SODIUM PYROPHOSPHATE AND SODIUM DIARSENATE

CRYSTAL STRUCTURES AND PHASE TRANSFORMATIONS
OF
SODIUM PYROPHOSPHATE AND SODIUM DIARSENATE

By

KIANG YIU LEUNG, B.Sc.

A Thesis
Submitted to the School of Graduate Studies
in Partial Fulfilment of the Requirements
for the Degree
Doctor of Philosophy

McMaster University

May 1973

DOCTOR OF PHILOSOPHY
(Physics)

McMASTER UNIVERSITY
Hamilton, Ontario

TITLE: Crystal Structures and Phase Transformations of Sodium Pyrophosphate and Sodium Diarsenate

AUTHOR: Kiang Yiu Leung, B.Sc. (University of Hong Kong)

SUPERVISOR: Professor Crispin Calvo

NUMBER OF PAGES: viii, 189

SCOPE OF CONTENTS:

An X-ray study of the various phases of anhydrous sodium pyrophosphate has been carried out. The system began with an ordered structure in orthorhombic space group $P2_12_12_1$ and ended with a completely disordered structure in hexagonal space group $P6_3/mmc$. All the intermediate phases were partially disordered.

The crystal structure of the first two phases of the system were determined while the rest were only partially solved due to the complexity of the disorder involved. A discussion on the symmetry aspects of the phase transformations was given and a model for the disorder of the hexagonal phase was proposed.

As an integral part of the study the room-temperature phase of sodium diarsenate was also investigated.

ACKNOWLEDGEMENT

It is with pleasure that I express my gratitude to Professor Crispin Calvo for supervising this work. His warm friendship and stimulating discussions throughout the experimental work and the writing of this thesis have been most beneficial.

I should also like to thank all the faculty members of the X-Ray Group for occasional discussions, particularly Dr. H.D. Grundy for his assistance in some programming problems. Many discussions with fellow graduate students, M.R. Anderson, D. DeLaMatter, Dr. R. Gopal and Dr. N. Panagiotopoulos have been most interesting.

Special thanks are due to my wife for her patience, understanding and encouragement throughout the course of my graduate studies.

The Ontario Government and the Department of Physics of McMaster University are cordially acknowledged for their financial assistance.

TABLE OF CONTENTS

LIST OF ILLUSTRATIONS

(continued)

LIST OF ILLUSTRATIONS
(continued)

LIST OF TABLES

(continued)

LIST OF TABLES
(continued)

CHAPTER I

INTRODUCTION

IT IS generally recognized that the properties of a substance do not depend merely on the types of atoms it contains; but rather they depend, to a large extent, on the configuration of the atoms building up the substance. One of the most interesting and useful applications of crystallography is therefore in the discussion of some observed properties of a substance in relation to its crystal structure.

Anhydrous sodium pyrophosphate, $Na_4P_2O_7$, has been observed by thermal differential analysis to exhibit a rich variety of reversible phase transformations [1,2]. Moreover, all these phase transformations exist within the crystalline state of the substance. We have, therefore, a problem which offers an opportunity to study phase transformations from a crystallographic point of view.

The mechanism of phase transformations has always been one of the most fascinating and one of the least understood of all physical problems. In recent years extensive studies has been carried out towards elucidating the various types of transformations that occur in crystals. However, most of the research is mainly on such critical phenomena as anomalies in specific heat, latent heat, elastic constants, electrical and thermal conductivities; and in ferromagnetic substances, changes in magnetic properties. With the focus being near the transition temperature, increasing attention is now being given to the structural aspects of crystal systems undergoing phase transformations, however. As early as 1937, Landau [3] had developed a theory on the possible changes of symmetry of a crystal at the transition point. It is convenient to distinguish between two types of phase transformations: (i) the so-called first-order phase transformation which usually involves a change of volume and/or entropy so that the symmetry properties of the phases before and after the transformation are uncorrelated, and (ii) the second-order phase transformation, or better, a transformation of the second kind, where the state of the phases before and after the transformation is the same. For such a transformation to be possible, Landau showed that the symmetry of the system must change in such a way that the space group of the lower symmetry form is a subgroup of the space group of the higher symmetry form. Furthermore, from a thermodynamical point of view, if the thermodynamic potential function of the system is expanded in powers of some order parameter which characterizes the transition, there should be no third power terms in the order parameter. In terms of the theory of group representations, this means that the triple product of the representation which corresponds to the transition, does not contain the unit representation [4]. In this thesis, therefore, apart from solving the structure of the various phases of the systems, an attempt will be made to apply Landau's theory to see if the transformations involved could be of second-order.

From the crystal chemical point of view, the system of $Na_4P_2O_7$ has merits of its own which deserve investigation. It belongs to a system with the stoichiometry $M_4X_2O_7$ where X_2O_7 is formed from two tetrahedrally coordinated X ions sharing a common "bridging" oxygen atom. Systems of MX_2O_7 and $M_2X_2O_7$ have been extensively studied in this laboratory as well as elsewhere. However, strange as it may seem, very little is known of the molecular geometry of $M_4X_2O_7$ systems where M is a monovalent metal such as Li, Na and K. To date, only powder pattern data on $Li_4P_2O_7$ and $Li_4As_2O_7$ [5] have been reported.

In recent years, much theoretical work has been done on the molecular geometry of various simple inorganic systems. Brown and Calvo [6] have discussed the crystal chemistry of large cation dichromates, pyrophosphates and related compounds with stoichiometry $X_2Y_2O_7$. They have observed that crystals for which the ionic radius of the Y atom is greater than 0.60 Å, crystallize into such structure as pyrochlore, $(Na,Ca)_2(Cb,Ti)_2(O,F)_7$ and weberite, Na_2MgAlF_7 [7] in which the Y atom is octahedrally coordinated. Of the rest, those in which the ionic radius of X is less than 0.97 Å tend to crystallize in one of the structures related to that of thortveitite, $(Sc,Y)_2Si_2O_7$ [8] while those in which X has an ionic radius greater than 0.97 Å usually crystallize in one of a series of structures closely related to those of alkaline metal dichromates. Recent results with $M_2V_2O_7$ groupings indicate that even this generalization must be viewed with caution [9]. In 1970, Baur [10] discussed bond-length variations and distorted coordination polyhedra and tested Pauling's Electrostatic Valency Principle first enunciated in 1929 which states that the sums of the average bond lengths around the cations and anions are approximately equal to their valence. He was able to predict with some accuracy the bond length, d_{A-X} between two ions A and X with the linear relationship

$$d_{A-X} = b + m\ p_X$$

where p_X is the electrostatic bond strength for anion X and b and m are coefficients determined from a large quantity of experimental data. More recently, in 1972 Brown and Shannon [11] did some calculations on the empirical bond strength, s, and bond length, r curves for oxides in the form

$$s = C_o(r_o/r)^n$$

where C_o is the formal charge divided by the "normal" coordination number and r_o and n are parameters to be determined by least squares based again on a large quantity of experimental data. It seems therefore apart from contributing to the knowledge of the system $M_4X_2O_7$, the validity of some of the general principles underlying these discussions could be tested.

As an integral part of the thesis, the system of sodium diarsenate, $Na_4As_2O_7$, was also investigated. Like sodium pyrophosphate, this system also exhibits a series of phase transformations as detected by differential thermal analysis. However, the nature of these transformations is quite different from sodium pyrophosphate. In sodium diarsenate, the first few minor transformations above room temperature are not very prominent and do not show any symmetry change detectable by a precession camera. Furthermore, these transformations are not immediately reversible and the reversibility depends on time. The major transformation at 692 °C. is immediately reversible, however; but the crystal invariably cracks at this temperature. Only the crystal structure at room temperature was therefore investigated.

CHAPTER II

SYMMETRY ASPECTS OF PHASE TRANSFORMATIONS

In 1937 Landau [3] put forward the thermodynamic theory of phase transformations of the second kind. In this Chapter, some of his results will be discussed first, and then, they will be applied to the system of sodium pyrophosphate to see if the various phases of the system could be of the second kind or not.

2.1. Phase Transformations of the Second Kind

The symmetry of a crystal can be described by means of a density function $\rho(\underline{r})$ which defines the probability $\rho(\underline{r})dV$ of finding one or more particles in a volume dV of the crystal. The set of all symmetry operators which leave $\rho(\underline{r})$ invariant forms the space group of the crystal. In general, a change of pressure p and temperature T will result in a change of $\rho(\underline{r})$. In a phase transformation of the second kind, $\rho(\underline{r})$ changes continuously in such a way that the symmetry of the crystal is different before and after the transformation. The thermodynamic function F which completely defines the system is a function of p, T, and ρ, and in a state of equilibrium, F is a minimum.

From thermodynamic considerations, Landau [12] showed that for a phase transformation of the second kind to be possible, it is necessary that the change of symmetry of the system at the transition point must be such that the space group of the lower symmetry form is a subgroup of the space group of the higher symmetry form.

It is convenient, in considering the symmetry of space groups, to use the mathematical formalism of the representation of groups. Seitz[13] showed that any irreducible representation of a space group could be given by a set of functions of the form

$$\phi_{\underline{k}n} = u_{\underline{k}n} e^{2\pi i(\underline{k}\cdot\underline{r})} \tag{2.1.1.}$$

where $\underline{k}$ is a vector which characterizes the representation in the reciprocal space, $u_{\underline{k}n}$ are periodic functions with the same periods as the direct lattice, and the suffix $n = 1, 2, \ldots.$ labels functions with the same $\underline{k}$.

In terms of the theory of the representation of groups, Landau's theory of phase transformations of the second kind requires that the change of symmetry of the crystal should correspond to a single irreducible representation of the space group of the higher symmetry form and that there should exist no third-order invariants corresponding to this irreducible representation[14]. Thus, according to Landau, a phase transformation of the second kind is only possible for representations with $\underline{k}$-vectors for which

$-\underline{k} = \underline{k} + \underline{Q}$ where $\underline{Q}$ is zero or a primitive vector of the reciprocal space, or with $\underline{k}$-vectors for which the proper symmetry group contains symmetry axes and planes intersecting at a point.

In the following Section, the phase transformations of sodium pyrophosphate will be examined along these lines.

2.2. Order of the Phase Transformations of $Na_4P_2O_7$

A full description of the phase transformations of the system of sodium pyrophosphate will be given in Chapter IV. Here, the observed phases of the system are summarized in Fig. 2.2.1.

At room temperature the structure of the system is orthorhombic in space group $P2_12_12_1$ with $\underline{a} = a_o = 9.37$, $\underline{b} = b_o = 5.39$, $\underline{c} = c_o = 13.48$ Å and $z = 4$. The space group becomes C2/c at 405 °C. with $\underline{a} = a_o$, $\underline{b} = b_o$, $\underline{c} = 2c_o$; $\beta = 93^o$ and $z = 8$. At 520 °C. the structure changes in such a way that the $\underline{a}$ axis becomes the unique axis and the $\underline{c}$ axis has a length of $3c_o$. The space group is now Cc, and $z = 12$. Between 540° and 600 °C. the diffraction pattern loses its superstructure reflections, i.e. those indexed with $l \neq 0$ (modulo 3), and simultaneously develops a 6-fold axis. The space group is now $P6_3/mmc$ with $\underline{a} = \underline{b} = b_o$ and $\underline{c} = c_o$.

Hysteresis effects (Section 4.6), common across the phase transformations and twinning (Section 4.3) indicate that the phase transformations are probably first-order.

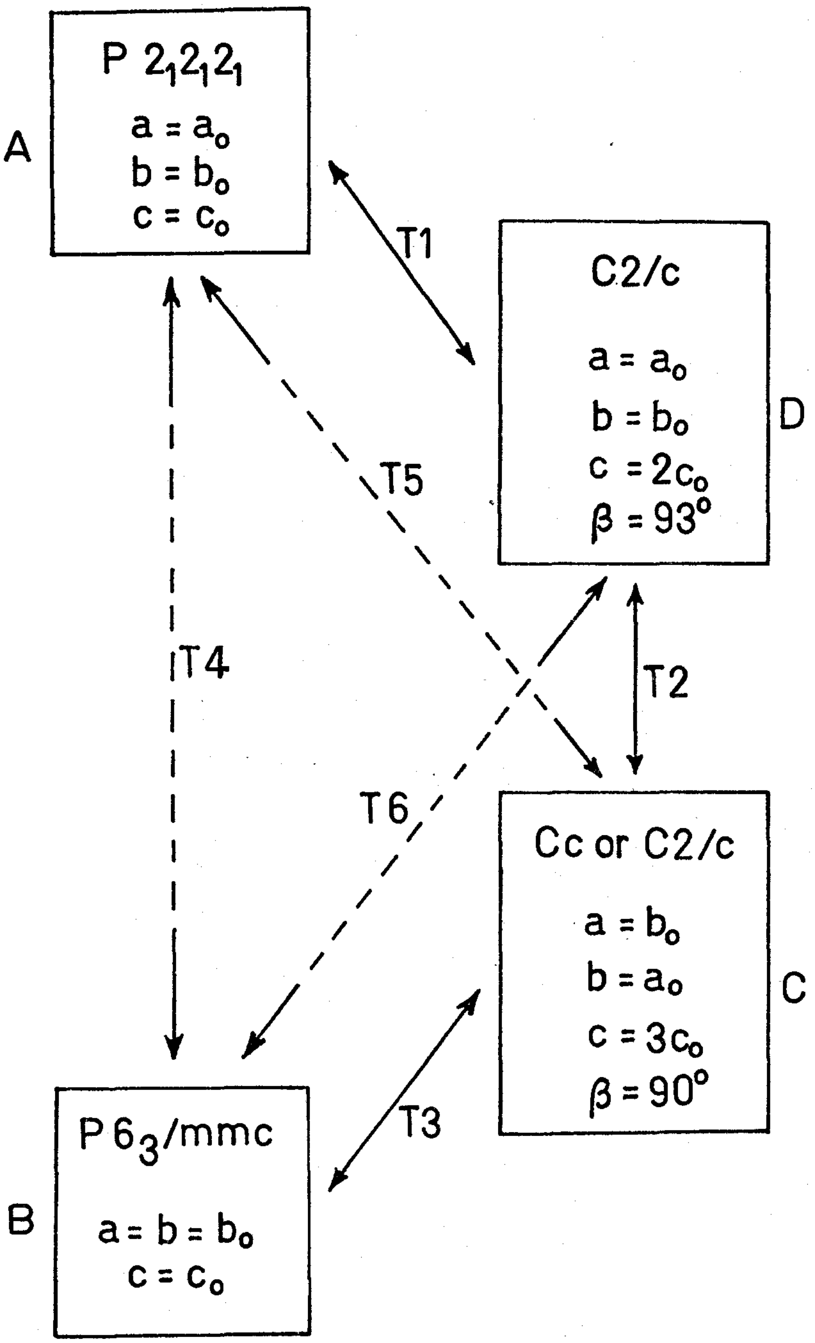

Fig. 2.2.1. Observed Phase Transformations of $Na_4P_2O_7$

It is, however, worthwhile to investigate the conclusions that can be drawn systematically from Landau's theory.

For phase D (Fig. 2.2.1), since $\beta = 93^\circ$ which cannot be readily expressed in terms of the angles of the other phases, transformations T1, T2 and T6 involving phase D at one end, must be eliminated as being of the second kind by the subgroup condition. Transformations T3 and T5 involve a tripled $\underline{c}$ axis; they are impossible as transformations of the second kind because each corresponds to a cell with lattice vectors $(0, 0, \frac{1}{3})$ which give rise to a function $e^{2\pi iz/3}$ which has a non-vanishing third-order invariant. The only transformation which might be of the second kind is probably T4. We will investigate this in more detail.

Phase A with space group $P2_12_12_1$ has a unit cell volume equal to twice that of phase B with space group $P6_3/mmc$. With reference to an orthogonal coordinate system $(\underline{i}, \underline{j}, \underline{k})$ the direct lattice vectors of A and B are given by

$$\text{(A)} \quad \begin{aligned} \underline{a} &= a\underline{i} \\ \underline{b} &= b\underline{j} \\ \underline{c} &= c\underline{k} \end{aligned} \qquad\qquad \text{(B)} \quad \begin{aligned} \underline{a} &= \tfrac{1}{2}a\underline{i} - \tfrac{1}{2}b\underline{j} \\ \underline{b} &= b\underline{j} \\ \underline{c} &= c\underline{k} \end{aligned}$$

The reciprocal lattice vectors of A and B are then

$$\text{(A)} \quad \begin{aligned} \underline{a}^* &= (1/a)\underline{i} \\ \underline{b}^* &= (1/b)\underline{j} \\ \underline{c}^* &= (1/c)\underline{k} \end{aligned} \qquad\qquad \text{(B)} \quad \begin{aligned} \underline{a}^* &= (2/a)\underline{i} \\ \underline{b}^* &= (1/a)\underline{i} + (1/b)\underline{j} \\ \underline{c}^* &= (1/c)\underline{k} \end{aligned}$$

The reciprocal lattice of B therefore consists of the points (200), (110), (001) etc. while the reciprocal lattice of A consists of the points (100), (010), (001) etc. Thus, the ordering corresponds to the three vectors

$$\underline{k}_1 = (100); \ \underline{k}_2 = (010); \text{ and } \underline{k}_3 = (001).$$

Since

$$\begin{aligned} -\underline{k}_1 &= \underline{k}_1 - (200) \\ -\underline{k}_2 &= \underline{k}_2 - (110) - (110) + (200) \\ -\underline{k}_3 &= \underline{k}_3 - (001) - (001) \end{aligned}$$

the condition $-\underline{k} = \underline{k} + \underline{Q}$ for a phase transformation of the second kind is fulfilled. We still have to check over the third-order invariants. Now, third-order invariants are possible if there exists a sum of three vectors equal to a primitive lattice vector of the reciprocal lattice of the higher symmetry form. This is the case here because

$$\begin{aligned} \underline{k}_1 + \underline{k}_2 + \underline{k}_3 &= (111) \\ &= (110) + (001) \end{aligned}$$

and the second line corresponds to a reciprocal lattice vector of B. Hence, transformation T4 cannot be of the second kind.

We have therefore shown that all the observed phase transformations of the system of sodium pyrophosphate could not be of the second kind. However, since there are a number of transformations of the system which are very close together, we could not conclude, pending further information on the structure of these phases, whether any of the totality of the phase transformations of the system of sodium pyrophosphate could be of the second kind or not.

CHAPTER III

PRINCIPLES OF STRUCTURE DETERMINATION

In the determination of a crystal structure various methods are employed depending on the degree of complexity of the structure. General principles of structure determination are discussed in a number of standard texts, e.g. Lipson and Cochran[15] and Stout and Jensen[16]. In this Chapter, no attempt is made to discuss all the principles involved; rather, only the principles of those methods which are pertinent to the present investigation will be discussed.

3.1. Basic Corrections

The structure of a crystal is revealed by the pattern and the magnitude of the intensities of the reflections formed when a beam of X-rays impinges on the crystal. These intensities are recorded either on a photographic film or with a counter. In either case corrections must first be made on their magnitudes before they can be used in a structure determination.

The corrections to be made are mainly due to the geometry of the instrument used in collecting the data and to the size of the crystal used. There are three effects for which corrections must be made, namely: the Lorentz factor, L, the polarization, p, and the absorption, K. If $I_o(H)$ is the observed intensity of a reflection H = (h,k,l)* relative to some arbitrary scale, the corrected intensity $I_c(H)$ relative to the same scale is given by

$$(3.1.1) \qquad I_c(H) = \frac{K}{L\ p} I_o(H).$$

The Lorentz factor arises from the fact that for a rotating crystal, various reflecting planes spend unequal times within the narrow angular range over which reflection occurs. It depends therefore on the technique used. For the equi-inclination Weissenberg, it is given by

$$L = \sin\theta/[\sin 2\theta\sqrt{(\sin^2\theta - \sin^2\delta)}]$$

where δ is the equi-inclination setting angle and θ is the usual Bragg angle. For a precession camera, the expression for L is very much more complicated; and a detailed discussion was given in an article by Waser [17].

The polarization term, p, arises because of the nature of the x-ray beam and the manner in which its reflection efficiency varies with the Bragg angle. It is given by

$$p = (1 + \cos^2 2\theta)/2$$

and is independent of the particular measurement technique used.

---

* "l" is the lower case of L. The numeral ONE is "1".

Of the three common types of corrections absorption is the most difficult and is often omitted when the data are not of high accuracy. The difficultyis due to the fact that the correction depends on the size and shape of the crystal. For each reflection it is necessary to calculate the absorption for the actual path length traversed within the crystal by the beam reflecting from each infinitesimal portion of the crystal and then integrate these results over the entire volume of the crystal. A general expression cannot be given for a crystal of an arbitrary shape. It is a general practice, therefore, to grind the crystal into a well-defined shape and the shape which is most easily obtained and consequently most often used, is a sphere. For a spherical crystal of radius R we have to calculate first the quantity μR where μ is defined by

$$\mu = D\sum_i \left[(A/M)_i(\mu/\rho)_i\right].$$

In this expression D is the density of the crystal, A is the atomic weight of the individual atom in the crystal, M is the molecular weight of the compound, and (μ/ρ) is the mass absorption coefficient depending on the wavelength of the radiation used. The summation is over all the distinct atoms in the unit cell. The values of (μ/ρ) for different atoms in common wavelengths as well as the absorption corrections for fixed values of μR in the range of θ from 0 to 90° are tabulated in the International Tables for X-Ray Crystallography[18]. The corrections are to be applied according to Equation (3.1.1).

3.2. Extinction Correction

In addition to the basic corrections discussed in Section (3.1), a further correction may be necessary depending on the apparent accuracy as indicated in the final stages of the refinement. It is the extinction correction. There are two types of extinction, namely, primary and secondary. Primary extinction relates to the interference effects on the diffracted beam as it is multiply reflected between the reflecting planes. The net result is to cause the intensity of the diffracted beam to be proportional to $|F|$ rather than $|F^2|$. A crystal for which this is strictly true is termed an ideally perfect crystal. However, due to the mosaic-block character of most crystals, very few specimens approach this ideal state and the intensity I is given by

$$I \propto |F|^n$$

where $1 < n < 2$, but is usually near 2. If primary extinction is neglected, $n = 2$ exactly.

Secondary extinction arises for reflections of such intensity that an appreciable amount of the incident radiation is reflected by the first planes encountered by the beam with the result that the deeper planes would receive less power and subsequently diffract less than they would do otherwise. Crystals in which the mosaic blocks are not well-aligned, will suffer less than those in which the alignment is more nearly parallel. A mosaic crystal in which secondary extinction is negligible is termed ideally imperfect. Secondary extinction is more pronounced for reflections at low values of sin θ/λ where the general level of the intensities is highest. Its existence is indicated by the observed values for the intense reflections being systematically less than their calculated values. If g is the secondary extinction coefficient which is characteristic of the crystal for a given radiation, then the observed (I_o) and calculated (I_c) intensities are related by

$$I_o = I_c \exp(-\, 2gI_c).$$

On expanding and neglecting terms in I_c higher than the first, we have

$$I_c = I_o(1 + 2gI_c).$$

A plot of I_c/I_o versus I_c should be linear with intercept 1 and slope 2g. If secondary extinction is present, $g > 0$ and its value is determined from the slope. Substituting this value of g in the above equation, we have

$$I_{\text{corrected}} = I_o(1 + 2gI_c).$$

3.3. The Method of Least Squares

An analytical method of refinement of great power and generality is that based on the principle of least squares. Consider a function G whose value is determined both by the "location" variables ($x_1, x_2, \ldots, x_N$) and the independent parameters ($p_1, p_2, \ldots, p_n$) which define the function. Thus

$$G = g(x_1, \ldots, x_N; p_1, \ldots, p_n). \tag{3.3.1}$$

If the values of the function are measured at m different points with m > N, the principle of least squares states that the best values for the parameters $p_1, \ldots, p_n$ are those which minimize the sums of the squares of the properly weighted differences between the observed G_o and the calculated G_c of the function for all the observation points. Thus, the quantity to be minimized is given by

$$D = \sum_{j=1}^{m} w_j (G_{oj} - G_{cj})^2 \tag{3.3.2}$$

where w_j is the weight assigned to each observation. Regarding the p_i's as variables, a minimum of D implies $\partial D/\partial p_i = 0$ for all i = 1, 2, ..., n. That is,

$$\sum_{j=1}^{m} w_j (G_{oj} - G_{cj}) \frac{\partial G_{cj}}{\partial p_i} = 0. \qquad (i = 1, \ldots, n) \tag{3.3.3}$$

The set of n equations in n unknowns is called the normal equations.

In X-ray diffraction the function of interest is the magnitude of the structure factor $|F|$ where the x variables are the Miller indices of each reflection, h, k, l and the p parameters are the atomic positions, temperature factors, multiplicities and scale factors. The indices h, k, l are often used in place of m. Writing H for (h, k, l), Equation (3.3.3) becomes

$$(3.3.4) \qquad \sum_{H} w(H)\Big[|F_o(H)| - |F_c(H)|\Big] \frac{\partial |F_c(H)|}{\partial p_i} = 0 \qquad (i = 1,\dots, n)$$

where, for simplicity, the scale factor usually in front of $|F_c|$ is absorbed into $|F_c|$ itself.

The set of Equations (3.3.4) involves the partial derivatives of $|F_c|$ with respect to each p_i. The mathematics would simplify considerably if $|F_c|$ were linear. However, in X-ray diffraction, the structure factor function is transcendental which can be expanded by a Taylor series. If $p = (p_1, \dots, p_n)$ is the true value which satisfies Equations (3.3.4) and $q = (q_1, \dots, q_n)$ is close to p so that $\delta_i = p_i - q_i$ are small for all i, then we have

$$(3.3.5) \qquad |F_c(H;p)| = |F_c(H;q)| + \sum_{i=1}^{n} \frac{\partial |F_c(H;q)|}{\partial p_i} \delta_i + O(\delta_i^2).$$

In the linear approximation, all terms of order higher than the first, $O(\delta_i^2)$, are ignored so that

$$(3.3.6) \qquad |F_c(H;p)| = |F_c(H;q)| + \sum_{i=1}^{n} \frac{\partial |F_c(H;q)|}{\partial p_i} \delta_i .$$

Substituting (3.3.6) in (3.3.4) and simplifying, we have

$$(3.3.7) \qquad \sum_{j=1}^{n} \sum_{H} w(H) \frac{\partial|F_c(H;q)|}{\partial p_j} \frac{\partial|F_c(H;q)|}{\partial p_i} \delta_j$$

$$= \sum_{H} w(H)\Big[|F_o(H)| - |F_c(H;q)|\Big]\frac{\partial|F_c(H;q)|}{\partial p_i} \qquad (i = 1, \ldots, n)$$

This is a system of n equations in n unknowns, the δ_j's. These equations are linear in the δ_j's and are solvable in them. Combining these with the initial approximation, the q_j's, gives better, although still approximate, values for the various parameters. These may be used to repeat the process until convergence is obtained, and successive cycles produce no further changes.

It is of importance to realize that the method of least squares is only applicable to refinements when the initial parameters are reasonably accurate. Thus, it is not possible to solve by this method for the parameters directly from the intensity data without first developing the structure by other methods such as the Patterson method or the direct methods.

3.4. Estimated Standard Deviations from Least Squares

In the set of equations (3.3.7), if we write

$$a_{ij} = \sum_H w(H) \frac{\partial |F_c(H;q)|}{\partial p_i} \frac{\partial |F_c(H;q)|}{\partial p_j} \tag{3.4.1}$$

and

$$c_j = \sum_H w(H)\Big[|F_o(H)| - |F_c(H;q)|\Big]\frac{\partial |F_c(H;q)|}{\partial p_j}$$

then (3.3.7) becomes

$$\begin{bmatrix} a_{11} & a_{12} & \cdots\cdots & a_{1n} \\ a_{21} & a_{22} & \cdots\cdots & a_{2n} \\ \cdots & \cdots & \cdots & \cdots \\ a_{n1} & a_{n2} & \cdots\cdots & a_{nn} \end{bmatrix} \begin{bmatrix} \delta_1 \\ \delta_2 \\ \cdot\cdot \\ \delta_n \end{bmatrix} = \begin{bmatrix} c_1 \\ c_2 \\ \cdot\cdot \\ c_n \end{bmatrix}$$

or, more compactly,

$$\underline{A}\,\underline{\delta} = \underline{c}. \tag{3.4.2}$$

The inverse matrix $\underline{A}^{-1}$ can be represented by $\underline{B} \equiv (b_{ij}) \equiv \underline{A}^{-1}$ and we are interested in the matrix elements b_{ij}.

In the least-squares refinement of a structure, it is a standard practice to solve the normal equations (3.3.7) in the matrix form (3.4.2) and to obtain both the new values of the parameters varied and their estimated standard deviations, σ. The general equation for calculating σ for any of the n parameters is

$$(3.4.3) \qquad \sigma_{p_i} = \sqrt{b_{ii}(\Sigma_H \; w(H) \left| |F_o(H)| - |F_c(H;q)| \right|^2)/(m - n)}$$

where m is the total number of reflections.

3.5. Weighting Functions

The function w(H) in Equation (3.3.4) is the weighting factor for each observation H. It should be a measure of the reliability of the observation. If properly chosen, it has the effect of adjusting the contribution of each observation to the normal equations in such a way as to produce the most reliable results. From statistical considerations, the best weight is equal to the square of the reciprocal of the standard deviation σ of the observation, i.e.

$$(3.5.1) \qquad w(H) = 1/\sigma^2(H).$$

One method of estimating $\sigma(H)$ has been given by Equation (3.4.3). It is not generally feasible, however, that in structure determinations involving a large number of reflections, the $\sigma(H)$'s could be reliably obtained. In 1961, Cruickshank[19] proposed a weighting scheme which requires that the averaged weighted discrepancy $\langle w(H) \left| |F_o(H)| - |F_c(H)| \right|^2 \rangle$ be a constant function of some systematic parameters such as $|F_o|$ or sin θ/λ. The functional form for the weight is usually taken to be

$$(3.5.2) \qquad w(H) = \left[A + B\,F_o(H) + C\,F_o^2(H) \right]^{-1}$$

where A, B, and C are constants determined experimentally. This weighting scheme, however, is only used in the last few cycles of a refinement when the constancy of the weighted discrepancy average could be obtained.

For reasonably good X-ray data, however, it is found that results from structure refinements are not strongly dependent on a particular weighting scheme although the use of proper weighting functions can produce a real, if small, improvement in the results from a given set of data.

3.6. The Temperature Factor

An atom in a crystal is not stationary; it is constantly vibrating about its mean position with amplitudes which might be different in different directions. This vibrational motion is temperature-dependent in particular, and the corrections to be applied are therefore termed the temperature factor. For the isotropic case in which the vibration is uniform in all direction, the temperature factor of an atom for a given set of planes (hkl) is given by

$$(3.6.1) \qquad \exp\left[-\frac{B}{4}\left(\frac{2\sin\theta}{\lambda}\right)^2 \right] = \exp\left[-\frac{B}{4}\left(\frac{1}{d_{hkl}}\right)^2 \right]$$

where $B = 8\pi^2\overline{u^2}$, $\overline{u^2}$ is the mean-square amplitude of vibration, and $1/d_{hkl}$ is the reciprocal of the interplanar spacing, given, for the general crystal system, by

(3.6.2) $$1/d_{hkl} = \sqrt{(h^2a^{*2} + k^2b^{*2} + l^2c^{*2} + 2hka^*b^*\cos\gamma^* + 2hla^*c^*\cos\beta^* + 2klb^*c^*\cos\alpha^*)}$$

For the anisotropic case, the temperature factor must have a parameter for every term in the expression (3.6.2) since each term represents a component perpendicular to the set of planes (hkl). The general temperature-factor expression is therefore

(3.6.3) $$\exp\left[-2\pi^2(U_{11}h^2a^{*2} + U_{22}k^2b^{*2} + U_{33}l^2c^{*2} + 2U_{12}hka^*b^*\cos\gamma^* + 2U_{13}hla^*c^*\cos\beta^* + 2U_{23}klb^*c^*\cos\alpha^*)\right]$$

where the U_{ij} are the thermal parameters expressed in terms of mean-square amplitudes of vibration in Ångstroms. Another expression for anisotropic factor is commonly used in the literature and in some computer programs; it is

(3.6.4) $$\exp\left[-(\beta_{11}h^2 + \beta_{22}k^2 + \beta_{33}l^2 + 2\beta_{12}hk + 2\beta_{13}hl + 2\beta_{23}kl)\right]$$

The relation between the β_{ij} and U_{ij} is therefore

(3.6.5) $$\beta_{ij} = 2\pi^2(\underline{e}_i^* \cdot \underline{e}_j^*)\, U_{ij}$$

where $\underline{e}_1^*$, $\underline{e}_2^*$, $\underline{e}_3^*$ stand for $\underline{a}^*$, $\underline{b}^*$, $\underline{c}^*$ respectively.

3.7. The Phase Problem

The intensity $I(\underline{H})$ of a reflection $\underline{H} = (h,k,l)$ is related to the amplitude of scattering $|F(\underline{H})|^2$ on an absolute scale, the relationship being

$$I(\underline{H}) = k|F(\underline{H})|^2 \tag{3.7.1}$$

where k is a scale constant. $F(\underline{H})$ is a complex quantity. It is the resultant of all the waves scattered in the direction of $\underline{H}$ by all the atoms in the unit cell. If $f_j(\underline{H})$ is the atomic scattering function for the j-th atom whose position vector in a coordinate system with axes parallel to the three basis vectors of the cell is $\underline{r}_j$, then

$$F(\underline{H}) = \sum_{j=1}^{N} f_j(\underline{H}) \exp\left[2\pi i(\underline{H}\cdot\underline{r}_j)\right] \tag{3.7.2}$$

where the summation is over all the atoms N in the unit cell. Equation (3.7.2) can be written in another form

$$F(\underline{H}) = |F(\underline{H})| \exp\left[i\phi(\underline{H})\right] \tag{3.7.3}$$

where $\phi(\underline{H})$ is known as the phase of the structure factor $F(\underline{H})$. A complete knowledge of $|F(\underline{H})|$ and $\phi(\underline{H})$ for each $\underline{H}$ would make structure determination a routine computational procedure. Unfortunately, however, in X-ray crystallography only $I(\underline{H})$ is measurable and therefore only the magnitude $|F(\underline{H})|$ is available. $\phi(\underline{H})$, in general, is missing. This lack of information about the phases of $F(\underline{H})$ is known as the Phase Problem.

There are two main approaches in structure determinations, each being typical in the way in which this missing information about the phase is handled. One approach is to ignore this missing information altogether in the initial stages and is generally known as the Fourier Method. The other is to try to retrieve in the beginning as much as possible this missing information by some statistical arguments. This latter approach is known as the Direct Method. In the present investigation, both methods have been used and the principles underlying each of them will be described briefly.

3.8. The Generalized Structure Factor

The structure factor as defined by Equation (3.7.2) has been considered as the resultant of adding the waves scattered in the direction of $\underline{H}$ by all the atoms in the unit cell. This approach was based on the assumption that the scattering power of the electron clouds surrounding each atom could be equated to that of the proper number of electrons concentrated at the atomic centre. The structure factor can also be viewed from another standpoint. It can be regarded as the sum of the wavelets scattered from all the infinitesimal volume elements of electrons in the unit cell. If $\rho(\underline{r})$ is the electron density at a point $\underline{r}$ in the unit cell, then in a small volume element dv about $\underline{r}$, the number of electrons is $\rho(\underline{r})\,dv$ and the exponential form of the wavelet scattered by this element is $\rho(\underline{r}) \exp[2\pi i(\underline{H}\cdot\underline{r})]\,dv$.

The resultant is then the integral of all the elements in the unit cell, i.e.

$$(3.8.1) \qquad F(\underline{H}) = \iiint_V \rho(\underline{r}) \exp[2\pi i(\underline{H}\cdot\underline{r})]\, dv$$

where V is the volume of the unit cell. Functions such as (3.8.1) can be Fourier-transformed to give

$$(3.8.2) \qquad \rho(\underline{r}) = \frac{1}{V} \iiint_H F(\underline{H}) \exp[-2\pi i(\underline{H}\cdot\underline{r})]\, dH.$$

The range of $\underline{H}$ is from $-\infty$ to $+\infty$ for each of the integral values of h, k, and l. Equation (3.8.2) can therefore be written in a more precise form as

$$(3.8.3) \qquad \rho(\underline{r}) = \frac{1}{V} \sum_{\underline{H}=-\infty}^{+\infty} F(\underline{H}) \exp[-2\pi i(\underline{H}\cdot\underline{r})] .$$

From Equation (3.7.3) we have

$$(3.8.4) \qquad \rho(\underline{r}) = \frac{1}{V} \sum_{\underline{H}=-\infty}^{+\infty} |F(\underline{H})| \exp[-2\pi i(\underline{H}\cdot\underline{r})]\, e^{i\phi(\underline{H})}.$$

Everything on the right hand side of Equation (3.8.4) is observable except $\phi(\underline{H})$. It is obvious therefore that the information of $\phi(\underline{H})$ is vital to a structure determination.

Once $\rho(\underline{r})$ is known throughout the unit cell, we can assume $\rho(\underline{r}) = \Sigma_i \rho_i(\underline{r} - \underline{r}_i)$ where $\rho_i(|\underline{r}|)$ is known about any i-th atom and determine $\underline{r}_i$ for all atoms in the unit cell.

3.9. The Patterson Function

In using the Fourier Method to determine the structure of a crystal, the initial step is to map out a function, known as the Patterson Function, first introduced by A.L. Patterson[20] in 1935. He pointed out that it was possible to use the phaseless quantities $|F(H)|^2$ to deduce information on the relative positions of the atoms in the unit cell. The argument is as follows: consider the function defined by

$$(3.9.1) \qquad P(\underline{s}) = V \iiint_V \rho(\underline{r})\ \rho(\underline{r} + \underline{s})\ dv$$

where $\underline{s}$ is a continuous variable similar to $\underline{r}$. Substituting Equation (3.8.3) for $\rho(\underline{r})$ and $\rho(\underline{r}+\underline{s})$ we have

$$P(\underline{s}) = \frac{1}{V} \iiint_V \sum_{\underline{H}'} F(\underline{H}') \exp\left[-2\pi i(\underline{H}'\cdot\underline{r})\right] \sum_{\underline{H}} F(\underline{H}) \exp\left[-2\pi i(\underline{H}\cdot(\underline{r}+\underline{s}))\right] dv$$

$$= \frac{1}{V} \sum_{\underline{H}} F(\underline{H}) \exp\left[-2\pi i(\underline{H}\cdot\underline{s})\right] \sum_{\underline{H}'} F(\underline{H}') \iiint_V \exp\left[-2\pi i(\underline{H}+\underline{H}')\cdot\underline{r}\right] dv$$

The volume integral is identically zero unless $\underline{H} = -\underline{H}'$ in which case its value is V. Hence, we have

$$(3.9.2) \qquad P(\underline{s}) = \sum_{\underline{H}} F(\underline{H}) \exp\left[-2\pi i(\underline{H}\cdot\underline{s})\right] F(-\underline{H})$$

From Equation (3.8.1) and from the fact that $\rho(\underline{r})$ is a real quantity, $F(-\underline{H}) = F^*(\underline{H})$ which is the complex conjugate of $F(\underline{H})$. Equation (3.9.2) therefore becomes

$$(3.9.3) \qquad P(\underline{s}) = \sum_{\underline{H}} |F(\underline{H})|^2 \exp\left[-2\pi i(\underline{H}\cdot\underline{s})\right]$$

Recalling $I(\underline{H}) = k|F(\underline{H})|^2$ we see that the Patterson Function $P(\underline{s})$ can be expressed as a series whose coefficients are the intensities $I(\underline{H})$.

The physical meaning of $P(\underline{s})$ can be obtained directly from its definition, Equation (3.9.1). Peak values of $P(\underline{s})$ at $\underline{s}$ will normally correspond to simultaneous peak values of $\rho(\underline{r})$ at $\underline{r}$ and $(\underline{r} + \underline{s})$. This implies there are atoms in the unit cell separated by a vector $\underline{s}$. If there is a heavy scatterer in the unit cell at $\underline{r}$, then $\rho(\underline{r})$ will have a large value and the product of $\rho(\underline{r})$ and $\rho(\underline{r}+\underline{s})$ for any other atom $(\underline{r} + \underline{s})$ will be appreciable. It is obvious therefore that in structure determinations if the positions of a heavy scatterer in the unit cell is known, the positions of other atoms relative to it could be more readily found than if a heavy scatterer is absent. On the other hand, it is also true, though less obvious, that if the atoms in the unit cell are in such relative positions as to make the vectors $\underline{s}$ nearly parallel and of the same length, the peaks in a Patterson map could be confusing and an interpretation could be extremely difficult. This was actually the case in the present investigation of the room-temperature phase of sodium pyrophosphate, and the situation was finally resolved using direct methods.

3.10. Direct Methods

Direct methods in structure determinations fall into two catagories, namely those which are applicable to centrosymmetric space groups and those which are applicable to noncentrosymmetric space groups. General theory of direct methods applicable of centrosymmetric space groups is described in a number of textbooks (e.g. Woolfson [21]) and is irrelevant to the present investigation which involves the noncentrosymmetric space group of $P2_12_12_1$. In what follows, methods which are pertinent to noncentrosymmetric space groups will be discussed and in particular, details will be confined to space group $P2_12_12_1$.

The basic theory of direct methods applicable to noncentrosymmetric space groups is largely due to Hauptman and Karle [22, 23] . Starting with the definition of structure factor $F(\underline{H})$ given by (3.7.2), since it is a complex quantity, it can be written as

$$F(\underline{H}) = F(\underline{H}) \exp i\phi(\underline{H})$$

$$\equiv A(\underline{H}) + i\, B(\underline{H})$$

where

$$A(\underline{H}) = \sum_{j=1}^{N} f_j(\underline{H})\, X(\underline{H}, \underline{r}_j)$$

and

$$B(\underline{H}) = \sum_{j=1}^{N} f_j(\underline{H})\, Y(\underline{H}, \underline{r}_j).$$

$X(\underline{H},\underline{r}_j)$ and $Y(\underline{H},\underline{r}_j)$ are trigonometric functions depending on the space group; e.g., for P1, we have

$$X(\underline{H},\underline{r}) = \cos 2\pi(\underline{H}\cdot\underline{r}) \qquad Y(H,r) = \sin 2\pi(\underline{H}\cdot\underline{r})$$

The exact forms of X and Y depend also on the choice of the origin and these have been tabulated in the International Tables for X-Ray Crystallography[24].

Next, the second moments of X and Y are defined:

$$m_2^0 = \iiint_V X^2(\underline{H}, \underline{r})\, dv \qquad m_0^2 = \iiint_V Y^2(\underline{H}, \underline{r})\, dv$$

For reflections which are pure imaginary, $m_2^0 = 0$, for reflections which are pure real, $m_0^2 = 0$, and for general reflections, $m_2^0 = m_0^2$. If the number of equivalent positions is n, we can define a small number $e = (m_2^0 + m_0^2)/2$. Obviously, e is space group dependent; but most important of all, it depends on $\underline{H}$. For space group $P2_12_12_1$, we have

$$\begin{aligned} e(\underline{H}) = e(h,k,l) &= 2 \text{ if } h = k = 0, \text{ or} \\ &\quad\ \text{if } k = l = 0, \text{ or} \\ &\quad\ \text{if } l = h = 0, \text{ and} \\ &= 1 \text{ otherwise.} \end{aligned}$$

In direct methods it is advantageous to introduce a normalized structure factor $E(\underline{H})$ defined by

$$(3.10.1) \qquad |E(\underline{H})|^2 = |F(\underline{H})|^2 / \left[e \sum_{j=1}^{N} f_j^2(\underline{H}) \right]$$

so that, statistically, $\overline{E(\underline{H})} = 0$ and $\overline{E^2(\underline{H})} = 1$. Apart from having mathematical convenience in probability calculations, values of $E(\underline{H})$ allow the normalization of all classes of reflections to a common basis. It is therefore possible to avoid a rather subtle source of error in the comparison of special sets of reflections.

The values of $|F(\underline{H})|^2$ in Equation (3.10.1) are not the "raw" data obtained from $I(\underline{H})$. They must be corrected for vibrational motion and must be placed on an absolute scale. The actual procedure to carry out this correction is described by Karle and Hauptman [23].

The principal formulae which are used in determining phases for noncentrosymmetric space groups are

$$\phi_{\underline{H}} \approx \langle \phi_{\underline{K}} + \phi_{\underline{H}-\underline{K}} \rangle_{\underline{K}_r} \tag{3.10.2}$$

and

$$\tan \phi_{\underline{H}} = \frac{\Sigma_{\underline{K}} |E_{\underline{K}} E_{\underline{H}-\underline{K}}| \sin(\phi_{\underline{K}} + \phi_{\underline{H}-\underline{K}})}{\Sigma_{\underline{K}} |E_{\underline{K}} E_{\underline{H}-\underline{K}}| \cos(\phi_{\underline{K}} + \phi_{\underline{H}-\underline{K}})} . \tag{3.10.3}$$

In Equation (3.10.2) the average on the right hand side is taken over the set of all reflections, $\underline{K}_r$ whose E-values are relatively large. Equation (3.10.3) is used to generate additional phases after the phases of a certain number of reflections have been obtained.

To apply Equation (3.10.2) it is convenient to divide the data into sets with respect to the behaviour of the components of the index upon inversion. This can be worked out directly from the real and imaginary parts of the structure factor which have been tabulated in the International Tables for X-Ray Crystallography [24]. For space group $P2_12_12_1$, the phase relationships among the various reflections of the same numerical values of h, k, and l are shown in TABLE III.1.

3.11. Phase Determination

In order to avoid lengthy digression in Chapter V, the practical detail of phase determination of $Na_4P_2O_7$ which had been carried out, is described in this Section.

There were altogether 493 unique reflections from precession films. Using Equation (3.10.1), the magnitude of the normalized structure factor $|E(h,k,l)|$ for each reflection was calculated. The reflections were then separated into eight groups according to their h, k, l values being even or odd; and in each group they were arranged in descending orders of magnitude of $|E|$, terminating at the arbitrarily chosen value of 1.5. The results were shown in TABLE III.2. There were only 101 reflections with $|E|$ values greater than 1.5 which amounted to about 20% of the total unique reflections.

To fix the origin and the enantiomorph in space group $P2_12_12_1$, it is convenient to use the phases of two-dimensional data since each of these is centrosymmetric. With the help of TABLE III.1, the origin and the enantiomorph were assigned as shown in TABLE III.3. Three other reflections were also assigned symbols, p, q, and r. They were reflections 119, 244 and 715 respectively. These reflections were chosen because they enter into many combinations for the average in

TABLE III.1

Phase Relationships in Space Group $P2_12_12_1$

NOTE: g stands for even and u stands for odd.

Reflection	h k l	$\bar{h}$ k l	h $\bar{k}$ l	h k $\bar{l}$
ggg, uuu	α	$-\alpha$	$-\alpha$	$-\alpha$
ggu, uug	α	$-\alpha$	$\pi - \alpha$	$\pi - \alpha$
gug, ugu	α	$\pi - \alpha$	$\pi - \alpha$	$-\alpha$
guu, ugg	α	$\pi - \alpha$	$-\alpha$	$\pi - \alpha$

0gg	$0, \pi$	g0g	$0, \pi$	gg0	$0, \pi$
0uu	$\pm\frac{1}{2}\pi$	u0g	$0, \pi$	ug0	$\pm\frac{1}{2}\pi$
0ug	$\pm\frac{1}{2}\pi$	g0u	$\pm\frac{1}{2}\pi$	gu0	$0, \pi$
0gu	$0, \pi$	u0u	$\pm\frac{1}{2}\pi$	uu0	$\pm\frac{1}{2}\pi$

TABLE III.2. Reflections with |E|>1.5

g g g

h	k	l	|E|
2	4	4	2.89
0	4	0	2.59
8	0	14	2.36
6	2	0	2.31
6	4	0	2.25
6	0	0	2.25
4	0	4	2.23
8	0	4	2.20
8	0	10	2.07
2	6	4	2.06
2	0	18	2.04
0	2	18	2.03
2	4	10	2.00
0	4	14	1.93
2	4	14	1.88
0	0	8	1.88
0	2	8	1.88
4	0	6	1.84
8	2	14	1.78
0	2	14	1.77
8	2	4	1.74
10	0	6	1.72
6	2	8	1.69
0	4	4	1.68
2	0	4	1.66
10	4	0	1.64
6	0	8	1.64
2	4	6	1.62
6	0	14	1.58
8	2	10	1.53
0	2	0	1.52
0	4	8	1.51

g u g

h	k	l	|E|
2	3	4	2.04
2	1	12	1.95
2	5	12	1.82
0	1	18	1.82
0	1	8	1.63
0	5	2	1.56
6	1	8	1.56

g g u

h	k	l	|E|
6	4	1	2.53
6	2	1	2.26
2	0	9	2.20
4	0	5	2.12
6	6	1	2.07
2	2	9	2.00
2	6	9	1.96
2	6	5	1.92
6	0	15	1.92
4	0	9	1.90
2	4	13	1.89
2	4	9	1.87
4	2	9	1.79
10	0	5	1.74
6	0	1	1.71
4	2	5	1.69
2	4	5	1.60
4	2	13	1.59
4	0	13	1.55
2	6	13	1.53
2	0	17	1.53
8	0	3	1.51

u u g

h	k	l	|E|
3	3	0	2.99
3	5	0	2.87
1	5	4	2.27
1	3	4	2.19
11	1	10	2.17
5	1	14	2.14
5	1	4	2.14
5	1	10	2.06
11	1	4	2.06
7	1	6	1.86
3	1	8	1.82
7	1	14	1.79
3	1	0	1.78
3	1	14	1.62

u g u

h	k	l	|E|
7	0	7	1.70

g u u

h	k	l	|E|
2	3	3	2.03
2	3	13	1.93
2	3	9	1.65

u u u

h	k	l	|E|
7	1	5	2.79
1	1	9	2.70
5	1	9	2.66
1	3	9	2.54
1	3	5	2.42
1	3	13	2.33
9	5	1	2.16
9	3	1	2.05
1	1	13	2.04
3	5	1	1.96
1	5	5	1.91
9	1	1	1.91
1	5	13	1.90
3	3	1	1.80
1	1	5	1.75
5	1	3	1.70
7	1	13	1.66
9	1	9	1.54
7	1	3	1.53
5	1	1	1.52

TABLE III.3

Assignment of Origin and Enantiomorph

h	k	l	$\vert E(h,k,l)\vert$	$\phi(h,k,l)$	
3	3	0	2.99	$+\frac{1}{2}\pi$	Origin
2	0	9	2.20	$+\frac{1}{2}\pi$	
3	0	12	1.82	0	
4	0	5	2.12	$+\frac{1}{2}\pi$	Enantiomorph
1	1	9	2.70	p	
2	4	4	2.89	q	
7	1	5	2.79	r	

Equation (3.10.2) and they were associated with relatively large $|E|$ values. Because they were not two-dimensional, the values of p, q, and r would lie in the range $-\pi < p,q,r \leqslant \pi$.

TABLE III.4 shows the application of Equation (3.10.2) in the determination of the phases of 28 reflections. To obtain a value for p and q, we looked at Steps (2) and (3) of TABLE III.4. These at once gave $p = q = 0$. From Step (1), $\frac{1}{2}\pi + p = r - \frac{1}{2}\pi$ implies $r = \pi$ when $p = 0$. These values of p, q, and r led to no apparent contradiction in all the steps shown. We could therefore obtain a set of phases for 35 reflections as shown in TABLE III.5.

3.12. Structure Determination

An E-map was first calculated with the 35 reflections using Equation (3.8.4) where the $|F(\underline{H})|$ was replaced by $|E(\underline{H})|$, i.e.

$$(3.12.1) \qquad \rho_E(r) = \frac{1}{V} \sum_{\underline{H}} |E(\underline{H})| \exp[-2\pi i(\underline{H}\cdot\underline{r})]\, e^{i\phi(\underline{H})}$$

Surprising enough, even with this small number of known phases, a grid of about 0.3 Å in three-dimensions showed the positions of peaks which could be identified as phosphorus and sodium, Fig. 3.12.1. It was also possible to introduce the three 2_1 axes of the system, thereby fixing the origin of the unit cell. An initial structure factor determination with only two phosphorus atoms on the 493 reflections resulted an R value of about 40%. Further Fourier syntheses disclosed gradually

TABLE III.4. Applications of Equation (3.10.2)

(1)

$$\begin{array}{rrrl} 4 & 0 & 5 & \pi/2 \\ 1 & 1 & 9 & p \\ \hline 5 & 1 & 14 & \pi/2 + p \end{array}$$

$$\begin{array}{rrrl} 7 & 1 & 5 & r \\ -2 & 0 & 9 & -\pi/2 \\ \hline 5 & 1 & 14 & r - \pi/2 \end{array}$$

(2)

$$\begin{array}{rrrl} 4 & 0 & -5 & \pi - \pi/2 \\ 1 & 1 & 9 & p \\ \hline 5 & 1 & 4 & \pi/2 + p \end{array}$$

$$\begin{array}{rrrl} 3 & 3 & 0 & \pi/2 \\ 2 & -2 & 4 & -q \\ \hline 5 & 1 & 4 & \pi/2 - q \end{array}$$

(3)

$$\begin{array}{rrrl} 2 & 4 & -4 & -q \\ -1 & -1 & 9 & -(-p) \\ \hline 1 & 3 & 5 & p - q \end{array}$$

$$\begin{array}{rrrl} 4 & 0 & 5 & \pi/2 \\ -3 & 3 & 0 & -\pi/2 \\ \hline 1 & 3 & 5 & 0 \end{array}$$

(4)

$$\begin{array}{rrrl} 2 & 4 & 4 & q \\ -1 & -1 & 9 & -(-p) \\ \hline 1 & 3 & 13 & p + q \end{array}$$

(5)

$$\begin{array}{rrrl} 2 & 0 & 9 & \pi/2 \\ 1 & 1 & -9 & -p \\ \hline 3 & 1 & 0 & \pi/2 - p \\ 3 & 1 & 0 & \pi/2 - p \\ \hline 6 & 2 & 0 & \pi - 2p \end{array}$$

(6)

$$\begin{array}{rrrl} 6 & 2 & 0 & \pi - 2p \\ -3 & 3 & 0 & -\pi/2 \\ \hline 3 & 5 & 0 & \pi/2 - 2p \end{array}$$

(7)

$$\begin{array}{rrrl} 4 & 0 & 5 & \pi/2 \\ 4 & 0 & 5 & \pi/2 \\ \hline 8 & 0 & 10 & \pi \end{array}$$

(8)

$$\begin{array}{rrrl} 4 & 0 & 5 & \pi/2 \\ -2 & 4 & 4 & -q \\ \hline 2 & 4 & 9 & \pi/2 - q \end{array}$$

(9)

$$\begin{array}{rrrl} -2 & 4 & 9 & -\pi/2 + q \\ 4 & 0 & 5 & \pi/2 \\ \hline 2 & 4 & 14 & q \end{array}$$

(10)

$$\begin{array}{rrrl} 4 & 0 & -5 & \pi - \pi/2 \\ -2 & 0 & 9 & \pi - \pi/2 \\ \hline 2 & 0 & 4 & \pi \\ -2 & 0 & 4 & -\pi \\ \hline 0 & 0 & 8 & 0 \end{array}$$

(11)

$$\begin{array}{rrrl} 2 & 4 & -4 & -q \\ -1 & 1 & 9 & -p \\ \hline 1 & 5 & 5 & -(p+q) \end{array}$$

(12)

$$\begin{array}{rrrl} 2 & 4 & 4 & q \\ -1 & 1 & 9 & -p \\ \hline 1 & 5 & 13 & q-p \end{array}$$

(13)

$$\begin{array}{rrrl} 7 & -1 & 5 & -r \\ -1 & 5 & -5 & -(p+q) \\ \hline 6 & 4 & 0 & -(p+q+r) \end{array}$$

$$\begin{array}{rrrl} 7 & 1 & -5 & -r \\ -1 & 3 & 5 & -(p-q) \\ \hline 6 & 4 & 0 & -(p-q+r) \end{array}$$

(14)

$$\begin{array}{rrrl} 3 & 3 & 0 & \pi/2 \\ -2 & 0 & 9 & -\pi/2 \\ \hline 1 & 3 & 9 & 0 \end{array}$$

(15)

$$\begin{array}{rrrl} -1 & -3 & 9 & 0 \\ 2 & 4 & 4 & q \\ \hline 1 & 1 & 13 & q \end{array}$$

(16)

$$\begin{array}{rrrl} 1 & 3 & 9 & 0 \\ 1 & -3 & 9 & 0 \\ \hline 2 & 0 & 18 & 0 \end{array}$$

(17)

$$\begin{array}{rrrl} 2 & 0 & -9 & \pi - \pi/2 \\ -1 & 1 & 9 & -p \\ \hline 1 & 1 & 0 & \pi/2 - p \\ 1 & 1 & 9 & p \\ \hline 2 & 2 & 9 & \pi/2 \end{array}$$

(18)

$$\begin{array}{rrrl} 1 & 1 & 0 & \pi/2 - p \\ 1 & -1 & 0 & \pi - (\pi/2 - p) \\ \hline 2 & 0 & 0 & \pi \\ 2 & 0 & 0 & \pi \\ \hline 4 & 0 & 0 & 2\pi \\ 2 & 0 & 0 & \pi \\ \hline 6 & 0 & 0 & \pi \end{array}$$

$$\begin{array}{rrrl} 3 & 3 & 0 & \pi/2 \\ 3 & -3 & 0 & \pi - \pi/2 \\ \hline 6 & 0 & 0 & \pi \end{array}$$

(19)

$$\begin{array}{rrrl} 6 & 0 & 0 & \pi \\ -2 & 0 & 9 & -\pi/2 \\ \hline 4 & 0 & 9 & \pi/2 \end{array}$$

(20)

$$\begin{array}{rrrl} -1 & 1 & 9 & -p \\ 1 & 1 & 9 & p \\ \hline 0 & 2 & 18 & 0 \end{array}$$

(21)

$$\begin{array}{rrrl} 2 & 2 & 9 & \pi/2 \\ 0 & 2 & -18 & 0 \\ \hline 2 & 4 & -9 & \pi/2 \\ 0 & 2 & 18 & 0 \\ \hline 2 & 6 & 9 & \pi/2 \end{array}$$

(22)

$$\begin{array}{rrrl} 1 & 1 & 0 & \pi/2 - p \\ 1 & 5 & 5 & -(p+q) \\ \hline 2 & 6 & 5 & \pi/2-2p-q \end{array}$$

(23)

$$\begin{array}{rrrl} 2 & 4 & 4 & q \\ -1 & 1 & 0 & p-\pi/2 \\ \hline 1 & 5 & 4 & p+q-\pi/2 \end{array}$$

(24)

$$\begin{array}{rrrl} 1 & 1 & 0 & \pi/2 - p \\ 1 & 5 & 4 & p+q-\pi/2 \\ \hline 2 & 6 & 4 & q \end{array}$$

(25)

$$\begin{array}{rrrl} -1 & 5 & 4 & \pi/2+p-q \\ 1 & -1 & 0 & \pi/2 + p \\ \hline 0 & 4 & 4 & \pi+2p-q \\ 1 & -1 & 0 & \pi/2+p \\ \hline 1 & 3 & 4 & 3\pi/2+3p-q \end{array}$$

(26)

$$\begin{array}{rrrl} 6 & 0 & 0 & \pi \\ -1 & 1 & 9 & -p \\ \hline 5 & 1 & 9 & \pi - p \end{array}$$

(27)

$$\begin{array}{rrrl} 1 & 1 & 0 & \pi/2 - p \\ -1 & 1 & 0 & -(\pi/2-p) \\ \hline 0 & 2 & 0 & 0 \\ 0 & 2 & 0 & 0 \\ \hline 0 & 4 & 0 & 0 \end{array}$$

(28)

$$\begin{array}{rrrl} 2 & 6 & -5 & \pi-(\pi/2-2p-q) \\ 2 & -6 & 9 & \pi-\pi/2 \\ \hline 4 & 0 & 4 & -(\pi-2p-q) \end{array}$$

TABLE III.5. Phases of 35 Reflections

NOTE: The phases are expressed within the range $-\pi < \phi \leqslant \pi$.

h	k	l	$\|E(h,k,l)\|$	$\phi(h,k,l)$
3	3	0	2.99	$\frac{1}{2}\pi$
2	0	9	2.20	$\frac{1}{2}\pi$
3	0	12	1.82	0
4	0	5	2.12	$\frac{1}{2}\pi$
1	1	9	2.70	0
2	4	4	2.89	0
7	1	5	2.79	π
5	1	14	2.14	$\frac{1}{2}\pi$
5	1	4	2.14	$\frac{1}{2}\pi$
1	3	5	2.42	0
1	3	13	2.33	0
6	2	0	2.31	π
3	5	0	2.87	$\frac{1}{2}\pi$
8	0	10	2.07	π
2	4	9	1.87	$\frac{1}{2}\pi$
2	4	14	1.93	0
0	0	8	1.88	0
1	5	5	1.91	0
1	5	13	2.33	0
6	4	0	2.24	π
1	3	9	2.54	0
1	1	13	2.04	0
2	0	18	2.04	0
2	2	9	2.00	$\frac{1}{2}\pi$
6	0	0	2.27	π
4	0	9	1.90	$\frac{1}{2}\pi$
0	2	18	2.03	0
2	6	9	1.96	$\frac{1}{2}\pi$
2	6	5	1.92	$\frac{1}{2}\pi$
1	5	4	2.27	$-\frac{1}{2}\pi$
2	6	4	2.06	0
1	3	4	2.19	$-\frac{1}{2}\pi$
5	1	9	2.66	π
0	4	0	2.59	0
4	0	4	2.23	π

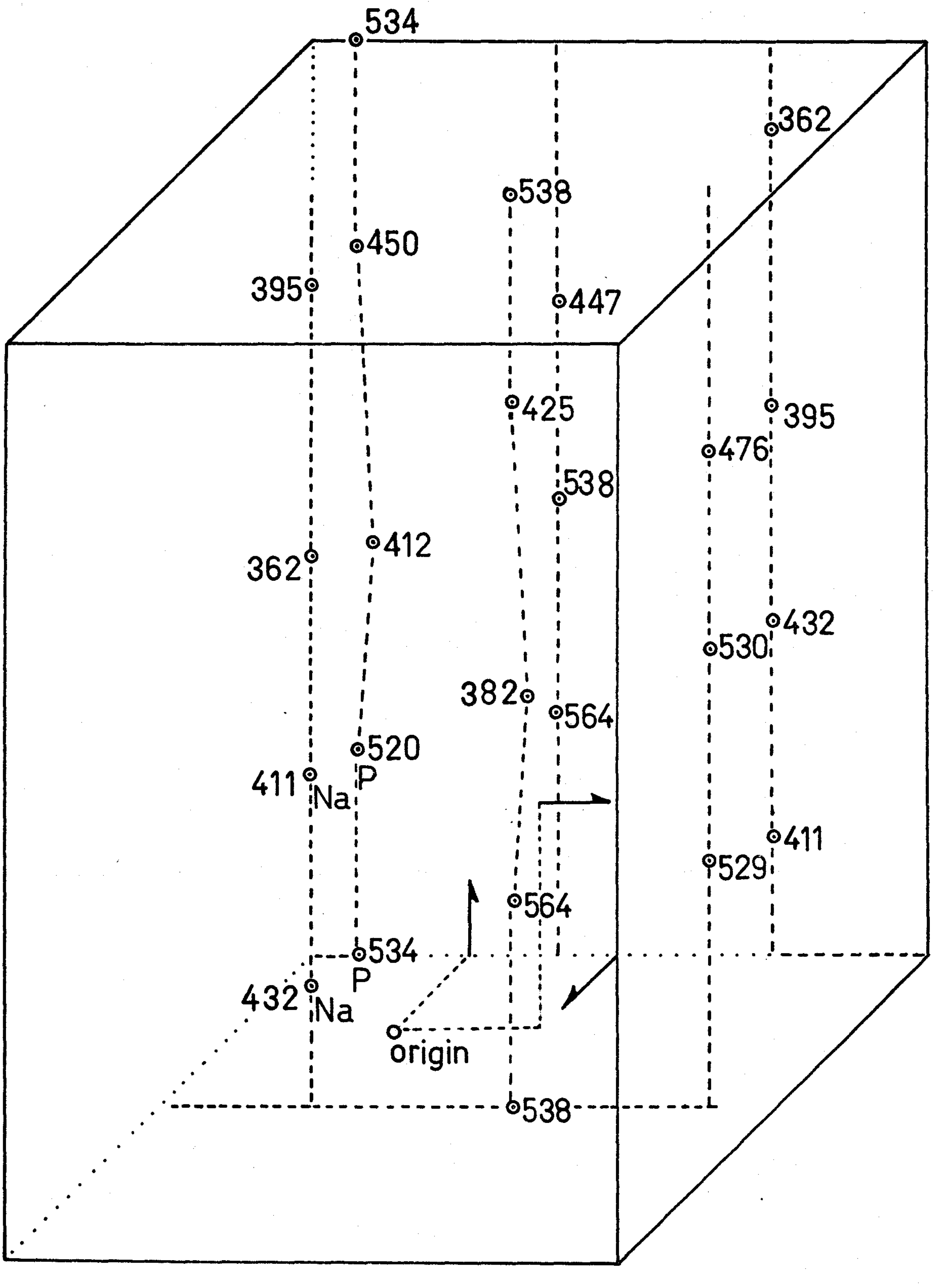

Fig. 3.12.1

A 3-D E-Map of $Na_4P_2O_7$ at 22°C. Only peak values shown.

the positions of the rest of the 11 atoms of oxygen and sodium. The final R value for the 493 film reflections with isotropic temperature factors is 10%. The rest of the refinement of the structure was then carried out with another set of more accurate diffractometer data and will be described fully in Chapter V.

CHAPTER IV

PHASE TRANSFORMATIONS OF SODIUM PYROPHOSPHATE AND SODIUM DIARSENATE

Differential thermal analyses (D.T.A.) showed that both $Na_4P_2O_7$ and $Na_4As_2O_7$ exhibited phase transformations in the range of temperature between 20 and 700 °C. $Na_4P_2O_7$, in particular, has a very rich variety of transformations. Although $Na_4P_2O_7$ and $Na_4As_2O_7$ are stoichiometrically equivalent, the changes in their various phases bear no immediate resemblance. In what follows, a description of the observed phenomena pertaining to the phases of these two compounds will be given.

4.1. The Phases of Sodium Pyrophosphate

A D.T.A. trace of sodium pyrophosphate is shown in Fig. 4.1.1. It is convenient to label the phases by Roman numerals as shown. Phase I is the room-temperature phase. At this temperature it is very stable and the space group is $P2_12_12_1$. The unit cell dimensions <u>a</u>, <u>b</u> and <u>c</u> are 9.367, 5.390 and 13.480 Å respectively. The transformation I-II takes place at 405 °C. and the space group becomes C2/c with $\beta = 93^\circ$ and the <u>c</u> axis double that of phase I. Phase II exhibits a "twinning" phenomenon which is discussed further

D.T.A. Traces of $Na_4P_2O_7$

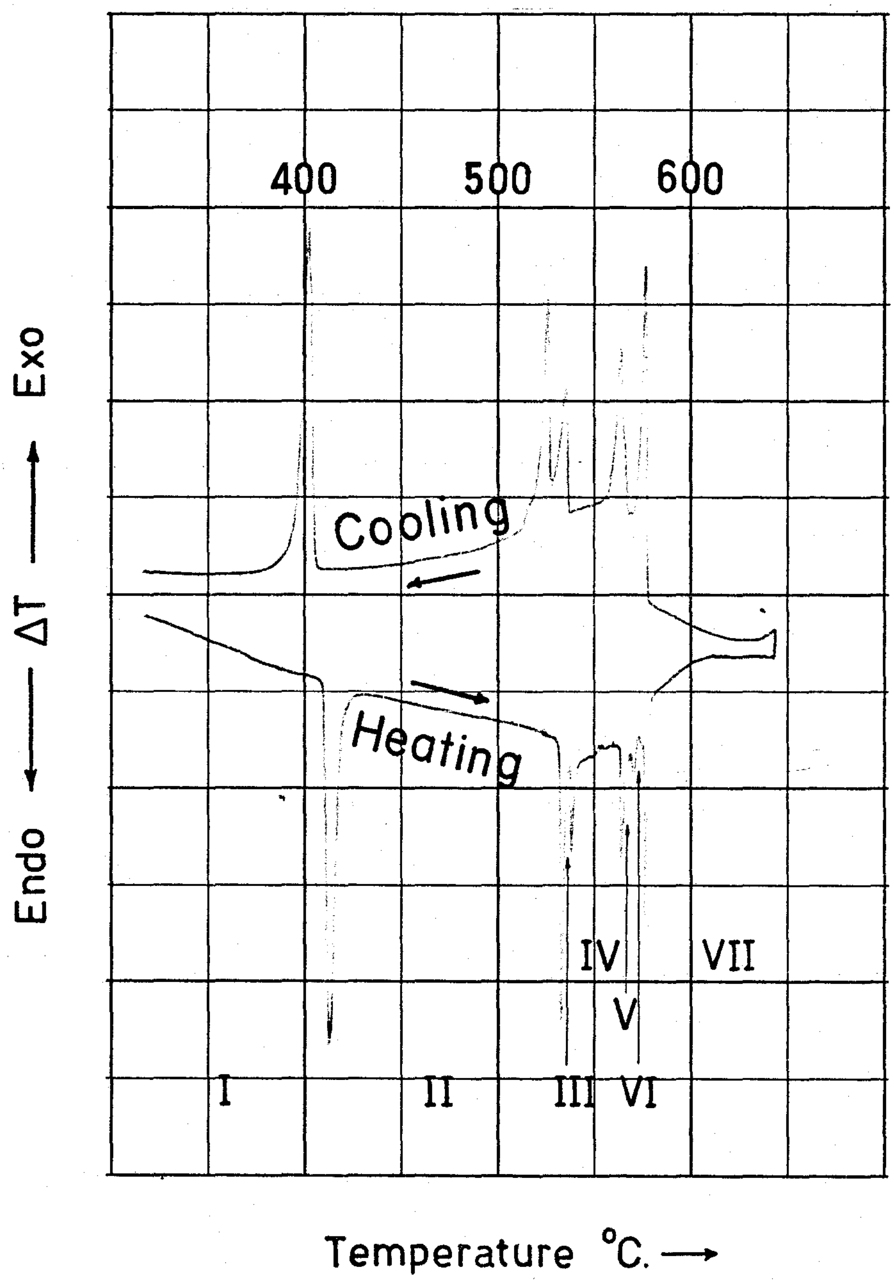

Fig. 4.1.1. Heating and Cooling D.T.A. of $Na_4P_2O_7$. Transition temperatures quoted in text have been corrected from charts supplied by manufacturer.

in Section (4.3).

The next two transformations II-III and III-IV occur at 517° and 522°C. respectively. Since these phases differ in temperature by only 5 degrees and the equipment for the precession camera was not designed to hold temperatures steady within that range, only data of the system in phase IV at the range 535 ± 5°C. were recorded. An attempt was also made to take precession photographs in the range 520 ± 5°C. They showed, in general, orthorhombic symmetry with occasional photographs showing slight deviations favouring a monoclinic system with $\beta = 90^\circ$. (This means that the reflections showed an overall orthorhombic symmetry with only a few reflections having intensities which were visually different from their orthorhombic equivalents.) The extinction conditions were: hkl: $h + k = 2n$; h0l: $l = 2n$; 0k0: $k = 2n$ which satisfied several C-centred space groups including Cc and C2/c. Here in phases III and IV, the c axis is triple that of phase I and this tripling of the axis imposes some limitations to the choice of space groups. (This aspect will be discussed more fully in Section (8.2) of Chapter VIII.) In space group Cc, the best R value in the refinement was 20%. Unfortunately, the refined structure did not show pseudo-C2/c symmetry and thus, this space group, C2/c, will be tested separately.

Around 555 ± 10°C. there were three phases V, VI and VII. Again only reflections of the system past the transition temperature within the phase field were recorded. The intermediate phase VI was very unstable and was nearly obliterated in the cooling process. This might be the reason why it was not detected at all by Kurian and Tamhankar [2] in their D.T.A. studies on the polymorphic transformations of the compound. Phase VII is hexagonal and the c axis becomes once again equal to that of phase I. This phase is highly disordered and refining in space group $P6_3/mmc$, an R value of 10% was obtained using a disordered model. Further evidence of disorder is shown by a rotation of the ab plane about the c axis (Section(4.4)) and by the existence of streaks (Section (4.5)).

4.2. Unit Cell Dimensions of Sodium Pyrophosphate

The rich variety of phases of sodium pyrophosphate can, to a large extent, be attributed to the special relationship between the two shorter axes a and b, and to the special arrangements of the pyrophosphate ions in the unit cell. Here in the room-temperature phase, $a = 9.367$ Å and $b = 5.390$ Å so that the ratio $a:b$ is close to $\sqrt{3}:1$. This special feature, coupled with an angle of 90° between these axes, has some very interesting geometric consequences. As shown in Fig. 4.2.1(a), the hypotenuse PQ is twice b so that the mid-point M of PQ forms an equilateral triangle with R and P. Also, still in the ab plane, it is possible to construct regular figures as shown in Fig. 4.2.1(b). The pyrophosphate and sodium ions seem to take good advantage of these interesting features. They occupy locations which are very close to the special positions, Fig. 4.2.1(c) and (d). This general arrangement

Fig. 4.2.1

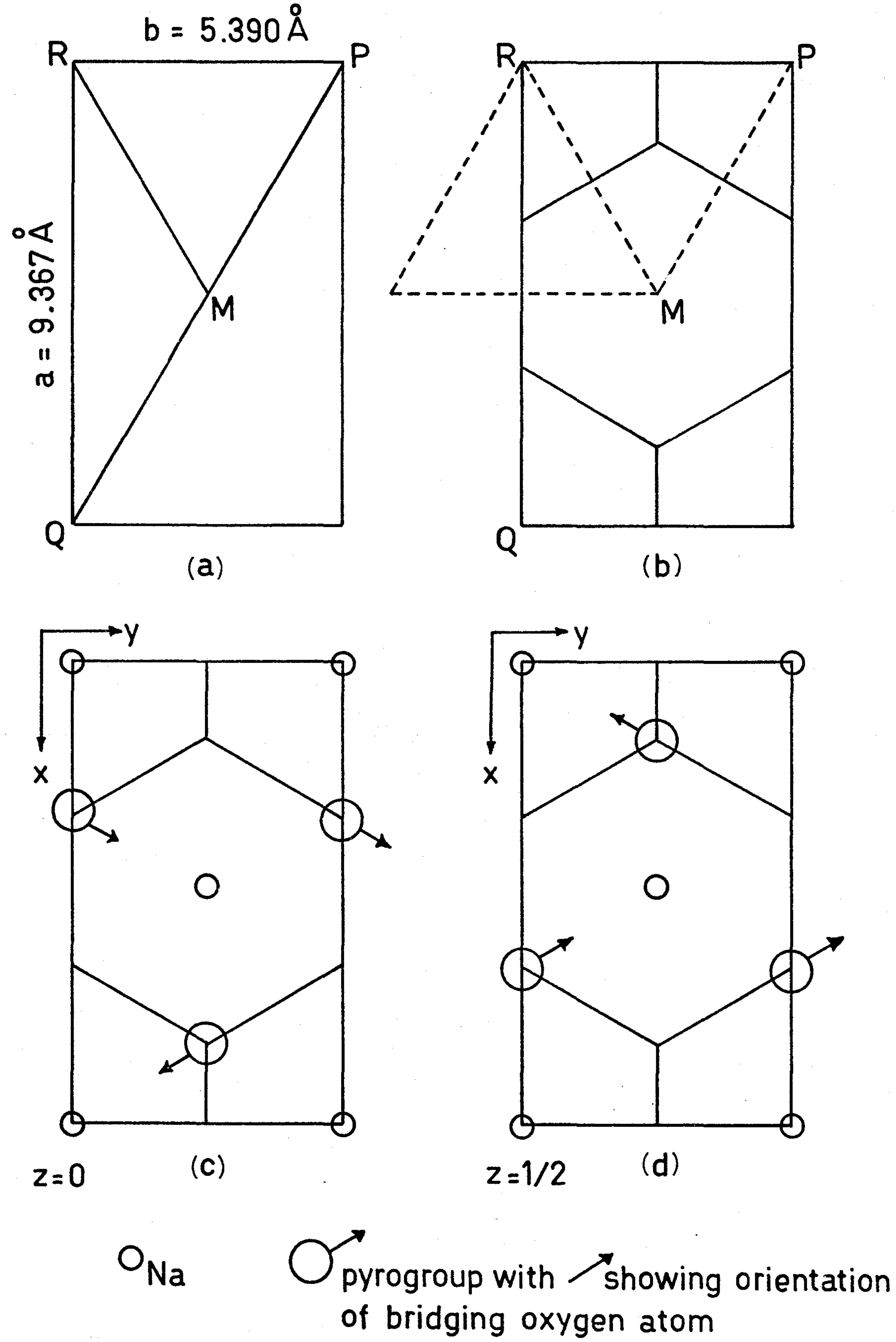
b = 5.390 Å
R
P
a = 9.367 Å
M
Q
(a)
R
P
M
Q
(b)
y
x
z=0
(c)
y
x
z=1/2
(d)
Na
pyrogroup with showing orientation of bridging oxygen atom

persists throughout the various phases. Each new phase results primarily from a change in the orientation of the bridging oxygen atom of the pyrophosphate ion. There are many possible orientations although some cannot co-exist with others in a crystal structure (Cf. Chapter IX).

4.3. "Twinning" of Sodium Pyrophosphate at 405 °C.

When sodium pyrophosphate transforms from phase I to phase II, disorder occurs resulting in what we have termed as a "twinning" phenomenon. Fig. 4.3.1 shows an arrangement of the reflections in the h0l projection. The angle $\underline{a}^*o\underline{c}^*$ is 90°. This pattern persists until the temperature of the crystal is near the transition point from I to II. At this temperature two things could happen. First, the angle $\underline{a}^*o\underline{c}^*$ becomes 87° and the h = odd reflections disappear. Second, a weak pattern which is the image of the new pattern reflected in a mirror perpendicular to $\underline{c}^*$ begins to superimpose on the existing pattern, Fig. 4.3.2. One way to describe the mechanism involved in this phenomenon is to assume that a small portion of the crystal is related to the main portion by a mirror through $\underline{b}^*$ and perpendicular to $\underline{c}^*$. This should not be surprising since the crystal started with an orthorhombic system at room temperature and becomes monoclinic at the transformation. In forming phase II, it is possible that a small portion prefers one orientation to the other, Fig. 4.3.3. This point of view is supported by the fact

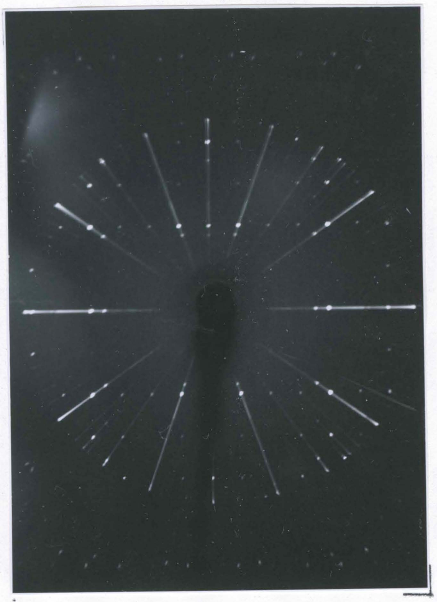

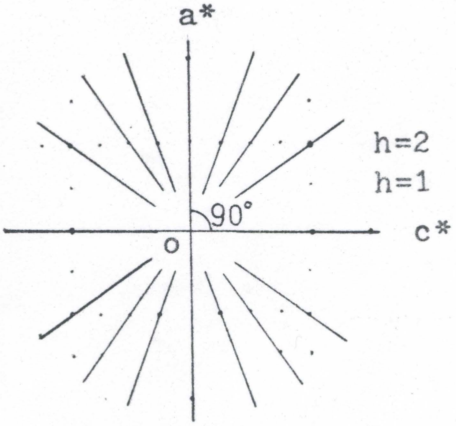

Fig. 4.3.1

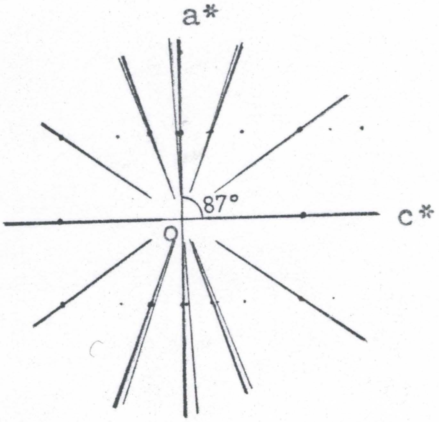

Fig. 4.3.2

Fig. 4.3.3

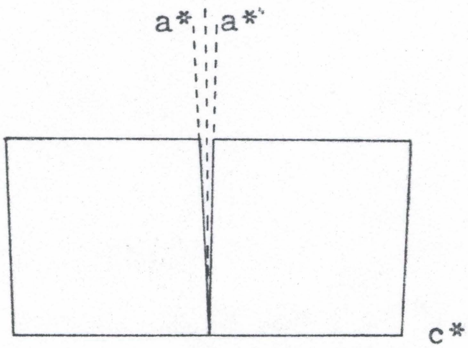

that the intensities of the weak and strong patterns in Fig. 4.3.2 become equal when the crystal is allowed to remain in phase II for a long time and also that it is possible to get little or no "twinning" at all in some cases. In these latter cases, the entire crystal would be oriented in one direction only. Furthermore, there is no observable "twinning" in the 0kl projection and this seems to be in favour of the present description.

The phenomenon of twinning persists until the transition II-III at which the angle $\underline{a}^*o\underline{c}^*$ becomes once again 90°.

4.4. Rotation of the ab Plane about the c Axis

If a crystal of sodium pyrophosphate was aligned with the c axis as the spindle axis on a precession camera, it was found that when the crystal was heated from room temperature to around 600 °C. and then cooled back to room temperature, there was a finite probability of finding a rotation of 60° about the c axis for the ab plane. This was indicated by a rotation of 60° necessary to retrieve the same projection as before the heating. Under normal circumstances this may be surprising; but in the present case it is not. The reason is that at 600 °C. the crystal developed a 6-fold axis parallel to the c axis in a hexagonal system. In this phase, therefore, there could be no distinction between the axes separated by 60°. The crystal simply "forgot" which was the previous a axis and settling down to the room-temperature phase, it might have chosen an axis which was 60° away. This point of view is supported by the fact that it is possible to have no rotation of the ab plane at all in the heating and cooling processes. Unfortunately, this rotation of the ab plane is more or less arbitrary so that this property of the system could not have any foreseeable application.

4.5. Streaks of Sodium Pyrophosphate at 600 °C.

Throughout the various phases of sodium pyrophosphate it is found that the orientation of the bridging oxygen atom in the pyrophosphate ion plays an important role in determining the final structure of the each phase. Because of the apparent ease in going from one orientation to another, "mistakes" are expected, especially in the ab plane where a layer arrangement predominates.

Streaks were observed in the hexagonal phase at a temperature around 600 °C. For projections up the c^* axis, they occurred at reflections where l = odd, and $h - k = 3n$, Fig. 4.5.1. These streaks were directed parallel to the a^* and b^* axes as is evident from the six-sided star formed by the reflections 101, 111, and their equivalents. From an h0l projection, Fig. 4.5.2, it is seen that streaks also occurred in a direction parallel to the c^* axes and at reflections with h = odd only which is consistent with the condition $h-k=3n$ above.

The mechanism for the streaks could be described in terms of the disordered nature of the orientations of the bridging oxygen atoms. Fuller discussions will be given

Fig. 4.5.1. hk1 projection

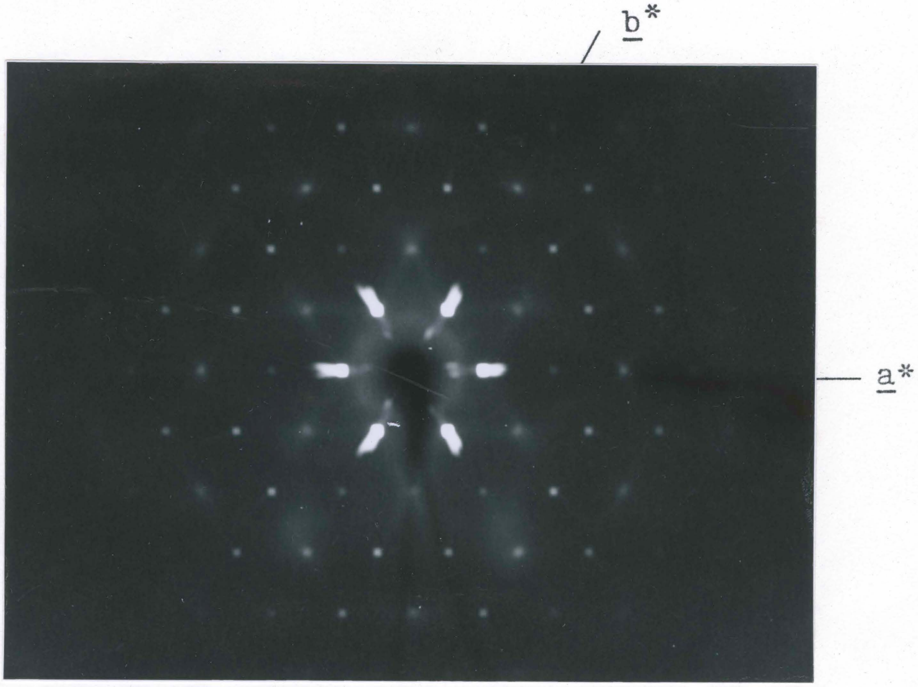

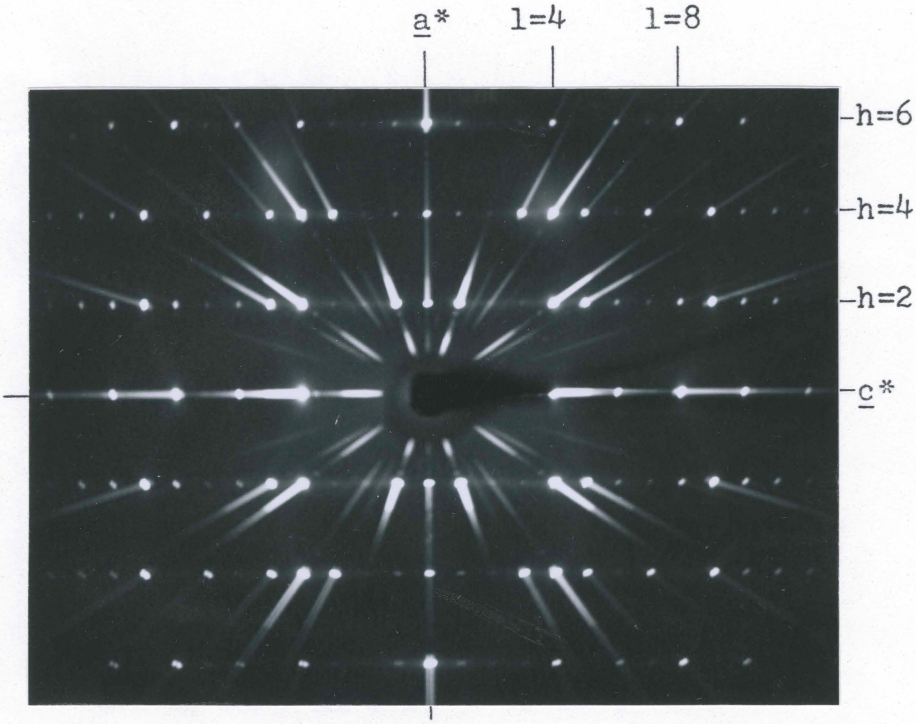

Fig. 4.5.2. h0l projection

in Chapter X where a model for the disorder of sodium pyrophosphate is described.

4.6. Variations of Cell Axes of Sodium Pyrophosphate

The lengths of the axes of the unit cell when measured as a function of temperature, show some interesting features, Figs. 4.6.1 - 3. It was found that both the a and c axes showed points of contraction in the heating process. This was rather unusual and might be considered to have been the result of structural changes within the unit cell. In these curves, peaks and troughs occurred at temperatures close to those observed in a D.T.A. trace for the various phase transformations.

It is of some interest to record here how the measurements were taken. A precession camera was used. The axis whose measurement was required, was aligned along the rotation axis of the camera. A full precession photograph was first taken at room temperature. The exposure time was about one hour. Then the temperature of the crystal was increased by a certain amount, the magnitude of which depended on the changes in the vicinity of that range of temperature. When the temperature was steady, the film holder was propped up about 1 mm. and the exposure for approximately the same time of one hour was taken. This process was repeated 5 or 6 times on the same film, each time with different temperatures. When another film was required to continue the process, the last recording on the previous film was repeated so that a

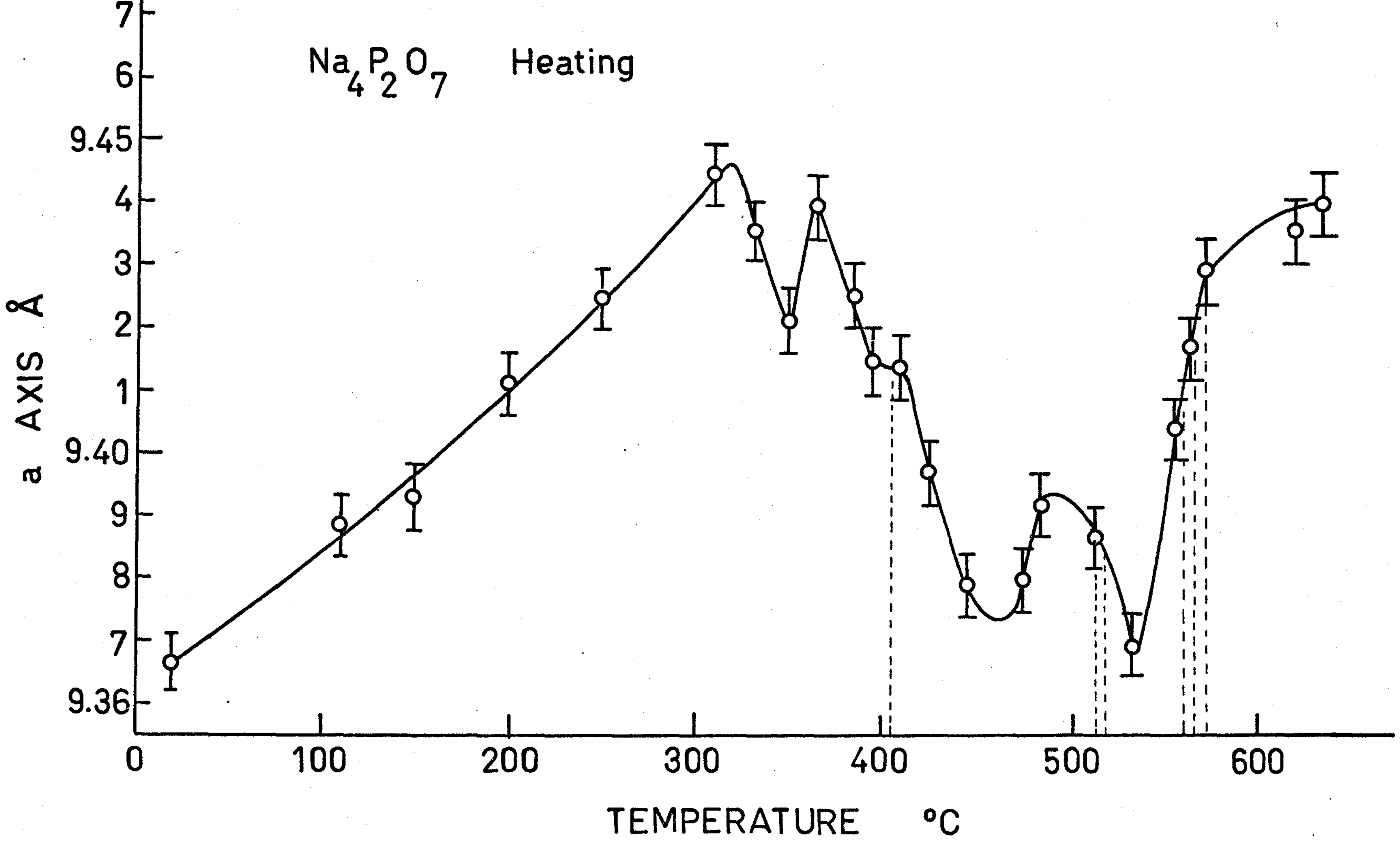

Linear Expansion of the a axis of $Na_4P_2O_7$. Dotted lines denote transition temperatures as detected by D.T.A.

Fig. 4.6.1

Linear Expansion of the b axis of $Na_4P_2O_7$. Dotted lines denote Transition Temperatures as detected by D.T.A.

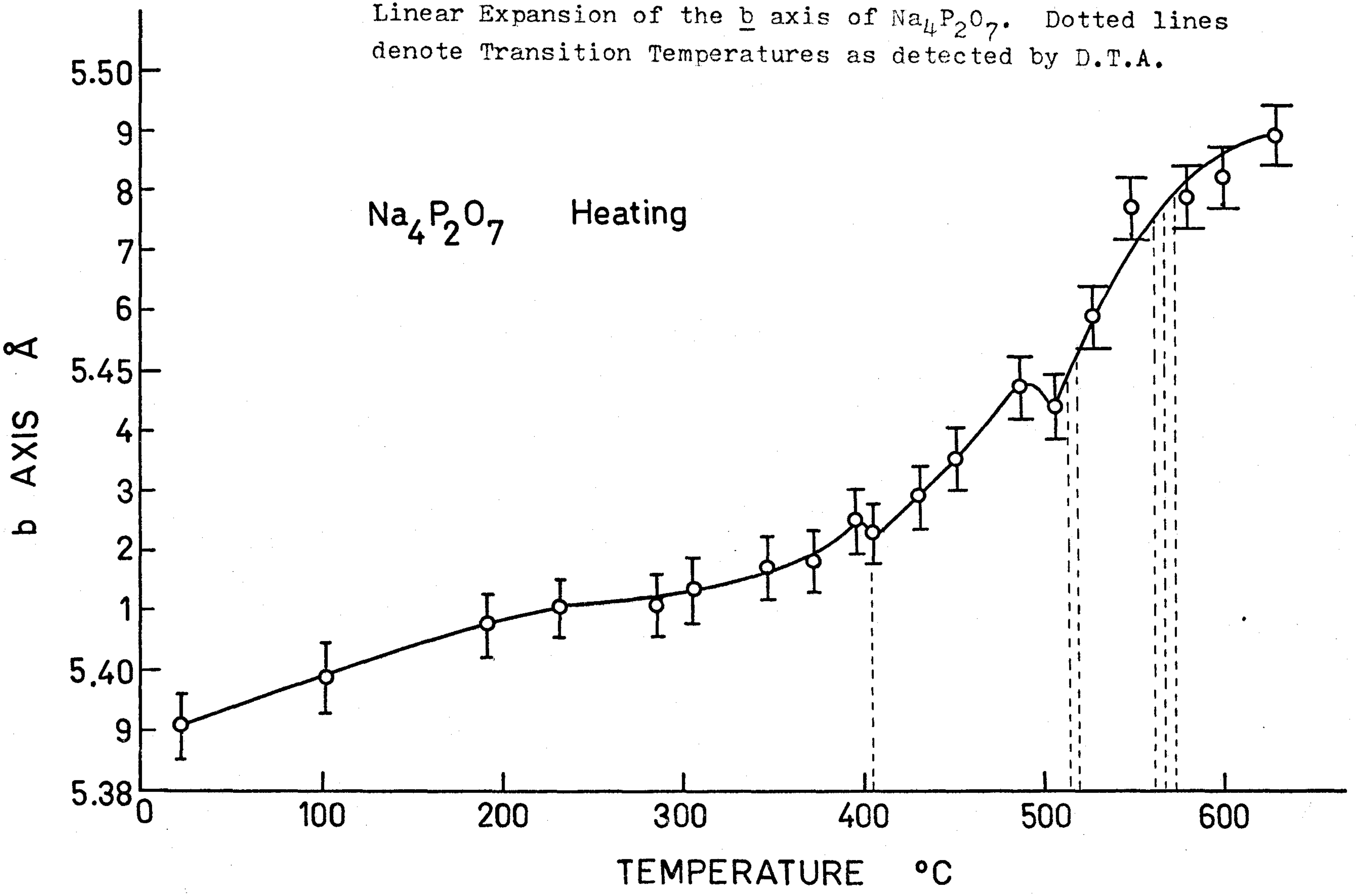

Fig. 4.6.2

Fig. 4.6.3

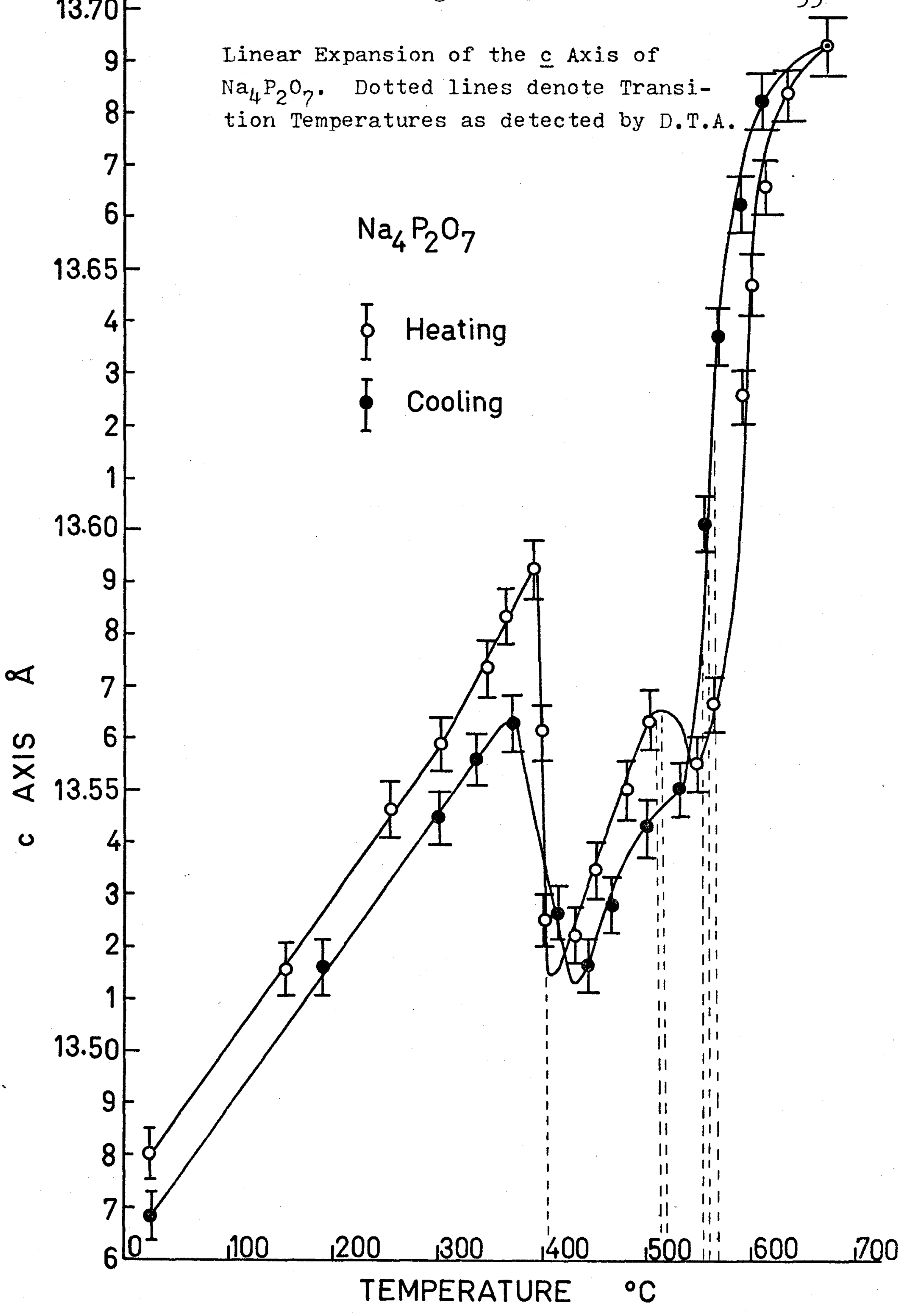

Linear Expansion of the c Axis of $Na_4P_2O_7$. Dotted lines denote Transition Temperatures as detected by D.T.A.

common scale could be established between the films. By so doing, shrinkage variations of the films could be eliminated in the relative values of the lengths of the axes.

The cooling curve was recorded in the same manner as the heating curve by reversing the control of the temperature. There was a contraction of about 0.01 Å of the c axis when it was cooled back to room temperature. It does not seem likely, however, this will go on indefinitely each time the crystal was heated and cooled because otherwise the crystal would become smaller and smaller. Rather, we would expect the contraction to relax back to its original value when allowed to stand by itself over a certain period of time, a process which might be similar to that observed in sodium diarsenate (Section 4.7 below).

4.7. The Phase Transformations of Sodium Diarsenate

Like sodium pyrophosphate, sodium diarsenate exhibits a series of phase transformations as detected by D.T.A. A trace of the transformations is shown in Fig. 4.7.1. However, unlike sodium pyrophosphate, the first few transformations of sodium diarsenate are not very prominent and they do not correspond to any symmetry change detectable with a precession camera. Furthermore, they are not immediately reversible; the crystal tends to retain its high-temperature phase for a certain period of time even though its temperature is returned to ambient. It is only after being left at the room temperature for a week or so that the crystal fully recovers its

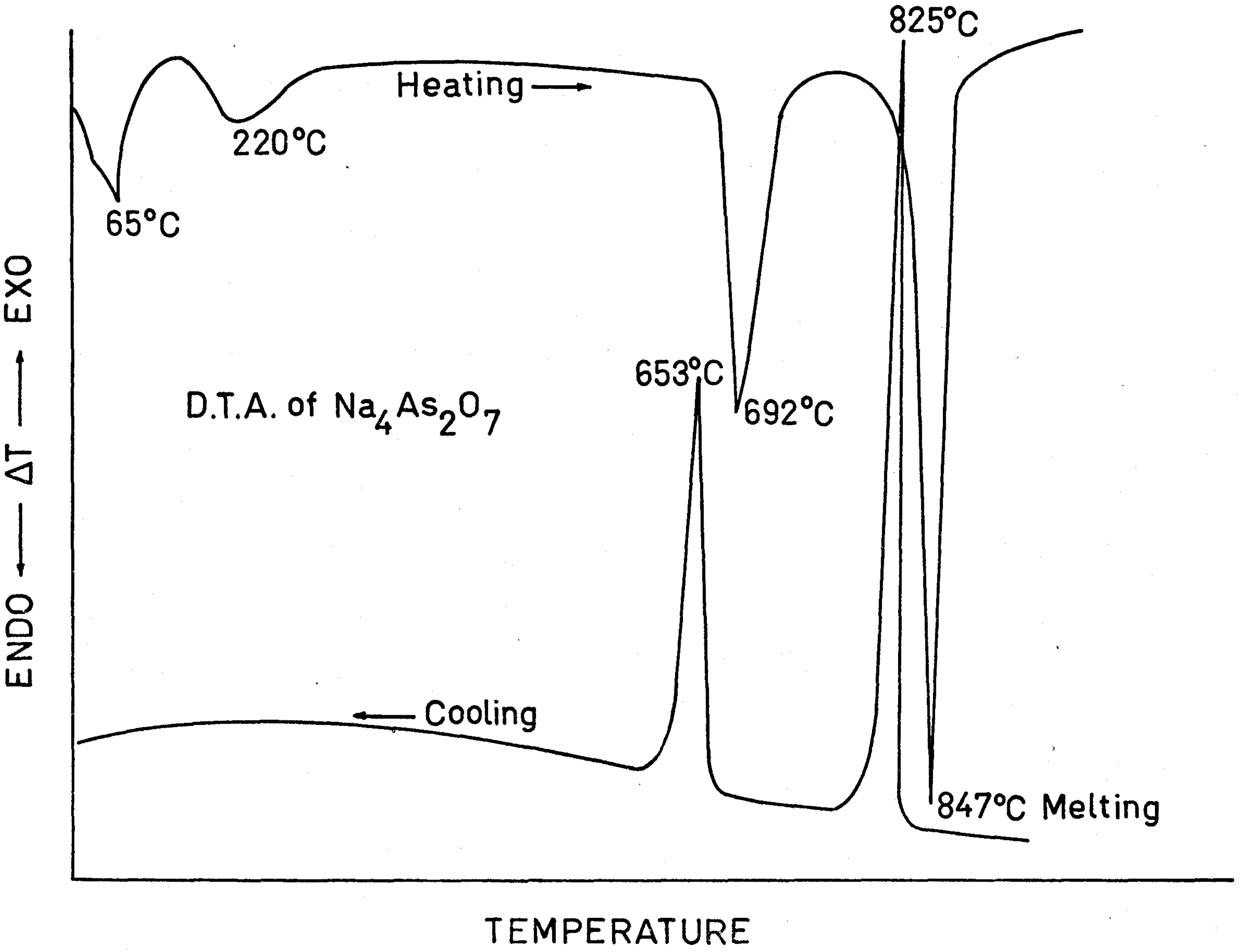

Fig. 4.7.1. D.T.A. Traces of $Na_4As_2O_7$. Note the disappearance of the minor transformations in the Cooling process.

normal ambient phase. The reversibility of the system as a function of time was studied and the result is shown in Fig. 4.7.2.

The major transformation occurring at 692 °C. is one in which the crystal invariably cracks. Consequently, in the present investigation, only the structure of sodium diarsenate at room temperature was studied.

Fig. 4.7.2. D.T.A. Heating Traces of $Na_4As_2O_7$

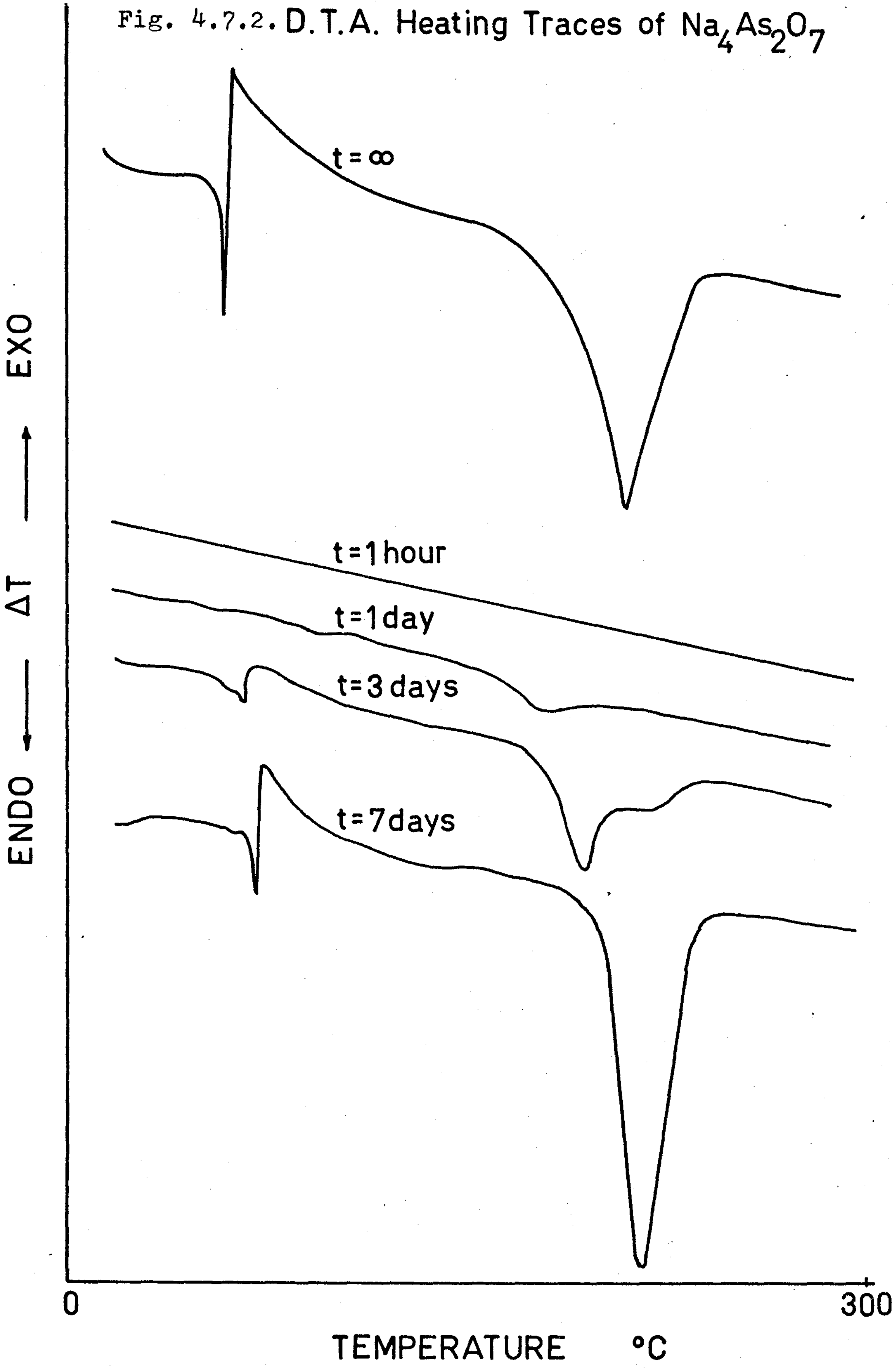

CHAPTER V

CRYSTAL STRUCTURE OF $Na_4P_2O_7$ AT 22°C.

SUMMARY

At room temperature sodium pyrophosphate, $Na_4P_2O_7$, crystallizes in the orthorhombic space group $P2_12_12_1$ with $\underline{a} = 9.367(5)$, $\underline{b} = 5.390(2)$, $\underline{c} = 13.480(8)$ Å and z = 4. The structure was solved initially by direct methods based on 493 unique reflections from films, to an R value of 10%, and then refined by full-matrix least-squares using 1337 reflections measured with a Syntex automatic diffractometer. The final R value is 0.022. The pyrophosphate anion has a configuration intermediate between staggered and eclipsed with a P-O-P angle of 127.5(1)°. The two bridging P-O bond lengths are 1.631(2) and 1.642(2) Å with terminal P-O bond lengths averages of 1.512 and 1.514 Å on either side of the anion. Two of the four sodium ions are coordinated to five oxygen atoms while the remainder are coordinated to six oxygen atoms. These are surrounded by six anions with the bridging oxygen atoms lying approximately at the corners of an octahedron with the P-P vector of the anion also paralleling the c axis. Adjacent anions along the c axis are separated by a pair of sodium ions.

5.1. Introduction

Although a large number of crystallographic studies have been devoted towards elucidating the phases and phase transformations of $M_2X_2O_7$ and MX_2O_7 systems where the X ions such as P, As and V, are tetrahedrally coordinated, sharing a common bridging oxygen atom, the $M_4X_2O_7$ system has largely been ignored. Various members of this series show phase transformations, for example: $Li_4P_2O_7$ [25], $Li_4As_2O_7$ [5], $Na_4As_2O_7$ and $Na_4P_2O_7$. However, $Na_4P_2O_7$ with six transformations as determined by D.T.A. [1], thermal expansion [26], and recent crystallographic studies [27] seems to be the most complex.

5.2. Crystal Data

Formula: $Na_4P_2O_7$ Formula Weight: 265.95

Crystal System: Orthorhombic;

$\underline{a} = 9.367(5)$, $\underline{b} = 5.390(2)$, $\underline{c} = 13.480(8)$ Å

Volume of Unit Cell: 679.33 $Å^3$

No. of Molecules/Unit Cell: $z = 4$

Specific Gravity: $\rho_{cal.} = 2.59$, $\rho_{obs.} = 2.53$

Systematic Extinctions: h00, 0k0 and 00l with h, k, l odd respectively

Space Group: $P2_12_12_1$

Wavelength of radiation used: $MoK_{\alpha_1} = 0.70926$ Å

5.3. Preparation of the Sample

The preparation of anhydrous sodium pyrophosphate required no special techniques. Chemically pure sodium pyrophosphate decahydrate ($Na_4P_2O_7.10H_2O$) was heated in a platinum crucible above its melting point and maintained at about 1000 °C. for several hours. The melt was then cooled at the rate of 10 °C. per hour to 500 °C. when the power of the furnace was shut off and the system allowed to cool to room temperature. (The cut-off temperature of 500 °C. is simply the minimum temperature of the furnace; it is not critical.) Good quality crystals of anhydrous sodium pyrophosphate suitable for X-ray work could be obtained. The crystals varied from colourless to pale blue-green depending upon the run, and often occurred in the form of flakes. Several well-shaped crystals were selected and the dimensions varied from 0.1 to 0.3 mm. These crystals were mounted as they were without being ground to a sphere because their natural cleavages made alignment along a particular direction easier for the precession camera. Spheres of diameters about 0.2 mm. were also obtained and these were used later on the Syntex $P\bar{1}$ automatic diffractometer in the collection of a more accurate data set.

5.4. Data Collection

Preliminary photographs using a precession camera were obtained to determine the space group of the crystal. Systematic extinctions along h, k, and l indicated unambiguously that the space group was $P2_12_12_1$. Initial cell dimensions were measured from the photographs. Nine layers of reflections along the three crystallographic axes were obtained using the precession camera. The intensities of these reflections were measured with a microdensitometer. After correcting for polarization and Lorentz factor, the intensities were scaled to a common level by making use of the common reflections among the layers. A total of 493 unique reflections were obtained. This data set was used to obtain a trial structure by direct methods.

A second data set, consisting of 1337 symmetry independent reflections was recorded utilizing the Syntex automatic diffractometer. The crystal used was a sphere of radius 0.25 mm. and the peaks were scanned in a $\theta/2\theta$ mode at a variable rate from 2° to 24° per minute depending upon the peak intensity. Data were recorded up to a sin θ/λ of 0.77 Å^{-1}. Backgrounds were measured at either side of the peak for the same period of time as the peak scan. Reflections whose intensity, corrected for background, exceeded 3σ[*] were considered observed. The remaining reflections were assigned a maximum possible value of 3σ. The data were corrected for absorption, Lorentz and polarization effects. The unit cell parameters were also refined using a program supplied with the diffractometer system of programs.

---

[*] σ is defined as $\sqrt{\sigma_I^2 + \frac{1}{2}(\sigma_1^2 + \sigma_2^2)}$ where $\sigma_I = (n_1+n_2)$ x scan rate with n_1 and n_2 being the front and rear background counts and σ_1 and σ_2 are the standard deviations of n_1 and n_2 determined by counting statistics.

5.5. Structure Determination

The set of 493 unique reflections obtained from films was used to construct a Patterson map. There was a predominantly strong peak along the c axis at a distance of about 3.2 Å from the origin. Experience suggested it was reasonable to assume that this peak was due to the P-P vectors of the pyrophosphate ions. However, an estimation of the relative magnitude of the peak showed that there were other contributions as well. The real difficulty came when the effects of symmetry were introduced in the interpretation of the map. The locations of the strong peaks offered so many alternatives that it soon became impracticable to try out all the possibilities. After many fruitless attempts, the Patterson approach was abandoned and direct methods were adopted.

The apparent failure of the Patterson method in this case, as pointed out in Section (3.9), was due to the special arrangement of the atoms in the unit cell. After the trial structure was obtained by direct methods, the situation was clear. It was found that many of the atoms gave rise to vectors of about 3.2 Å parallel to the c axis in addition to the P-P vectors of the pyrophosphate ions. Worse still, all the atoms are of comparable atomic weights (Phosphorus 15, Sodium 11, Oxygen 8) and this made identification of the peaks extremely difficult.

In Sections (3.11) and (3.12), the actual procedures carried out in the direct methods were fully described. After an R value of 10% was obtained with the 493 unique film reflections, a new set of data was obtained with the automatic diffractometer as described in Section (5.4). It was with this latter set that the final refinements of the structure were carried out. As initial parameters, the final coordinates obtained with the film data were used. They were refined by full-matrix least-squares using a program written by J.S. Stephens for the computer CDC 6400. Atomic scattering factors for Na^+, P^{3+} and O^{--} were taken from the International Tables for X-Ray Crystallography [28]. Unit weights were chosen since there seemed to be no systematic variation in $|F_o - F_c|$ with F_o. When a minimum had been obtained with isotropic temperature factors, the refinement was completed with individual anisotropic thermal parameters. The final R value, determined when the shift was less than 0.2σ was 0.022. The final atomic parameters are found in TABLE V.1 and the observed and calculated structure factors in TABLE V.2. Sixteen reflections too strong to be measured with the diffractometer were included in TABLE V.2 with their film measured values, but they had been excluded from the refinement. A final difference electron density map showed no residual peaks larger than 0.1 of an oxygen atom peak and the refinement was considered complete. There was no systematic variation of $|F_o - F_c|$ with $\sin \theta/\lambda$ either.

TABLE V.1. Atomic and Thermal Parameters of $Na_4P_2O_7$ with Estimated Standard Deviations in Parentheses

Atom	x	y	z	U_{11}^{*}	U_{22}	U_{33}	U_{12}	U_{13}	U_{23}
Na(1)	0.4725(1)	0.4992(2)	-0.01678(7)	0.0146(4)	0.0144(4)	0.01591(4)	0.0009(5)	-0.0006(3)	0.0008(4)
Na(2)	0.4919(1)	0.4848(2)	0.23603(7)	0.0197(5)	0.0193(5)	0.0180(4)	-0.0034(5)	0.0059(4)	-0.0019(5)
Na(3)	0.1221(1)	0.4961(2)	0.15454(7)	0.0165(5)	0.0198(5)	0.0179(4)	0.0006(5)	0.0023(3)	-0.0020(5)
Na(4)	0.6654(1)	-0.0368(2)	0.16744(8)	0.0161(5)	0.0161(5)	0.0210(4)	-0.0013(4)	0.0008(4)	-0.0006(4)
P(A)	0.30704(6)	0.0113(1)	-0.10609(4)	0.0088(2)	0.0091(2)	0.0082(2)	-0.0001(2)	-0.0001(2)	0.0001(2)
P(B)	0.31380(6)	-0.0223(1)	0.11128(4)	0.0090(2)	0.0100(2)	0.0083(2)	-0.0006(2)	0.0006(2)	0.0000(2)
O(CE)	0.3602(2)	0.0971(3)	0.0040(1)	0.0152(8)	0.0140(7)	0.0081(6)	-0.0051(6)	0.0002(5)	0.0000(6)
O(A1)	0.3444(2)	0.2338(3)	-0.1693(1)	0.025(6)	0.0119(7)	0.0132(7)	0.0005(6)	0.0004(6)	0.0052(6)
O(A2)	0.3953(2)	-0.2131(3)	-0.1339(1)	0.0179(9)	0.0119(7)	0.0140(7)	0.0055(7)	0.0019(6)	-0.0018(6)
O(A3)	0.1490(2)	-0.0447(4)	-0.1019(1)	0.0087(8)	0.0275(10)	0.0152(7)	-0.0019(7)	-0.0006(5)	-0.0043(8)
O(B1)	0.4264(2)	0.0803(4)	0.1805(1)	0.0122(8)	0.0241(9)	0.0115(7)	-0.0027(7)	-0.0035(5)	-0.0028(7)
O(B2)	0.3205(2)	-0.3017(3)	0.1009(4)	0.0205(9)	0.0093(7)	0.0206(8)	-0.0009(7)	0.0063(7)	0.0001(6)
O(B3)	0.1654(2)	0.0744(4)	0.1333(1)	0.0110(8)	0.0191(8)	0.0149(7)	0.0018(6)	0.0032(5)	-0.0023(6)

* U_{ij}'s in $\mathring{A}^2$ are computed from $\beta_{ij}=2\pi^2 \underline{b}_i \cdot \underline{b}_j U_{ij}$ where $T=\exp\{-[\beta_{11}h^2 + 2\beta_{12}hk + \ldots]\}$ appears in the structure factor expression and $\underline{b}_j$ are reciprocal lattice cell vectors.

TABLE V.2

TABLE OF OBSERVED REFLECTIONS OF NA4P2O7 AT 29 DEGREES C.   UNOBSERVED REFLECTIONS ARE MARKED WITH * AND UNRELIABLE REFLECTIONS WITH * .

```
              FOBS FCAL                  FOBS FCAL

 K    L        H =   0          5    5     287  288
                                5    6      44   46
 0    6      206  262           5    7      40   47
 0   10      203  201           5    8      82   78
 0   12      149  153           5    9     137  137
 0   14      260  258           5   10      54   53
 0   16       26   26           5   11      26   25
 0   18      149  200           5   12      85   85
 1    3       34   34           5   13     140  142
 1    4      119  129           5   14 *     5   20
 1    6      131  132           6    1      31   28
 1    7       47   44           6    2      40   42
 1    8      302  300           6    3      32   33
 1    9      101   99           6    5      36   33
 1   10        9    7           6    6      36   38
 1   11       48   49           6    7      43   42
 1   12      151  153           6    8      89   89
 1   13       68   48           6    9 *     4   18
 1   14       81   78           6   10      22   23
 1   16       71   73           6   11      61   59
 1   17       41   42           7    0      24   25
 1   18      135  135           7    1      47   49
 2    1      104  101           7    2      62   61
 2    2       18   15           7    3      66   65
 2    3      138  134           7    4     131  133
 2    4      138  134           7    5     129  128
 2    5       63   64           7    6      87   89
 2    6       16   12           7    7      52   54
 2    7       28   16
 2    8      322  320           K    L       H =   2
```

5.6. Description of the Structure

The structure of anhydrous sodium pyrophosphate can be described as a deviant from a simple idealized structure shown in Fig. 5.6.1. This ideal structure consists of diphosphate ions formed by a pair of PO_4^{3-} groups sharing a bridging oxygen atom with a P-O-P angle of 180°. The oxygen atoms of the anion are in an eclipsed configuration as viewed down the P-P vector, with this vector parallel the c axis. These anions lie in layers such that the bridging oxygen atoms lie at the corners of an octahedron elongated parallel to the c axis with adjacent layers related by a 6_3 axis, Fig. 5.6.2. Chains of Na^+ ions coincide with the 6_3 axis with Na(1) coplanar with the bridging oxygen atoms and Na(2) lying in an octahedral site between layers formed by the terminal oxygen atoms of six separate anions. The terminal oxygen atoms are coplanar with a plane perpendicular to the 6_3 axis. Two additional Na^+ ions per formula unit, Na(3) and Na(4) are collinear with the P-P vectors separating the pyrophosphate groups in adjacent cells along the c axis.

Na(1) in this idealized structure has a coordination number of nine as a result of sharing the bridging oxygen atom and one terminal oxygen atom from each end of three pyrophosphate groups. This configuration, with the bridging oxygen atom lying $b\sqrt{3}$ Å from three Na(1) ions, is unstable relative to a bent anion where the Na(1) ion forms a strong bond with only one bridging oxygen atom. It is of interest that an

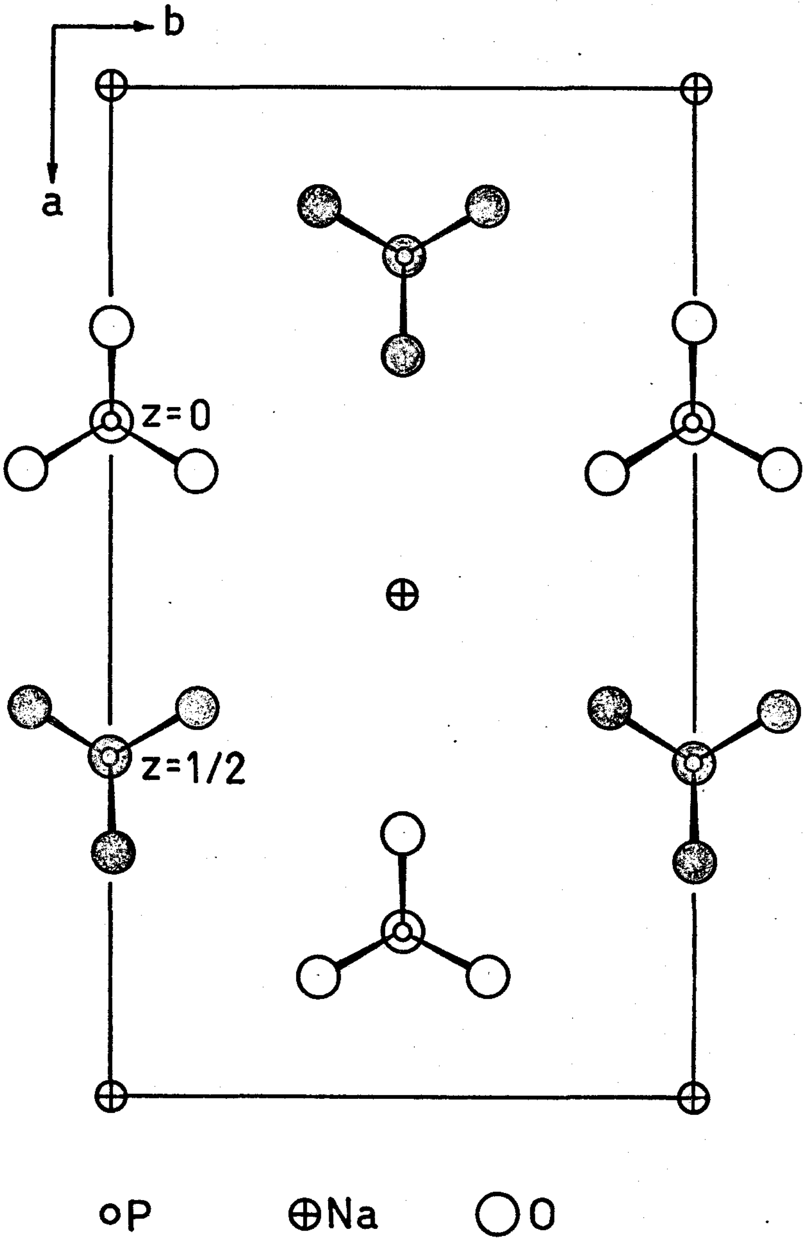

Fig. 5.6.1. The idealized structure of $Na_4P_2O_7$ projected onto the ab plane.

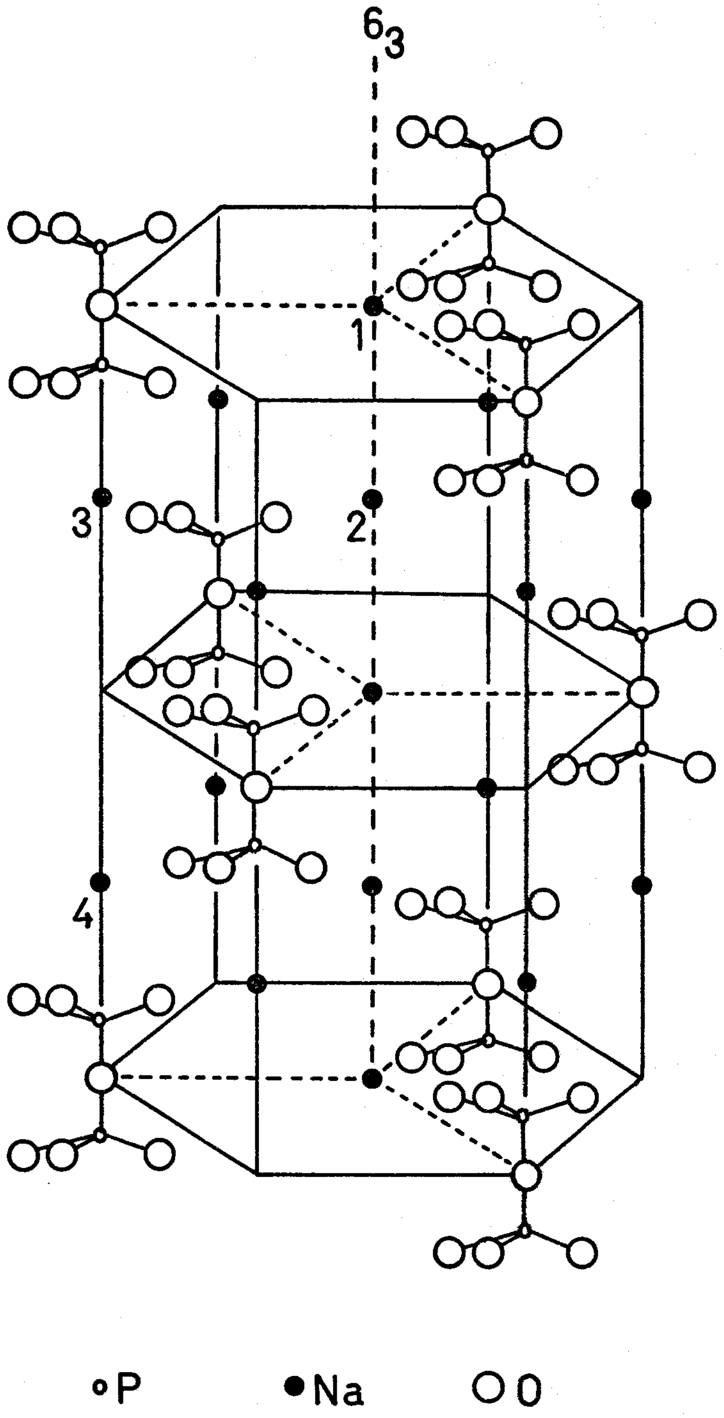

Fig. 5.6.2. The idealized structure of $Na_4P_2O_7$ in 3-Dimensions.

infinite number of configurations are possible for an infinite layer where the only constraint is that each Na(1) is bonded to one and only one bridging oxygen atom, and vice versa. If further constraints of translational periodicity corresponding to the determined a and b axes are imposed, three configurations are possible. The arrangement shown in Fig. 5.6.3(a) is found in the present structure while that in Fig. 5.6.3(b) is found in the structure at 410°C. (Chapter VII). The configuration seen in Fig. 5.6.3(c), consistent with both a 2_1 axis and a C-centering in a layer, may occur for some of the layers in the structure near 500°C.

In the actual structure, the pyrophosphate ion bends at the bridging oxygen atom, and the plane of terminal oxygen atoms no longer coincides with the ab plane. In addition, the two ends of the anion twist slightly destroying the eclipsed configuration and the anion rotates as a whole so that the P-P vector is no longer collinear with the c axis. However, as can be seen in Fig. 5.6.4 the gross features of the idealized model remain in the structure. These distortions lead to coordination numbers of five for Na(3) and Na(4) rather than three as expected from the idealized model.

Na(1) shares two oxygen atoms with three pyrophosphate ions and shows bond lengths ranging from 2.313(2) to 2.777(2) Å, TABLE V.3. As predicted this ion shares oxygen atoms from either end of two anions and shares an edge with one of the tetrahedra of a third anion. One of the oxygen atoms in this

Schematic representations of possible arrangements of bent anions. The arrows indicate the direction of the displacements of the bridging oxygen atoms.

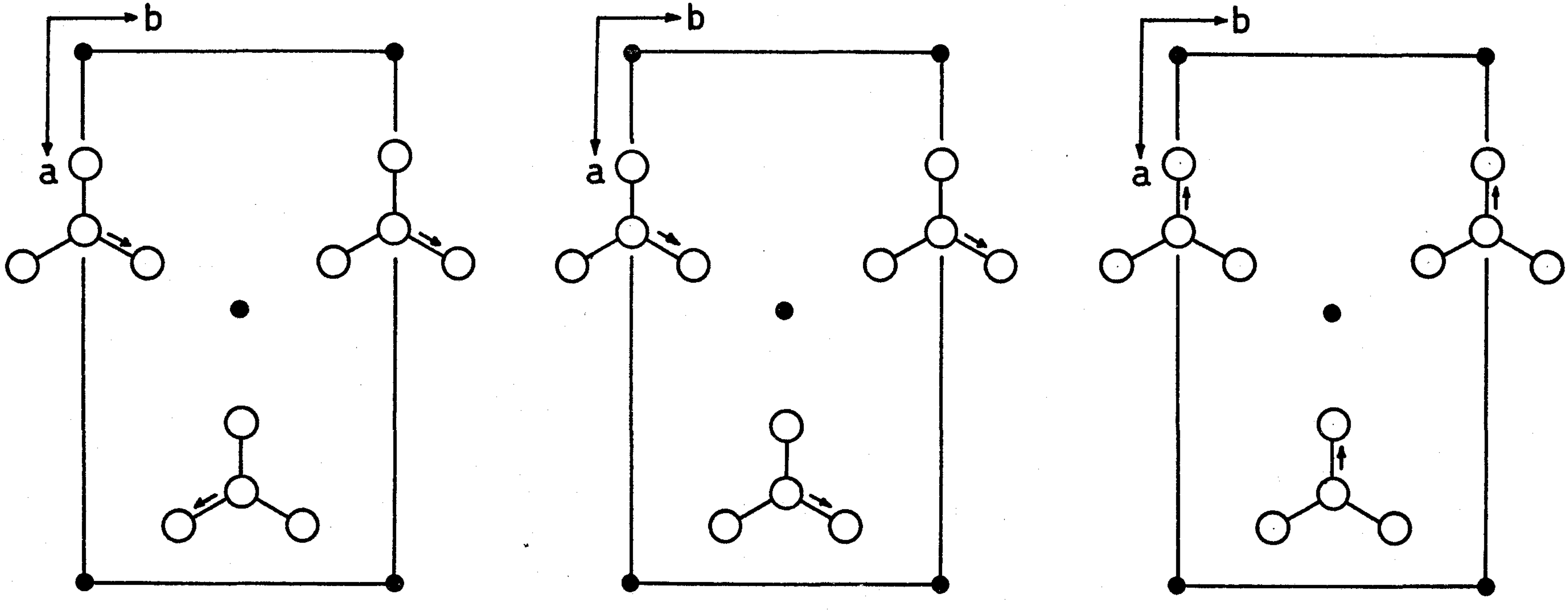

(a) (b) (c)

Fig. 5.6.3

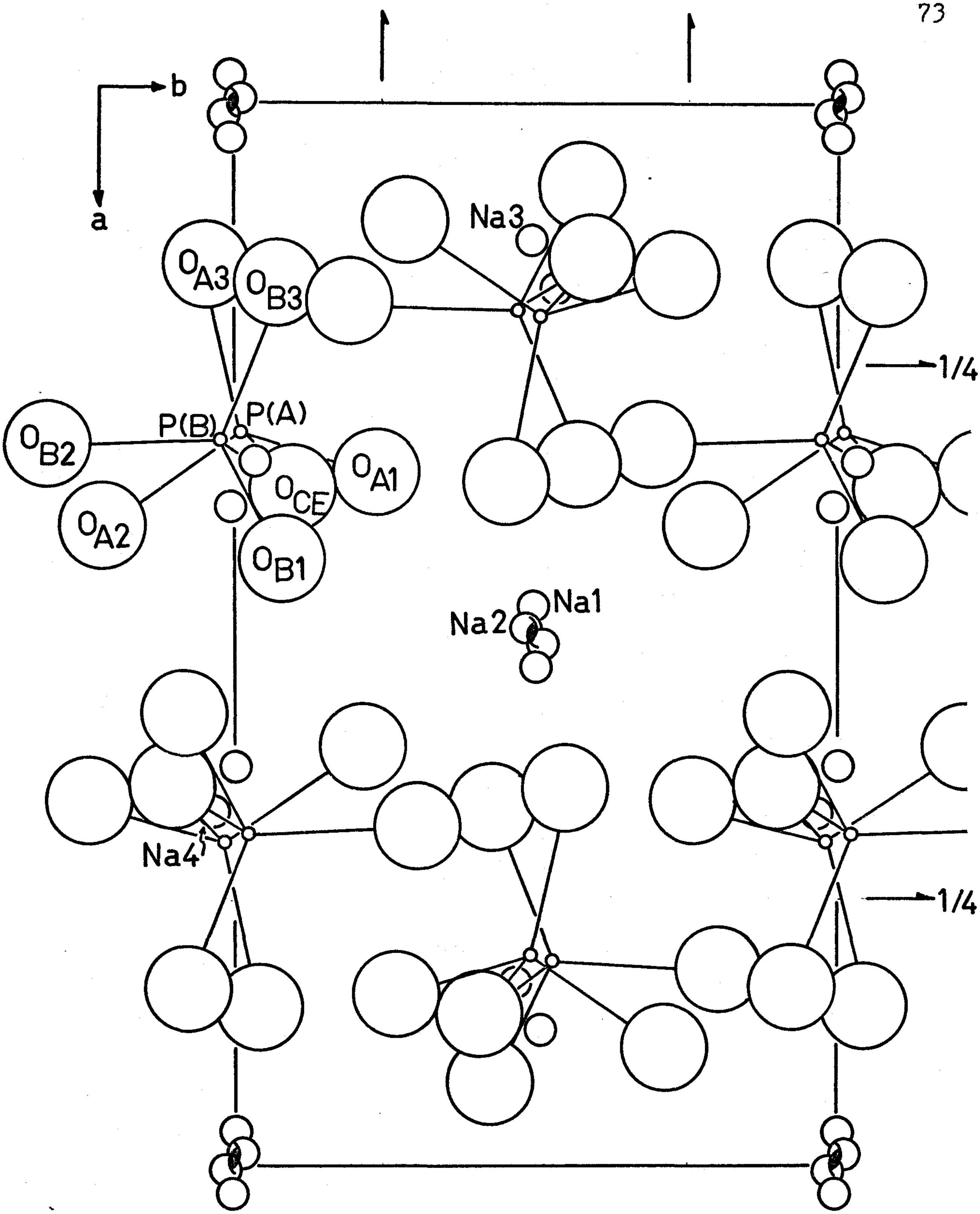

$Na_4P_2O_7$ 22°C.

Fig. 5.6.4

The structure of $Na_4P_2O_7$ projected onto the a b plane

Fig. 5.6.5

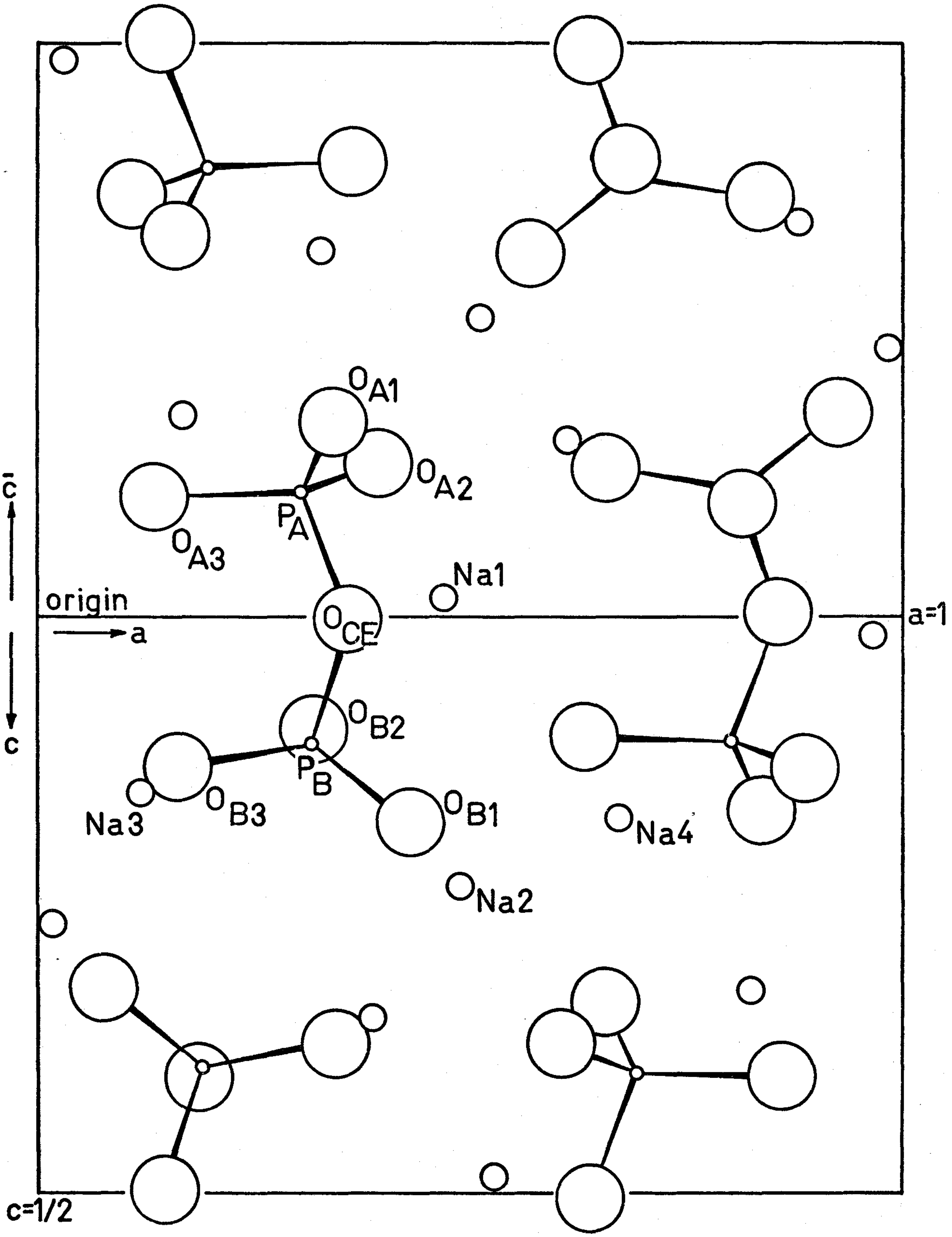

The structure of $Na_4P_2O_7$ projected onto the ac plane

TABLE V.3

Bond Distances and Angles in $Na_4P_2O_7$ at 22 °C.

Distance*	(Å)	Angle	(°)	Angle	(°)
P(A)-O(CE)	1.631(2)	O(CE)-P(A)-O(A3a)	108.8(1)	O(A3a)-P(A)-O(A2a)	112.6(1)
-O(A3a)	1.512(2)	-O(A2a)	106.6(1)	-O(A1a)	113.9(1)
-O(A2a)	1.512(2)	-O(A1a)	102.5(1)	O(A2a)-P(A)-O(A1a)	111.6(1)
-O(A1a)	1.512(2)				
P(B)-O(CE)	1.642(2)	O(CE)-P(B)-O(B2a)	107.3(1)	O(B2a)-P(B)-O(B1a)	113.1(1)
-O(B2a)	1.514(2)	-O(B1a)	102.4(1)	-O(B3a)	113.5(1)
-O(B1a)	1.513(2)	-O(B3a)	106.4(1)	O(B1a)-P(B)-O(B3a)	113.2(1)
-O(B3a)	1.514(2)				
P(A)-P(B)	2.936(1)	P(A)-O(CE)-P(B)	127.5(1)		
Na(1)-O(CE)	2.426(2)	O(CE)-Na(1)-O(A1a)	55.78(5)	O(A1a)-Na(1)-O(A2a)	72.95(6)
-O(A1a)	2.777(2)	-O(A2a)	122.57(7)	-O(B2a)	117.77(7)
-O(A2a)	2.329(2)	-O(B2a)	93.79(6)	-O(B3b)	76.02(6)
-O(B2a)	2.387(2)	-O(B3b)	104.59(7)	-O(A3b)	151.08(7)
-O(B3b)	2.427(2)	-O(A3b)	108.98(7)	O(A2a)-Na(1)-O(B2a)	88.04(7)
-O(A3b)	2.313(2)	O(B2a)-Na(1)-O(B3b)	161.42(8)	-O(B3b)	84.33(7)
		-O(A3b)	85.36(7)	-O(A3b)	128.34(8)
				O(B3b)-Na(1)-O(A3b)	86.15(6)
Na(2)-O(B1a)	2.386(2)	O(B1a)-Na(2)-O(B2a)	91.43(6)	O(B2a)-Na(2)-O(B3a)	92.60(7)
-O(B2a)	2.687(2)	-O(B3a)	105.19(7)	-O(A2c)	166.47(7)
-O(B3a)	2.347(2)	-O(A2c)	78.17(6)	-O(A3b)	78.12(6)
-O(A2c)	2.517(2)	-O(A3b)	92.59(7)	-O(A1c)	116.83(7)
-O(A3b)	2.353(2)	-O(A1c)	150.52(8)	O(B3a)-Na(2)-O(A2c)	81.99(6)
-O(A1c)	2.506(2)	O(A2c)-Na(2)-O(A3b)	110.63(7)	-O(A3b)	160.22(9)
		-O(A1c)	74.97(6)	-O(A1c)	82.96(7)
				O(A3b)-Na(2)-O(A3c)	85.73(7)

(Continued)

TABLE V.3 (Continued)

Distance*	(Å)	Angle	(°)	Angle	(°)
Na(3)-O(A1b)	2.888(2)	O(A1b)-Na(3)-O(B3a)	75.30(6)	O(B3a)-Na(3)-O(A2b)	127.29(7)
-O(B3a)	2.327(2)	-O(A2b)	55.23(6)	-O(B2a)	106.67(7)
-O(A2b)	2.441(2)	-O(B2a)	164.63(7)	-O(B1d)	110.11(7)
-O(B2a)	2.272(2)	-O(B1d)	80.86(6)	O(A2b)-Na(3)-O(B2a)	116.47(7)
-O(B1d)	2.315(2)	O(B2a)-Na(3)-O(B1d)	111.84(7)	-O(B1d)	81.08(6)
Na(4)-O(B1a)	2.333(2)	O(B1a)-Na(4)-O(A3b)	102.60(7)	O(A3b)-Na(4)-O(A2b)	60.23(6)
-O(A3b)	2.428(2)	-O(A2b)	162.83(8)	-O(A1b)	134.22(7)
-O(A2b)	2.580(2)	-O(A1b)	119.87(8)	-O(A1c)	85.50(6)
-O(A1b)	2.341(2)	-O(A1c)	90.78(7)	O(A2b)-Na(4)-O(A1b)	76.61(6)
-O(A1c)	2.445(2)	O(A1b)-Na(4)-O(A1c)	108.67(7)	-O(A1c)	87.82(6)

Tranformations: $a = x, y, z$

$b = \frac{1}{2}+x, \frac{1}{2}-y, \bar{z}$

$c = \bar{x}, \bar{y}, \frac{1}{2}+z$

$d = \frac{1}{2}-x, \frac{1}{2}+y, \frac{1}{2}-z$

* Includes all interactions less than 3.0 Å except a P(A)-Na(4) interaction of 2.998 Å

edge is a bridging oxygen atom. The second cation, Na(2), lies at the centre of a distorted octahedron formed by six oxygen atoms arising from six separate anions. The bond lengths range from 2.347(2) to 2.687(2) Å. The environment of Na(3) consists of a very irregular arrangement of five oxygen atoms contributed by four separate anions. Here the bond lengths range from 2.272(2) to 2.441(2) Å for Na(3)-O(A1b). The five neighbouring oxygen atoms to Na(4) also arise from four separate anions but with the tighter range of 2.333(2) to 2.580(2) Å.

The P-O bridging bond lengths at 1.631(2) Å for side A and 1.642(2) Å for side B are significantly longer than the terminal P-O bond lengths which all lie between 1.512 and 1.514 Å. The individual terminal P-O bond lengths are significantly different. The P-O-P bond angle, at 127.5(1)°, is the smallest reported for a diphosphate ion. As commonly found for this anion the O-P-O bond angles involving the bridging oxygen atom are less than the ideal tetrahedral value in every case while those involving only terminal oxygen atoms are all larger than the ideal.

5.7. Discussion

It is of some interest to compare the geometries of the $P_2O_7^{4-}$ ion in the three sodium pyrophosphate studied to date. In $Na_4P_2O_7.10H_2O$ [29] the anion has a nearly staggered configuration with cryatallographic two-fold axis through the bridging oxygen atom. The P-O-P bond angle is 130.2° while the O-P-O angles involving the bridging oxygen atom range from 101.8 to 108.9°. The O-P-O angles among only terminal oxygen atoms range from 111.1 to 115.0°. The average terminal P-O bond length is 1.513 Å while the P-O(-P) bond is 1.612(5) Å long. The two unique Na^+ ions are coordinated to six oxygen atoms but only one is bonded directly to the anion; involving O(2) and O(4). These P-O bonds are the longer of the three at 1.510 and 1.526 Å respectively, although they do not differ significantly from the remaining terminal P-O bond length of 1.503 Å.

In $Na_2H_2P_2O_7.6H_2O$ [30], the anion again contains a crystallographic two-fold axis and has a nearly staggered configuration. The P-O-P bond angle is 136.1° with O(bridge)-P-O angles ranging from 103.4 to 108.8°. The remaining O-P-O angles of the PO_4 group range from 109.9 to 117.7°. The terminal P-O(-H) bond is 1.569(2) Å long while the remaining terminal P-O bond lengths are within 0.002 of 1.493 Å. These two oxygen atoms are bonded to the sodium ion which is coordinated to a total of six oxygen atoms. In this case, the P-O(-P) bond is shortened to 1.598(1) Å.

It is also of some interest to compare the observed P-O bond lengths in the above structures as well as the present structure with the predictions of Baur [10]. In order to do so, it is necessary to calculate first the electrostatic bond strength at the oxygen atom under consideration which can be defined as

$$(5.7.1) \qquad p_O = \Sigma_i \, (z/CN)_i$$

where z is the formal charge of the cation and CN is the coordination number of the cation contributing to the oxygen atom and the summation is over all contributing cations. The predicted bond length d_{P-O} between a phosphorus and an oxygen atom is then given by

$$(5.7.2) \qquad d_{P-O} = 1.322 + 0.109 \; p_O \quad \text{angstroms}$$

(Baur [10], p.136).

The following calculation illustrates the construction of TABLE V.4. Referring to TABLE V.3, each phosphorus atom is bonded to four oxygen atoms, i.e. CN = 4. Taking z = 5+ for P, then $(z/CN)_P = 5/4$. Suppose now $d_{P-O(CE)}$ is required. O(CE) receives the following contributions to the electrostatic bond length: 1/6 from Na(1), 5/4 from each of the two phosphorus atoms, P(A) and P(B). That is,

$$\begin{aligned} p_{O(CE)} &= 1/6 + 5/4 + 5/4 \\ &= 2.666. \end{aligned}$$

TABLE V.4

Correlation between Predicted and Experimental P-O Bond Lengths in Sodium Pyrophosphate Systems

	Bond	Observed Length (Å)	Predicted Length (Å)
$Na_4P_2O_7$	P-O(CE)	1.631 1.642	1.61
	P-O(A3)	1.512	1.49
	P-O(A2)	1.512	1.54
	P-O(A1)	1.512	1.56
	P-O(B2)	1.514	1.52
	P-O(B1)	1.513	1.52
	P-O(B3)	1.514	1.52
$Na_4P_2O_7 \cdot 10H_2O$*	P-O(1)	1.612	1.60
	P-O(2)	1.510	1.47
	P-O(3)	1.503	1.47
	P-O(4)	1.526	1.47
$Na_2H_2P_2O_7 \cdot 6H_2O$†	P-O(1)	1.598	1.60
	P-O(2)	1.492	1.47
	P-O(3)	1.495	1.47
	P-O(4)	1.569	1.57

* From Ref.29

† From Ref.30

Substituting this value in Equation (5.7.2), we have

$$d_{P-O(CE)} = 1.322 + 0.109 \times 2.666$$
$$= 1.612 \text{ angstroms.}$$

The rest of the entries in TABLE V.4 was obtained in a similar way. It is clear that the predicted values are, except with a few glaring exceptions, not far off the mark. In particular, the predicted value for the P-O(A1) bond length in $Na_4P_2O_7$ results from including the two rather long Na-O bonds in the calculation. It is clear that weighting the contribution to the electrostatic bond strength by some function inversely related to the atomic separation would improve the agreement. The P-O-P bond angle is small in $Na_4P_2O_7$ probably because the bridging oxygen atom is coordinated to a sodium ion. A similar effect has been noted in comparing the $Zn_2V_2O_7$ structure [31] to those of $Mg_2V_2O_7$ [31] and $Co_2V_2O_7$ [32]. This effect can be rationalized in the sense that Baur's relationship [10] would predict a lengthened P-O(-P) bond while Cruickshank's considerations [29] suggest that as the ratio of P-O(-P) to P-O increases, the P-O-P angle must contract.

Finally, the vibrational motion of the sodium and oxygen atoms in the $Na_4P_2O_7$ structure deserves some attention, TABLE V.5. The major components of vibration for P(A), P(B) and O(CE) are in the ab plane as would be expected either from the nature of the bonding or if some errors occur in the directions of the bending of the anion relative to the

Principal Axes of the Thermal Ellipsoids in $Na_4P_2O_7$

RMS Amplitude	Direction Cosines to			RMS Amplitude	Direction Cosines to			RMS Amplitude	Direction Cosines to		
	a	b	c		a	b	c		a	b	c
Na(1)				O(CE)				O(B2)			
0.128	0.1319	-.3911	-.9108	0.140	-.7277	0.6856	-.0198	0.164	-.7158	0.0399	-.6971
0.124	-.8110	-.5709	0.1276	0.097	0.6805	0.7253	0.1041	0.122	0.6899	-.1141	-.7149
0.115	-.5699	0.7219	-.3925	0.089	-.0857	-.0623	0.9944	0.096	-.1080	-.9927	0.0541
Na(2)				O(A3)				O(B1)			
0.163	-.6922	0.4588	-.5572	0.170	-.0812	0.9555	-.2837	0.158	-.1701	0.9735	-.1530
0.133	0.2296	0.8718	0.4327	0.118	0.1861	-.2651	-.9461	0.126	-.7274	-.0193	0.6859
0.114	-.6843	-.1716	0.7088	0.094	0.9792	0.1297	0.1563	0.086	0.6648	0.2279	0.7114
Na(3)				O(A2)				O(B3)			
0.146	-.2088	0.7625	-.6124	0.147	0.8762	0.4738	0.0877	0.142	-.0468	-.9305	0.3633
0.137	0.6405	0.5798	0.5036	0.123	-.0998	0.3566	-.9289	0.129	0.5528	0.2788	0.7853
0.119	0.7390	-.2871	-.6094	0.088	0.4714	-.8052	-.3597	0.092	0.8320	-.2376	-.5014
Na(4)				O(A1)							
0.146	-.2286	0.1787	-.9570	0.158	0.9959	0.0639	0.0646				
0.131	0.6757	-.6786	-.2881	0.134	0.0907	-.6508	-.7538				
0.122	-.7009	-.7125	0.0344	0.085	-.0061	0.7565	-.6539				

Angle between Principal Component of the Thermal Ellipsoid of X and P-X Bond Vector

Atom X	O(CE)	O(A3)	O(A2)	O(A1)	O(B2)	O(B1)	O(B3)	
Angle P(A) - X	7.5	8.5	9.8	1.4				in ($^{\circ}$)
Angle P(B) - X	5.3				5.6	2.2	20.0	

TABLE V.5

idealized structure. The fact that Na(1) vibrates nearly isotropically and with an amplitude comparable to the remaining cations suggests that the structure has very little residual configurational disorder at room temperature. The thermal motions of the oxygen atoms are significantly anisotropic with the largest component nearly perpendicular to the P-O bond.

A paper on the crystal structure of sodium pyrophosphate at 22°C. by K.Y. Leung and C. Calvo has been published in the Canadian Journal of Chemistry (1972)[53].

CHAPTER VI

CRYSTAL STRUCTURE OF $Na_4As_2O_7$ AT 22°C.

SUMMARY

Sodium diarsenate at room temperature is monoclinic with $\underline{a}$ = 5.969(1), $\underline{b}$ = 10.126(1), $\underline{c}$ = 12.272(3) Å and β = 92.87(2)°. There are four formula units per unit cell with space group C2/c. The structure was refined by full-matrix least-squares to a final R value of 0.027 utilizing 1157 reflections measured on the Syntex P$\bar{1}$ automatic diffractometer. The anion, consisting of two AsO_4 tetrahedra sharing a common oxygen atom, with a bridging angle of 123.5° at that oxygen atom, lies on a two-fold axis. The bridging As-O bond lengths are 1.783 Å and the average terminal As-O bond length is 1.658 Å. Both sodium ions show five-fold coordination to oxygen atoms with average Na-O bond lengths of 2.386 and 2.462 Å. One of these sodium ions has a long interaction (2.852 Å) with the bridging oxygen atom of the anion. Sodium diarsenate undergoes a series of phase transformations between room temperature and 220°C. and a further major transformation near 690°C.

6.1. Introduction

To date little accurate data exists on the structure of systems containing condensed tetrahedral AsO_4 groups. A number of diarsenates have been found to crystallize as analogues of the mineral thortveitite [33]; but in these cases, as in all other structures isotypic with thortveitite, ambiguity exists as to the detailed bonding because of disorder at the bridging oxygen atom [34, 35]. An additional interest in this system arises because its chemical analogue, $Na_4P_2O_7$, manifests a rich variety of phase transformations between room temperature and 600°C. (Chapter V).

6.2. Crystal Data

Formula: $Na_4As_2O_7$

Formula Weight: 353.79

Crystal System: Monoclinic;

$\underline{a} = 5.969(1)$, $\underline{b} = 10.126(1)$, $\underline{c} = 12.272(3)$ Å

$\beta = 92.87(2)^\circ$

Volume of Unit Cell: 740.85 $Å^3$

No. of Molecules/Unit Cell: z = 4

Specific Gravity: $\rho_{cal.} = 3.17$, $\rho_{obs.} = 3.12$

Space Group: C2/c

Wavelength of Radiation used: $MoK_{\alpha_1} = 0.70926$ Å

6.3. Preparation of the Sample

Like anhydrous sodium pyrophosphate, sodium diarsenate $Na_4As_2O_7$ required no special technique in its preparation. Chemically pure di-sodium hydrogen orthoarsenate hydrated, $Na_2HAsO_4.7H_2O$ was first heated in a platinum crucible to about 900°C. and maintained at that temperature for several hours. The melt was then cooled at the rate of 10°C. per hour to 500°C. when the power was shut off and the system allowed to cool to room temperature. The crystals were colourless and slightly opaque. Some of them were well-shaped and had the proper dimensions for X-ray work. Spheres of diameter about 0.15 mm. were also obtained to be used on the Syntex $P\bar{1}$ automatic diffractometer for data collection.

6.4. Data Collection

Preliminary photographic work was carried out on the precession camera and established the space group to be either Cc or C2/c on the basis of the extinction conditions: $h + k$ = odd for general h, k, l, and l = odd for $h\ 0\ l$.

A ground sphere, 0.01 cm. in radius, was used to collect data both for accurate parameters and for the resolution of the crystal structure. The 2θ values of 15 reflections were accurately centred using the diffractometer and the lattice parameters fitted to these values by least-squares. The results were obtained at room temperature using MoK_{α_1} radiation monochromatized with graphite. Peaks were scanned at a rate varying between 2 and 24° per minute, depending upon the peak count rate. Backgrounds were counted on either side of the peak for the same time period as used in scanning the peak. Reflections whose intensity, after correction for background, were less than 3σ where σ was determined from counting statistics, were regarded as unobserved. A total of 1157 unique reflections were collected of which 1011 were regarded as observed. These were corrected for Lorentz, polarization, absorption and extinction ($\mu R = 0.59$) effects.

6.5. Structure Determination

The positions of the arsenic atoms were determined from a Patterson map. Unlike the case of sodium pyrophosphate, the peaks could be identified fairly easily. From the extinction conditions: $h\ k\ l$: $h + k = 2n$; $h\ 0\ l$: $l = 2n$, ($h = 2n$); and $0\ k\ 0$: $k = 2n$, the space group should be either Cc or C2/c. A trial structure was first made with the choice of C2/c and was proven by the subsequent resolution of the structure to be correct. The structure factor calculation was first carried out with only the arsenic atom; further electron density difference syntheses determined the positions of the remaining sodium and oxygen atoms. The structure was refined with full-matrix least-squares. Atomic scattering factors were obtained from the International Tables for X-ray Crystallography[28]. Convergence was first obtained with unit weights and isotropic thermal parameters and then independent anisotropic thermal parameters were varied. Near the final stages of the refinement, plots of $\langle|F_o - F_c|\rangle$ versus $\langle\sin\theta/\lambda\rangle$ and $\langle|F_o|\rangle$ were obtained, Figs. 6.5.1 - 2. There were indications that some systematic variations were in existence and extinction corrections were subsequently carried out. For the final refinement, weights were set equal to $(7.4 - 0.26\ F_o + 0.0031\ F_o^2)^{-1}$ with coefficients chosen so that $w|F_o - F_c|^2$ would be independent of F_o. The final R value is 0.027 while $R_w = 0.037$ where

$$R_w = \left[\frac{\Sigma\ w|F_o - F_c|^2}{\Sigma\ w\ F_o^2}\right]^{\frac{1}{2}}$$

No residual peaks could be discerned in the final electron density map. The final atomic positional parameters are found in TABLE VI.1 and the observed and calculated structure factors in TABLE VI.2.

Variations of $\langle |F_o - F_c| \rangle$ as a function of $\langle \sin\theta/\lambda \rangle$

Fig. 6.5.1

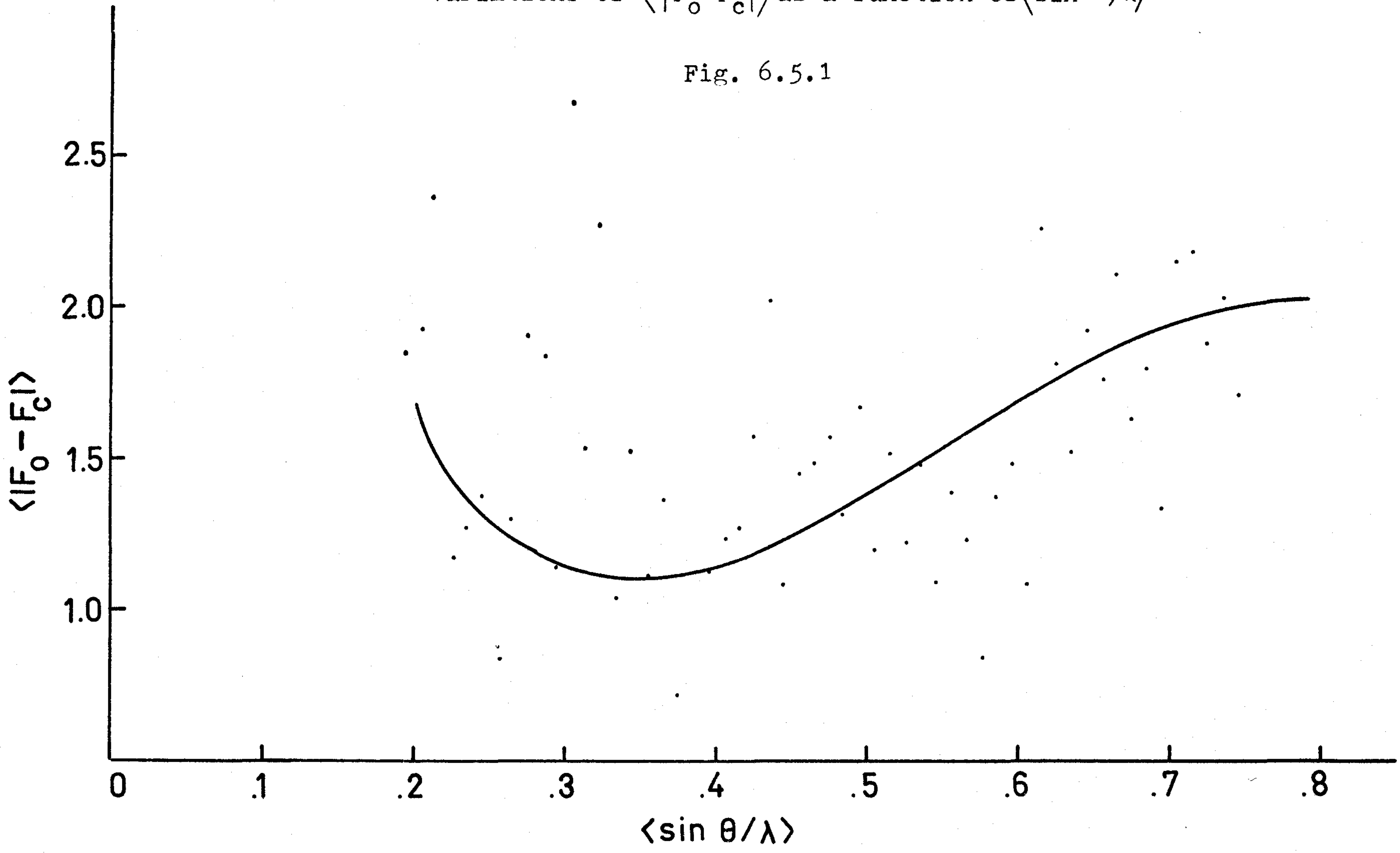

Variations of $\langle|F_o - F_c|\rangle$ as a function of $\langle F_o\rangle$

Fig. 6.5.2

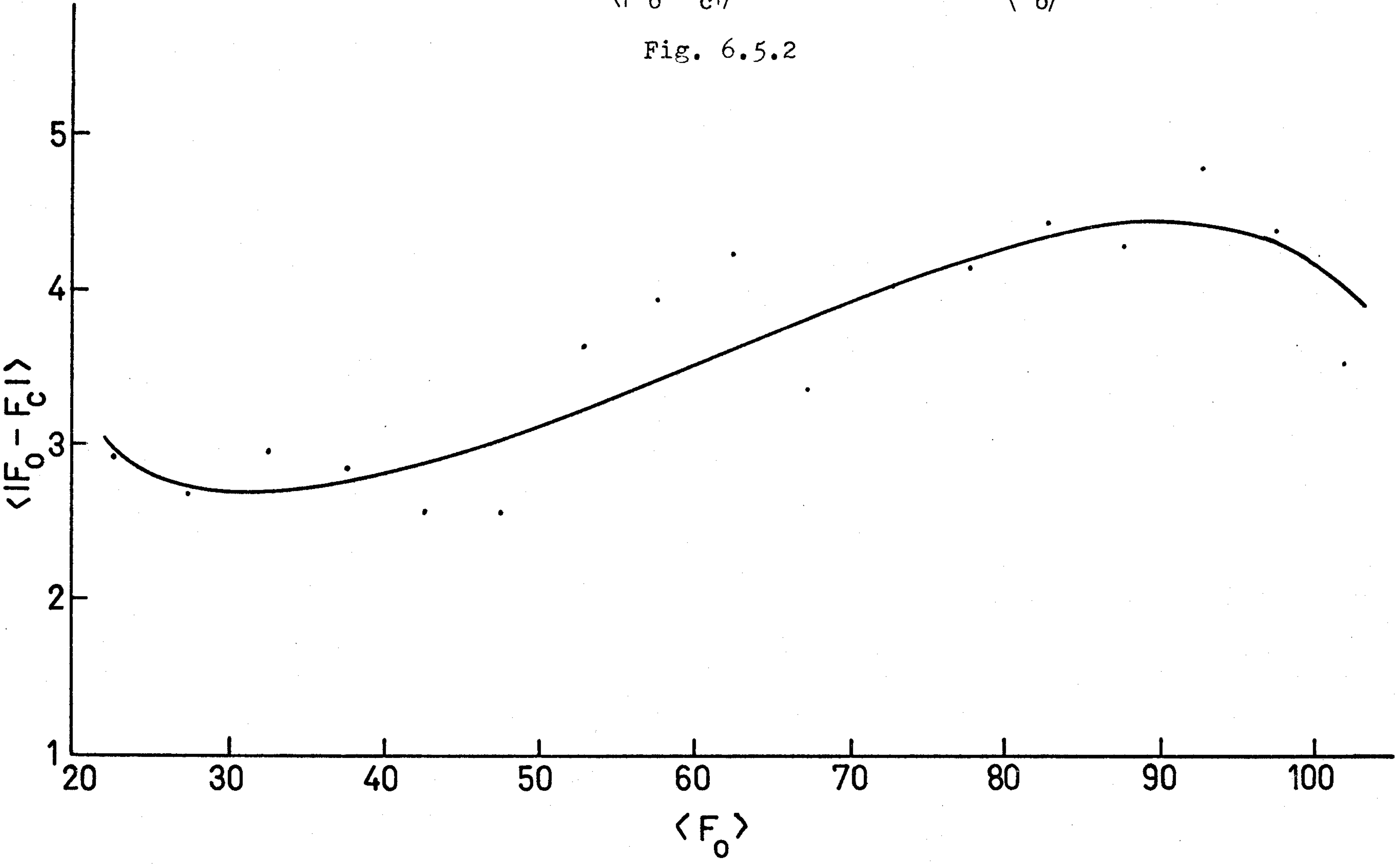

TABLE VI.1. Atomic and Thermal Parameters of $Na_4As_2O_7$ with Estimated Standard Deviations in Parentheses

	x	y	z	U_{11}^*	U_{22}	U_{33}	U_{12}	U_{13}	U_{23}
Na(1)	0.3438(2)	0.3216(2)	0.1273(1)	0.0157(8)	0.0194(7)	0.0146(7)	-.0024(5)	0.0010(5)	0.0021(5)
Na(2)	0.3118(2)	-.0155(2)	0.0958(1)	0.0137(8)	0.0209(7)	0.0224(7)	-.0011(5)	0.0017(6)	0.0023(5)
As	0.14474(5)	0.15226(3)	0.36050(2)	0.0067(2)	0.0084(2)	0.0079(2)	0.0006(1)	0.0004(1)	0.0012(1)
O(1)	0	0.0689(3)	1/4	0.025(2)	0.009(1)	0.017(1)	-	-.013(1)	-
O(2)	0.2649(4)	0.2870(2)	0.3133(2)	0.015(1)	0.014(1)	0.015(1)	-.005(1)	0.000(1)	0.0029(8)
O(3)	0.3219(4)	0.0360(3)	0.4046(3)	0.012(1)	0.016(1)	0.019(1)	0.005(1)	-.004(1)	0.0016(8)
O(4)	-.0605(5)	0.1787(3)	0.4442(2)	0.019(2)	0.030(1)	0.016(1)	0.007(1)	0.012(1)	0.005(1)

* U_{ij}'s in Å^2 are computed from $\beta_{ij} = 2\pi^2 \underline{b}_i \cdot \underline{b}_j U_{ij}$ where $T = \exp -(\beta_{11}h^2 + \ldots + 2\beta_{12}hk + \ldots)$ appear in the structure factor expression and $\underline{b}_i$'s are the reciprocal lattice vectors.

TABLE VI.2

TABLE OF OBSERVED AND CALCULATED STRUCTURE FACTORS OF NA4AS2O7 AT 22 DEGREES C. UNOBSERVED REFLECTIONS ARE MARKED WITH * AND UNRELIABLE REFLECTIONS WITH + .

K	L	|F-O|	|F-C|
		H = 0	
[illegible]	[illegible]	[illegible]	[illegible]

6.6. Description of the Structure

The structure of $Na_4As_2O_7$ consists of anions formed from corner-shared As_2O_7 groups. These anions are arranged in layers parallel to the ab plane and at a thickness equal to half the c axis, Fig. 6.6.1. In each layer, the anions in adjacent unit cells form a triangularpattern, Fig. 6.6.2, with the As-As vector of any anion at 32.6° to the c axis. The anion contains a crystallographic two-fold axis through the bridging oxygen atom O(1) and the angle As-O(1)-As is 123.5°. Two of the terminal oxygen atoms O(3)a and O(2)a lie within $\frac{1}{4}$ Å of the same z = constant plane but the third terminal oxygen atom O(4)a and its symmetry-equivalent counterpart O(4)c do not lie within the same range, Fig. 6.6.1.

Na(1) lies between the terminal oxygen atoms of two anions in one layer and is nearly directly below another anion in an adjacent layer, Fig. 6.6.1. It is coordinated to five oxygen atoms three of which being contributed by the same anion, TABLE VI.3. The two oxygen atoms bonded to this cation, O(2)c and O(4)a arise from opposite ends of the anion. Na(1) and As c lie nearly in the same z = constant plane. Na(2) which is also coordinated to five oxygen atoms, shares a bridging oxygen O(1) and a terminal oxygen atom O(2)c with one anion while the remaining oxygen atoms arise from two additional anions, TABLE VI.3. The bridging oxygen atom of the anion lies on a two-fold axis separated by 1.783(2) Å from the As atom (TABLE VI.3). The terminal As-O bond

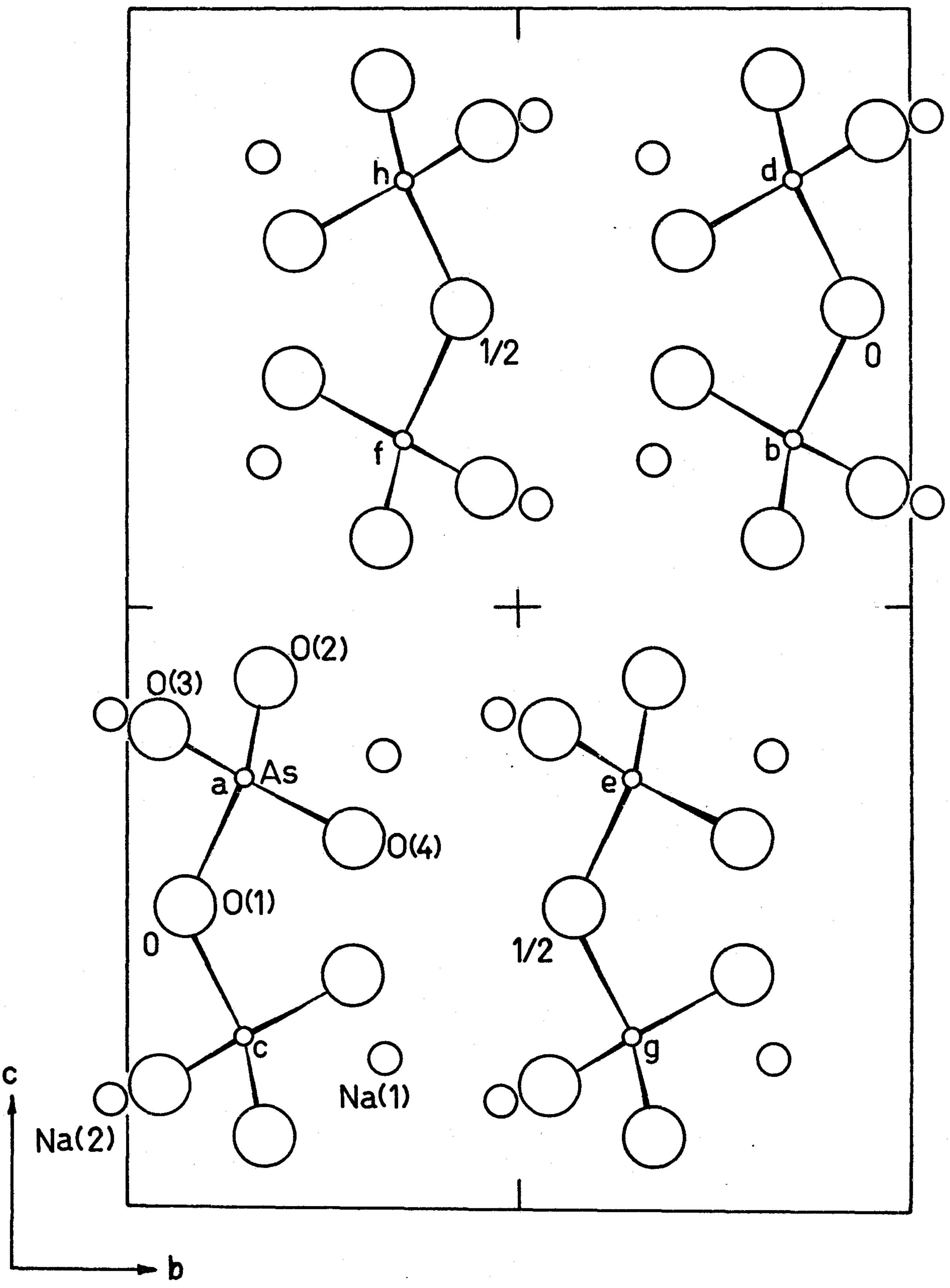

Fig. 6.6.1

The structure of $Na_4As_2O_7$ projected onto the <u>bc</u> plane

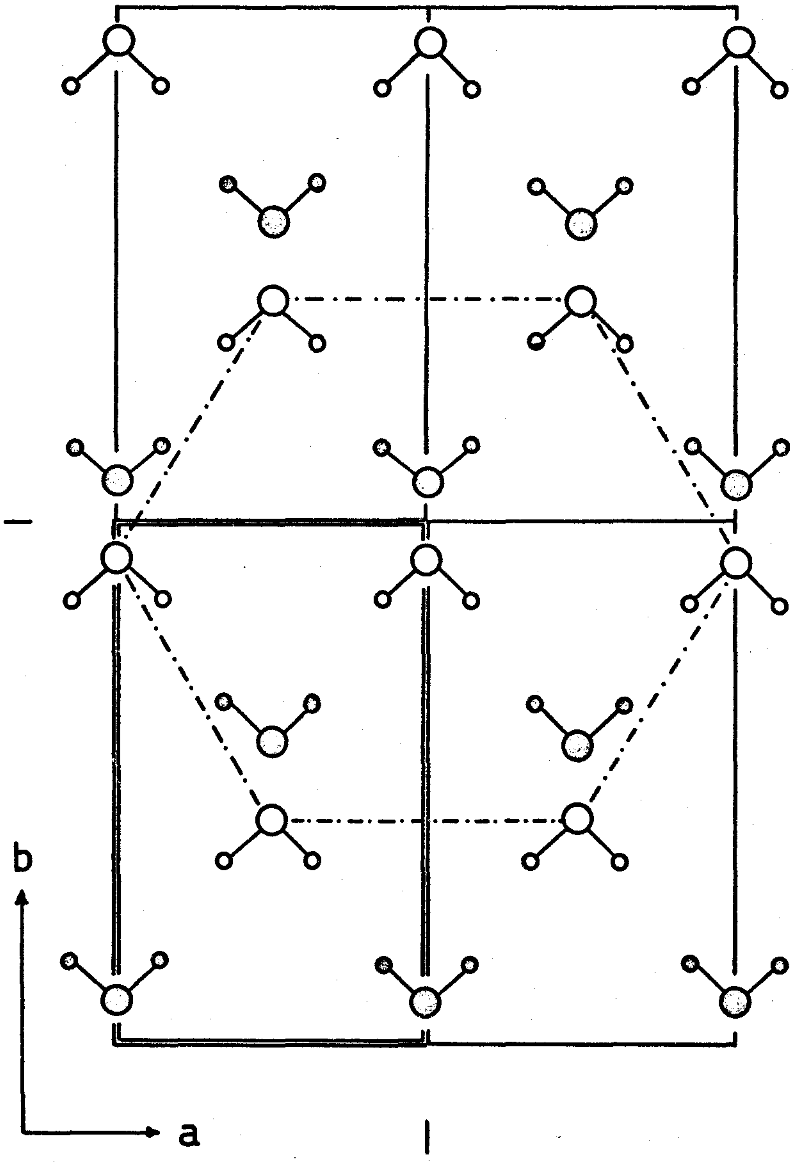

Fig. 6.6.2

Diarsenate groups projected onto the <u>a</u> <u>b</u> plane. Only the bridgen oxygen atom and the two arsenic atoms are shown in each group.

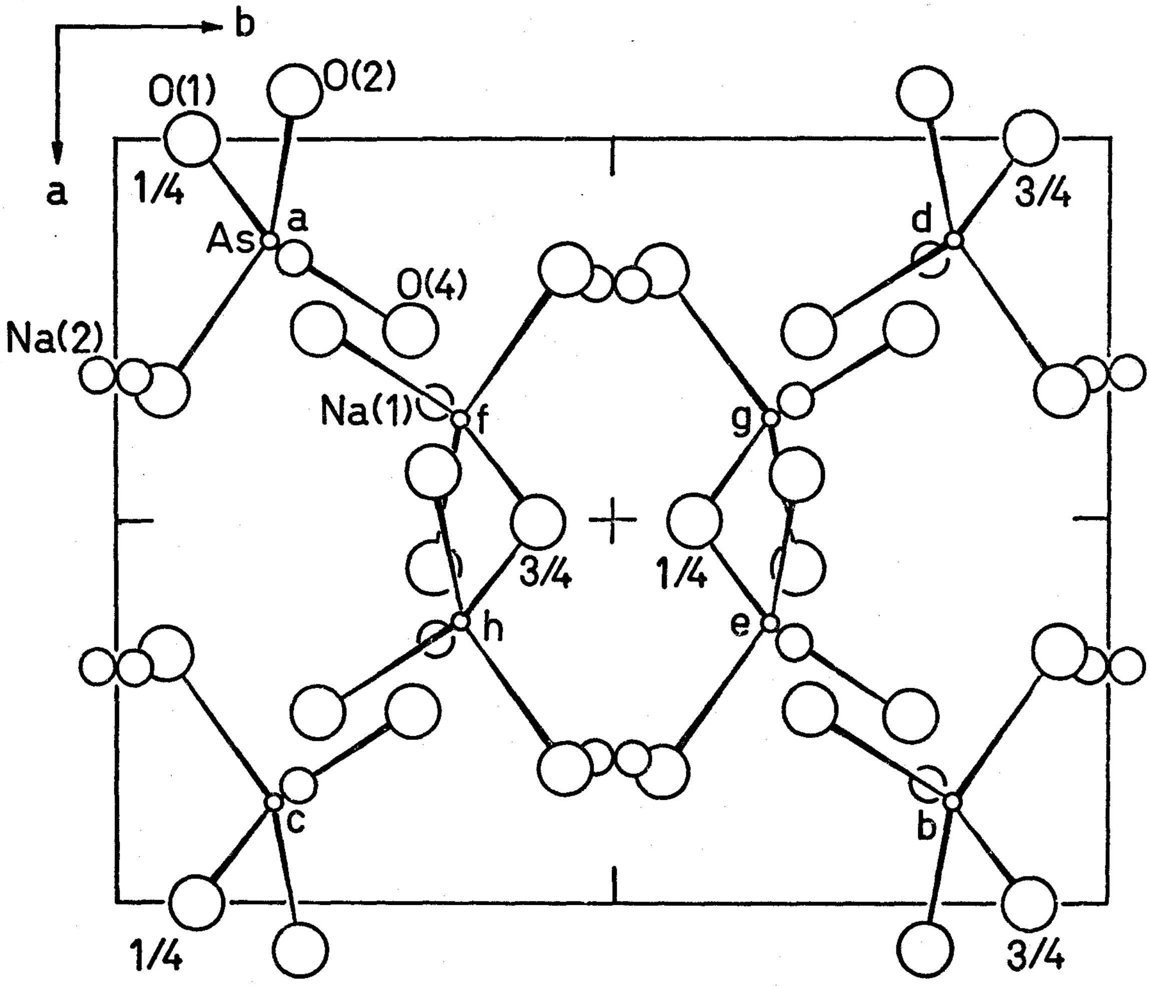

Fig. 6.6.3

The structure of $Na_4As_2O_7$ projected onto the ab plane

TABLE VI.3

Bond Distances and Angles in $Na_4As_2O_7$

Distance	Å	Angle	Degrees	Angle	Degrees
As-O(1)a,c	1.783(2)*	O(1)-As-O(2)	101.7(1)	O(2)-As-O(3)	113.1(1)
-O(2)a,c	1.659(3)	-O(3)	100.9(1)	-O(4)	115.4(1)
-O(3)a,c	1.655(3)	-O(4)	109.0(1)		
-O(4)a,c	1.659(3)			O(3)-As-O(4)	114.7(1)
As-As c	3.142(3)	As-O(1)-As	123.5(2)		
Na(1)-O(2)c	2.362(3)	O(2)c-Na(1)-O(2)h	81.2(1)	O(2)h-Na(1)-O(3)g	87.9(1)
-O(2)h	2.347(3)	-O(3)g	102.2(1)	-O(4)a	171.1(1)
-O(3)g	2.409(3)	-O(4)a	95.4(1)	-O(4)c	90.6(1)
-O(4)a	2.379(3)	-O(4)c	132.9(1)	O(3)g-Na(1)-O(4)a	100.9(1)
-O(4)c	2.437(3)	O(4)a-Na(1)-O(4)c	85.7(1)	-O(4)c	123.9(1)
Na(2)-O(1)a	2.852(2)	O(1)a-Na(2)-O(2)c	59.4(1)	O(2)c-Na(2)-O(3)d	85.4(1)
-O(2)c	2.506(3)	-O(3)d	137.4(1)	-O(3)c	113.0(1)
-O(3)d	2.359(3)	-O(3)c	126.8(1)	-O(4)g	129.2(1)
-O(3)c	2.248(3)	-O(4)g	77.9(1)	O(3)d-Na(2)-O(3)c	86.9(1)
-O(4)g	2.346(1)	O(3)c-Na(2)-O(4)g	114.4(1)	-O(4)g	114.3(1)

Transformations: a = x,y,z b = -x,-y,-z c = $-x,y,\frac{1}{2}-z$ d = $x,-y,\frac{1}{2}+z$

e = $\frac{1}{2}+x,\frac{1}{2}+y,z$ f = $\frac{1}{2}-x,\frac{1}{2}-y,-z$ g = $\frac{1}{2}-x,\frac{1}{2}+y,\frac{1}{2}-z$ h = $\frac{1}{2}+x,\frac{1}{2}-y,\frac{1}{2}+z$

* Errrors include those arising from the lattice constants in addition to the individual parameter errors.

lengths are substantially and significantly shorter, ranging from 1.655 to 1.659 Å. Individual terminal As-O bond lengths are not significantly different. All the O-As-O angles in a tetrahedron that involve the bridging oxygen atom are less than the ideal value while the remaining angles are all larger than ideal. The As-O-As angle is rather small at 123.5° and results, in part, from the interaction of the bridging oxygen atom with two Na(2) ions.

Each sodium ion has only five oxygen atoms within 3 Å. The Na(1)-O bond lengths are fairly uniformly distributed between 2.347(3) and 2.437(3) Å and the $Na(1)-O_5$ configuration is a distorted trigonal bipyramid with O(2)h and O(4)a as the axial oxygen atoms. The four nearest oxygen atoms to Na(2) form a distorted tetrahedron with the O(2)c-O(4)g edge enlarged to accommodate the fifth oxygen atom, O(1). The O(1)-O(2) edge is shared with one of the anions. About the $Na(2)-O_4$ tetrahedron, the Na(2)-O distances range from 2.248 to 2.506 Å and the angles lie between 85.4 and 129.2°. The Na(2)-O(1) interaction is 2.852 Å long and compares with an interaction of 2.426 Å between the bridging oxygen atom and Na(1) in sodium pyrophosphate (Chapter V).

6.7. Discussion

The structure of $Na_4As_2O_7$ bears considerable resemblance to that of the room-temperature polymorph of $Na_4P_2O_7$. The latter structure is orthorhombic with space group $P2_12_12_1$ and unit cell dimensions of a = 9.367, b = 5.390 and c = 13.480 Å (Chapter V). The anion is formed from two PO_4 groups sharing a common oxygen atom with a bridging P-O-P angle of 127.5° compared to an As-O-As angle of 123.5° in $Na_4As_2O_7$. The angle that the P-P vector of the anion subtends with the c axis is 9°. This structure also contains layers of pseudo-hexagonally arranged anions and as a result of small displacements, assumes a C-centred cell, with a doubled c axis at 405°C. Three ansions in one layer and three in an adjacent layer are approximately related by a 6_3 axis which becomes a crystallographic symmetry element above 550°C. Half of the sodium cations lie near this pseudo-axis as shown in Fig. 6.7.1(a). The remaining cations lie between the anion layers and are coordinated to five oxygen atoms. Each anion is stabilized with a non-linear X-O-X group by an interaction with one sodium ion in contrast to two for $Na_4As_2O_7$. In $Na_4P_2O_7$ the anion deviates by about 25° from an eclipsed configuration when viewed parallel to the P-P vector while the comparable average dihedral angle in $Na_4As_2O_7$ is 11°.

As Fig. 6.7.1(b) shows, the bridging oxygen atoms in adjacent layers in $Na_4As_2O_7$ nearly superimpose in projection

A comparison between the structures of $Na_4P_2O_7$ and $Na_4As_2O_7$ projected onto the ab plane

same scale

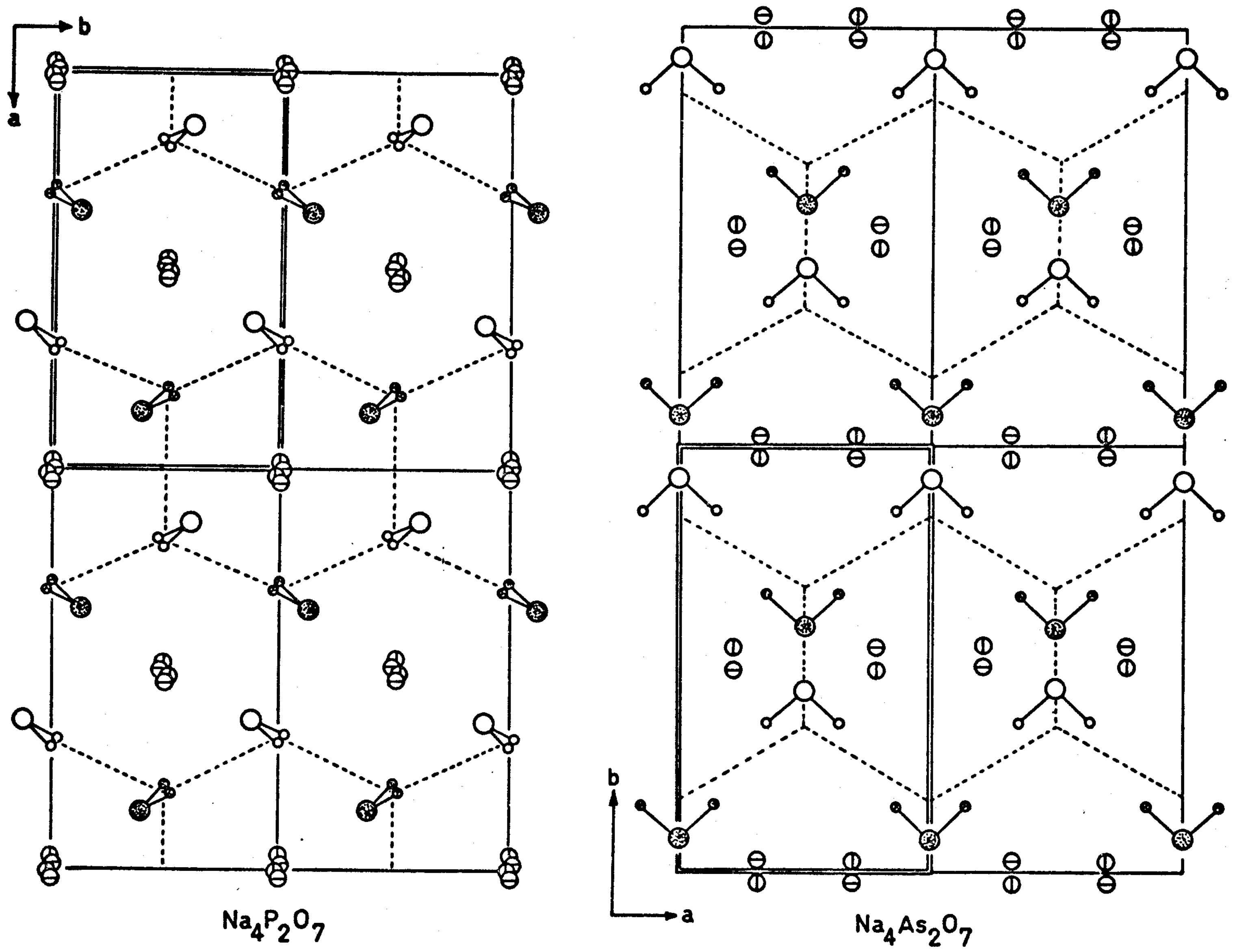

(a) Fig. 6.7.1 (b)

and a relative shift of about 1.8 Å is needed to establish a pseudo 6_3 axis relationship between the oxygen atoms. However, the acute side of the anion opens towards -b in one layer and +b in the next, as required by the two-fold axis, so that the anion configurations are not consistent with a pseudo 6_3 axis. Another major difference between the two structures is the Na^+ configuration relative to the anion. All the Na^+ are approximately between the oxygen atom layers in $Na_4As_2O_7$ although the Na-O interactions are not restricted to those oxygen atoms corresponding to the top of one layer and the bottom of the next adjacent one, as found in $Na_4P_2O_7$. In order to obtain the $Na_4P_2O_7$ structure from that of $Na_4As_2O_7$, the two-fold axis must be lost with one of a pair of Na(2) ions moving to the pseudo 6_3 axis and to a z plane nearly coplanar with the bridging oxygen atoms. The second Na(2) ion must also be near the same 6_3 axis but displaced by about $\frac{1}{4}$c from the first Na(2) ion. Further, each Na(1) must be displaced so as to coordinate with four oxygen atoms at nearly the same z coordinate as the Na ion with a fifth oxygen atom arising from the adjacent layer. One of these Na(1) ions must share a face of a PO_4 group formed from three terminal oxygen ions at one end of the anion.

TABLE VI.4 summarized the thermal behaviour of the atoms in $Na_4As_2O_7$. All the atoms show significant anisotropic motion but the ratio of the maximum to the minimum amplitudes

TABLE VI.4

Root Mean Squared Atomic Displacements and Angles of Principal Axis with respect to the Unit Cell Edges

atom	r_i	root mean square amplitude	angle of r_i with a	b	c
As	r_1	.097	81.5	37.8	54.1
	r_2	.085	123.4	115.7	42.3
	r_3	.080	145.3	64.4	109.3
O(1)	r_1	.159	173.8	90.0	80.9
	r_2	.150	90.0	0.0	90.0
	r_3	.131	96.2	90.0	170.9
O(2)	r_1	.193	60.1	40.7	66.6
	r_2	.145	122.6	49.3	120.4
	r_3	.079	47.2	92.2	140.0
O(3)	r_1	.147	124.6	107.0	37.1
	r_2	.137	72.9	36.8	59.6
	r_3	.084	140.2	58.5	109.3
O(4)	r_1	.145	49.5	130.0	116.0
	r_2	.121	118.6	86.0	148.3
	r_3	.094	126.3	139.7	73.1
Na(1)	r_1	.145	67.1	151.7	106.9
	r_2	.124	40.4	81.8	53.6
	r_3	.114	121.2	116.9	41.3
Na(2)	r_1	.155	88.5	127.0	143.0
	r_2	.140	102.5	39.1	125.5
	r_3	.115	167.4	100.9	80.9

for both As and the bridging oxygen atoms is surprisingly small. Although the typical behaviour in X_2O_7 systems would show O(1) with the largest amplitude, in $Na_4As_2O_7$, O(2), one of the terminal oxygen atoms has the largest amplitude. This may be a result of the fact that O(1) is bonded to two cations, whereas in the previous cases the bridging oxygen atom of the X_2O_7 group bonds strongly to at most one cation. These thermal amplitudes provide no strong evidence for the impending phase transformation near 65°C. but may be interpretable, ex post facto, when the nature of high temperature phases have been ascertained.

The diarsenate ion, with two Na(2) ions bonded weakly to the bridging oxygen atom, shows a large distortion from equivalent As-O bond lengths. The Pauling electrostatic valency [36] is 2.90 at O(1) and 1.85 at the terminal oxygen atoms. From Baur's [10] linear relationship between bond length and electrostatic valency with coefficients derived by Krishnamachari [37] which has the form

$$(6.7.1) \qquad d_{As-O} = 1.49 + 0.10\ p_O \text{ angstroms,}$$

the predicted bond length difference would be 0.105 Å and lengths of 1.780 Å and 1.675 Å for the As-O(-As) and As-O bond lengths respectively. On the other hand, ignoring the Na(2)-O(1) bonds would lead to a greater discrepancy.

Brown and Shannon [11] have shown that the bond strength, s, can be fitted with a curve of the form

(6.7.2) $s = C_o(r_o/r)^n$

where r_o and n are found by least squares and C_o is given by the formal charge divided by the "normal" coordination number. TABLE VI.5 shows the individual bond strengths and how well the sum about each element compares with the formal charge. In TABLE VI.6 the individual X-O bond lengths are compared with those predicted on the assumption that the calculated valency contribution from the sodium ion is errorless and the difference between the formal charge on the oxygen atom and its formal charge is used to calculate the X-O bond length. Errors in these predicted bond lengths arises from two sources: the individual errors in the Na-O bond lengths and the errors in the estimated values of n and r_o. Only the former contributions are included in TABLE VI.6.

The agreement in $Na_4As_2O_7$ has to be regarded as reasonably good, despite the fact that correction for the effects of thermal motion on the apparent bond lengths have not been applied to either the data that were used to determine n and r_o or to the experimental values in $Na_4As_2O_7$ and $Na_4P_2O_7$. Systematic deviations leading to predicted values of bridging P-O(-P) bonds and smaller terminal ones seem to appear in both these compounds and in $KAlP_2O_7$ [38] .

A paper on the crystal structure of $Na_4As_2O_7$ at 22°C. by K.Y. Leung and C. Calvo has been accepted for publication in the Canadian Journal of Chemistry (1973) [54].

TABLE VI.5. Bond Strengths in $Na_4As_2O_7$ and $Na_4P_2O_7$*

$Na_4As_2O_7$

	As	Na(1)	Na(2)	ΣS_{anion}
O(1)	0.982 0.982		0.071 0.071	2.11
O(2)	1.319	0.203 0.211	0.146	1.88
O(3)	1.332	0.182	0.205 0.268	1.99
O(4)	1.319	0.195 0.171	0.211	1.90
ΣS_{cation}	4.95	0.96	0.90	

$Na_4P_2O_7$

	P(1)	P(2)	Na(1)	Na(2)	Na(3)	Na(4)	ΣS_{anion}
OCE	1.023	1.007	0.176				2.21
O1A	1.312		0.227	0.208		0.175	1.92
O1B	1.309		1.221	1.142	0.168	0.124	1.96
O1C	1.306		0.082	0.146	0.066	0.214 0.168	1.98
O2A		1.304	0.192	0.092	0.253		1.85
O2B		1.306		0.192	0.228	0.219	1.95
O2C		1.304	0.194	0.211	0.221		1.91
ΣS_{cation}	4.95	4.92	1.07	1.00	0.94	0.90	

---

* Calculated from $S_i = C_i(R_{oi}/R_i)^{n_i}$ with

Atom(i)	C_i	R_{oi}(Å)	n_i
Na^+	1/6	2.449	5.6
As^{5+}	5/4	1.681	4.1
P^{5+}	5/4	1.534	3.2

TABLE VI.6

Observed and Predicted As-O and P-O Bond Lengths in $Na_4As_2O_7$ and $Na_4P_2O_7$

Bond	Observed	Predicted*
As-O(1)	1.783(2)	1.807(5)
As-O(2)	1.659(3)	1.624(10)
As-O(3)	1.655(3)	1.651(10)
As-O(4)	1.659(3)	1.629(10)
P(1)-OCE	1.633(2)	1.742(4)
P(1)-O1A	1.511(2)	1.475(6)
P(1)-O1B	1.512(2)	1.490(6)
P(1)-O1C	1.513(2)	1.498(6)
P(2)-OCE	1.641(2)	1.753(4)
P(2)-O2A	1.514(2)	1.452(6)
P(2)-O2B	1.513(2)	1.485(6)
P(2)-O2C	1.514(2)	1.474(6)

* Calculated by adjusting the X-O bond length so as to yield $\Sigma S_{O^{2-}} = 2.00$.

CHAPTER VII

CRYSTAL STRUCTURE OF $Na_4P_2O_7$ AT 410°C.

SUMMARY

At 405°C. sodium pyrophosphate becomes monoclinic in space group C2/c with $\underline{a} = 9.415(5)$, $\underline{b} = 5.425(5)$, $\underline{c} = 27.035(10)$ Å, $\beta = 93^\circ$, and $z = 8$. The structure was refined by full-matrix least squares using 580 unique reflections recorded with a precession camera. The final R value is 0.054. The anions assumed a staggered configuration with an average dihedral angle of 65° compared to a semi-eclipsed configuration with an average of 32° in the room-temperature structure. The $P\text{-}O_{bridge}\text{-}P$ angle is 132.4(6)°. The two bridging P-O bond lengths differ significantly, being 1.577(6) and 1.644(7) Å with terminal P-O bond-length averages of 1.485 and 1.475 Å on either side of the anion. These averages are significantly shorter than for $Na_4P_2O_7$ at room temperature. Corrections based on a rigid-body motion librating about the centre of mass of the anion were carried out. In addition, a rigid-group refinement based upon the room-temperature structure was also carried out, and the R value is 0.073. It is suspected that a certain amount of configurational disorder exists in the present structure.

7.1. Introduction

The first phase transformation of sodium pyrophosphate above room temperature takes place at 405 °C. and the system goes from the orthorhombic space group $P2_12_12_1$ to the monoclinic space group C2/c with a doubled c axis while the other two axes a and b remain essentially the same. There is a high probability that the crystal becomes twinned at this temperature (Section 4.3); but the structure reported here corresponds to one at 410 °C. without any twinning.

7.2. Crystal Data

Formula: $Na_4P_2O_7$ Formula Weight: 265.95

Crystal System: Monoclinic;

$\underline{a} = 9.415(5)$, $\underline{b} = 5.425$, $\underline{c} = 27.035(10)$ Å

$\beta = 93^\circ$

No. of Molecules/Unit Cell: $z = 8$

Space Group: C2/c

Wavelength of Radiation used: $MoK_\alpha = 0.7114$ Å

Temperature of Crystal: 410 ± 5 °C.

7.3. Experimental

In order to record intensities with a precession camera above room temperature, a small furnace, eight inches long, was constructed, Fig. 7.3.1. The heating element was made of nichrome wire. Air from a tap in the laboratory was first passed into a large flask where it was dried and directed through the inner Mullite tube which housed the heating element. The air pressure was adjusted by operating on the opening of the tap. The electric current through the heating element was controlled by a small variac.

The temperature was recorded by a thermocouple made of fine chromel-alumel (Gauge 36). The system was first tested for temperature gradient by setting up a second thermocouple at the position normally occupied by the crystal. It was found that if the pressure of the air-flow was about half an inch of water, the temperature difference between the two thermocouples was negligibly small, the lower thermocouple registering about 1% less than the upper thermocouple. Without an enclosure about the camera, the fluctuation was about 5°C. when the temperature of the system was 500 °C. This stability is satisfactory when the phases extend over ranges of temperature of more than 10 °C. In the investigation of the phase transformations of sodium pyrophosphate, there are phases around 525 °C. which are separated by only several degrees (Fig. 4.1.1) and this set-up, without modification, is not suitable. A furnace of greater stability could be

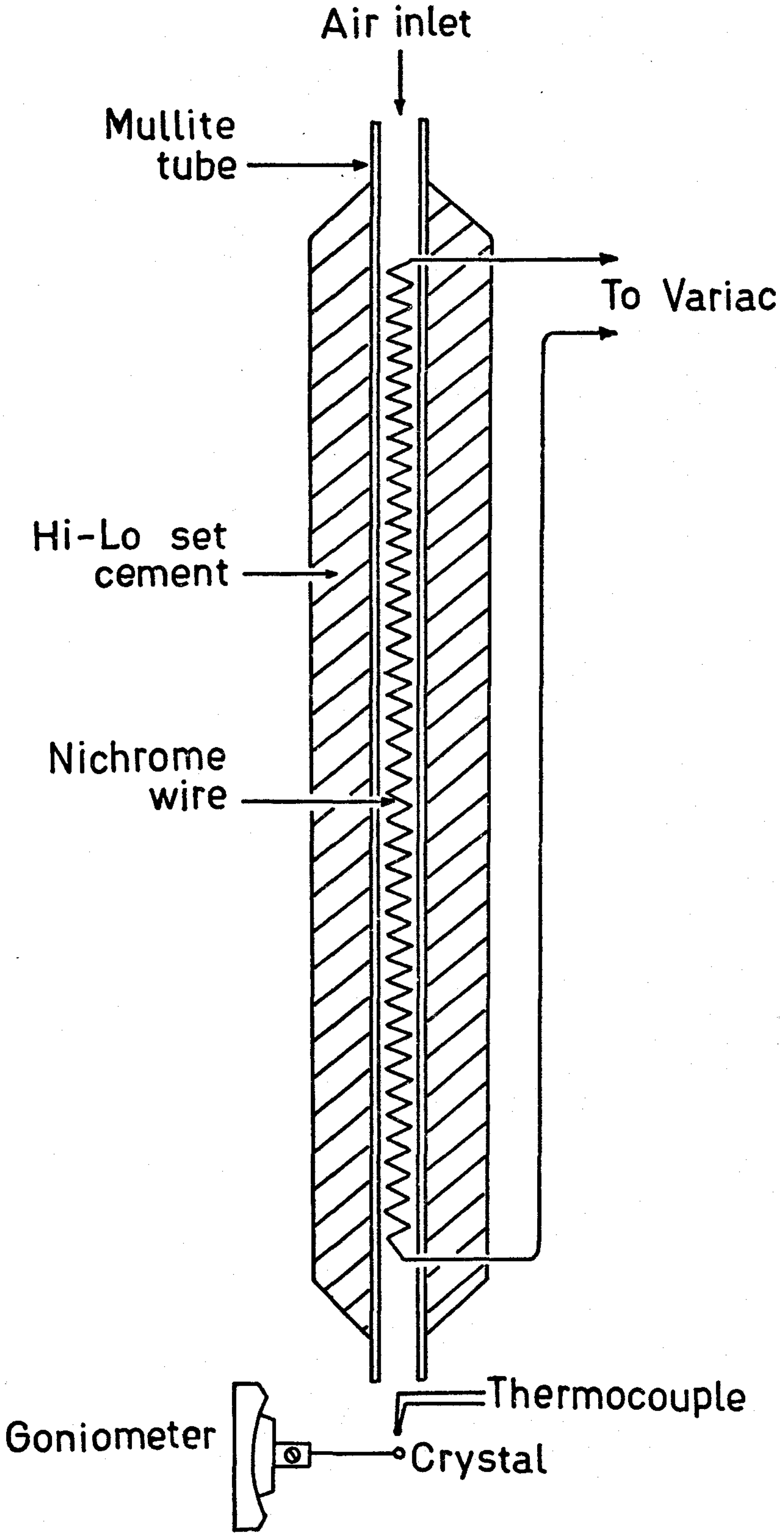

Fig. 7.3.1. A Furnace for the Precession Camera

obtained, of course, by covering the entire camera, thus minimizing the effect of draughts in the laboratory and, further, by installing a feedback system for a better control of the heating current. The furnace could attain a temperature of 800 °C. and is very inexpensive to build.

The glue used in mounting the crystal for high temperature work was a commercial "Silicone Seal" by General Electric. When the tube was fresh, the glue was satisfactory up to 650 °C. However, when the tube was left in the laboratory for a period of time - about half a year or so, the glue inside the tube began to harden and even the remaining soft portion were not suitable for high temperatures because the glue would become brittle at times and the crystal would be lost.

7.4. Data Collection

The crystal was aligned on a precession camera at room temperature with the c axis of the crystal parallel to the spindle axis. The furnace described in Section 7.3 was then placed in position and the current was slowly increased in steps corresponding to about 25 °C. at half-hour intervals. This procedure was followed in order to avoid uneven setting of the glue which might disturb the alignment of the crystal. Also slow heating decreased the chance of getting a twinned crystal at the transition temperature 405°C. When the temperature of the crystal was close to 390 °C. the increment of temperature was reduced (about 5 - 7°C.) and the time interval between steps was extended to about an hour. Meanwhile, alignment photographs of the h0l projection were taken and the necessary adjustments on the arcs of the goniometer and the spindle were made. From the photographs, it was possible to decide whether the crystal has undergone its phase transformation by observing the disappearance of the h = odd reflections or by the appearance of the "twinning" lines (Section 4.3). Very often both phenomena occurred simultaneously. When twinning lines appeared, the temperature of the crystal was lowered and the approach to the transition point was again attempted by slowly increasing the temperature. Thus, it was sometimes possible to eliminate twinning by this process. However when twinning persisted, it was necessary to select another crystal. It is worth mentioning that an untwinned crystal would remain untwinned even though there might be slight fluctuations in the temperature of the system provided the lower limit of the fluctuation did not extend into the lower phase.

The temperature of the untwinned crystal was brought to 410 °C. (as recorded by the thermocouple) which was slightly beyond the transition temperature. Full precession photographs of h0l, h1l, h2l, h3l, and 0kl, 1kl, 2kl were obtained with varying number of cycles in each case. The intensities of the reflections were measured with a microdensitometer and corrected for polarization and Lorentz effects. Common reflections were used to place all the intensities on a common scale and 580 unique reflections were obtained.

The lengths of the unit cell axes at this temperature as well as at all higher temperatures, were obtained from the linear expansion curves shown in Figs. 4.6.1 - 3. In these curves the axes of the room-temperature structure were taken as standards since their values had been directly obtained and refined. The angle β, however, was obtained from a full precession h0l photograph.

7.5. Determination of the Structure

Since the c axis of the system at 410 ^{o}C. was twice that of the room-temperature structure, a trial structure was derived by taking a unit cell double the size of the room-temperature structure along the c axis. An origin was first chosen so that the locations of the pyrophosphate anions could be generated by the symmetry operations of the space group. The C-centering as indicated by the extinction condition: $h + k = 2n$, required the bridging oxygen atoms of the anions in the same layer to have the same displacement relative to the coplanar sodium atom, a feature rather than the screw axis relationship of the room-temperature structure. Since it was not known a priori which way the bridging oxygen atom would bend, this oxygen atom as well as all the terminal oxygen atoms of the anion were left out in the initial calculation of the structure factors. Of the eight sodium atoms located along the 6_3 axis of the idealized structure (Chapter V), four had to be generated from two types, Na(8) and Na(9), in special four-fold sites. Na(7), because of its location in the z direction, need not be in any special position, though its x and y coordinates were close to 0 and ½ respectively.

This model, with two phosphorus and the five sodium atoms, yielded an R value of about 50%. A least squares refinement, with some major shifting on the atoms, gave an R value of about 40%. At this stage, electron density maps were constructed in slices up the c axis at levels where the oxygen atoms would be expected to lie. The peaks on these maps corresponding to the seven oxygen atoms could be identified and their coordinates were used in subsequent refinements. The structure was refined by full-matrix least squares using unit weights and isotropic temperature factors. When the R value was 15%, anisotropic temperature factors for each atom were used. For the final refinement, weights were set equal to $(18.11 - 0.69 F_o + 0.0067 F_o^2)^{-1}$ with coefficient chosen so that $w|F_{obs} - F_{cal}|^2$ would be independent of F_{obs}. The final value is 0.068 where $R_w = 0.054$ with

$$R_w = \left[\frac{\Sigma\, w|F_o - F_c|^2}{\Sigma\, w\, F_o^2} \right]^{\frac{1}{2}}$$

The final atomic positional parameters are found in TABLE VII.1 and the observed and calculated structure factors in TABLE VII.2.

TABLE VII.1. Atomic and Thermal Parameters of $Na_4P_2O_7$ at 410 °C. with Estimated Standard Deviations in Parentheses

Atom	x	y	z	U_{11}*	U_{22}	U_{33}	U_{12}	U_{13}	U_{23}
P-A	0.1758(3)	0.0146(7)	0.4284(1)	0.028(1)	0.032(2)	0.024(1)	-.001(1)	-.002(1)	0.001(1)
P-B	0.1813(3)	0.1038(7)	0.3209(1)	0.028(1)	0.026(2)	0.030(1)	0.003(2)	-.001(1)	0.003(1)
Na-3	0.3440(1)	0.5974(13)	0.2961(2)	0.065(3)	0.057(5)	0.069(3)	-.002(4)	-.010(2)	-.003(3)
Na-4	0.3451(6)	0.5251(16)	0.4567(2)	0.059(3)	0.061(6)	0.082(3)	-.001(3)	0.001(2)	0.011(4)
Na-7	0.0099(4)	0.5552(11)	0.3804(1)	0.050(3)	0.046(5)	0.049(2)	0.005(3)	-.006(2)	0.000(2)
Na-8	0	$\frac{1}{2}$	0	0.042(3)	0.041(3)	0.036(3)	-.001(3)	-.009(2)	0.006(3)
Na-9	0	0.6018(20)	$\frac{1}{4}$	0.081(4)	0.060(6)	0.062(4)	-	-.010(3)	-
O-CE	0.1371(7)	-.0363(19)	0.3722(2)	0.059(4)	0.061(8)	0.032(3)	-.026(6)	-.005(3)	0.006(4)
O-A1	0.1513(10)	0.2849(23)	0.4379(4)	0.072(6)	0.040(9)	0.097(7)	0.008(8)	-.001(5)	-.001(6)
O-A2	0.0772(25)	-.1489(25)	0.4542(3)	0.052(5)	0.071(10)	0.064(5)	-.033(6)	-.000(4)	0.016(5)
O-A3	0.3255(6)	-.0580(22)	0.4366(3)	0.036(4)	0.044(10)	0.075(5)	0.004(5)	-.011(3)	0.009(6)
O-B1	0.0731(9)	0.2931(18)	0.3105(3)	0.060(5)	0.060(8)	0.049(4)	0.034(6)	-.002(4)	-.003(5)
O-B2	0.1721(11)	-.0926(23)	0.2826(3)	0.128(8)	0.056(8)	0.049(5)	-.007(9)	0.000(4)	-.024(5)
O-B3	0.3264(8)	0.2023(21)	0.3285(3)	0.048(5)	0.086(11)	0.083(6)	-.022(6)	-.012(4)	0.054(6)

* U_{ij}'s in Å^2 are computed from $\beta_{ij} = 2\pi^2 \underline{b}_i \cdot \underline{b}_j U_{ij}$ where $T = \exp - \beta_{11}h^2 + \ldots + 2\beta_{12}hk + \ldots$ appears in the structure factor expression and $\underline{b}_i$ are the reciprocal lattice cell vectors.

TABLE VII.2

TABLE OF OBSERVED AND CALCULATED STRUCTURE FACTORS OF NA4P2O7 AT 410 DEGREES C.

UNOBSERVED REFLECTIONS ARE MARKED WITH * AND UNRELIABLE REFLECTIONS WITH + .

K = 0

H	L		IF-OI	IF-CI
8	0		198	181
8	-6		81	94
8	-8		419	398
6	0		759	781
6	-6		214	199
6	-8		182	181
6	-10		65	80
6	-14		87	87
6	-16		276	247
6	-20		136	139
4	-2		61	55
4	-6		121	120
4	-8		389	346
4	-10		104	104
4	-12		96	89
4	-14		92	87
4	-16		109	129
4	-18		331	327
4	-22		113	131
4	-26		133	131
2	26		77	67
2	16		116	123
2	12		167	166
2	-2		421	392
2	-4		51	17
2	-6		59	21
2	-8		859	856
2	-10		230	262
2	-12		42	32
2	-14		63	69
2	-16		66	69
2	-18		350	359
2	-20		214	223
2	-22		67	97
2	-24		62	60
2	-26		189	205
2	-28		140	145
0	10	+	64	81
0	8		963	940
0	-16		598	578
0	-18		127	122
0	-20		228	199
0	-24		119	115
0	-28		193	180
-2	0		299	253
-2	-2		540	523
-2	-4		126	120
-2	-8		689	640
-2	-10		48	62
-2	-14		216	221
-2	-18		369	373
-2	-20		148	155
-2	-22		95	97
-2	-24		120	126
-4	0		387	367
-4	-2		53	30
-4	-6		199	181
-4	-8		744	705
-4	-10		337	348
-4	-12		273	275
-4	-14		252	244
-4	-18		239	227
-4	-22		57	99
-4	-26		210	213
-6	-2		150	150
-6	-4		104	103
-6	-6		83	85
-6	-8		204	201
-6	-10		66	68
-6	-12		176	168
-6	-16		225	226
-6	-18		81	116
-6	-20		174	176
-8	-2		57	63
-8	-6		123	139
-8	-8		334	319
-8	-12		159	157

K = 1

H	L		IF-OI	IF-CI
11	20		74	82
11	8		97	106
11	2		28	45
11	0		33	49
9	28		72	75
9	20		36	41
9	19		43	47
9	18		46	56
9	16		51	66
9	11		46	62
9	10		40	51
9	8		39	55
9	6		75	82
9	5		48	39
9	3		93	101
9	2		140	142
9	1		48	47
7	26		133	140
7	25		46	48
7	23		40	41
7	22		53	50
7	19		35	38
7	18		120	124
7	17		124	118
7	16		47	38
7	15		93	97
7	14		51	65
7	13		46	57
7	12		142	144
7	11		108	108
7	10		298	302
7	9		115	114
7	8		149	146
7	6		113	115
7	5		34	33
7	4		50	37
7	3		122	132
7	2		121	124
7	1		88	83
5	28		100	90
5	26		85	83
5	25		32	31
5	24		93	79
5	23		70	77
5	22		63	80
5	20		166	168
5	18		342	351
5	17		106	100
5	16		87	96
5	15		81	90
5	14	*	15	2
5	13	*	28	27
5	12		169	172
5	10		182	192
5	9		200	207
5	8		318	310
5	7		178	170
5	6		175	176
5	5	*	21	15
5	4	*	20	12
5	3		108	115
5	2		284	315
5	1		23	38
5	0		35	21
3	28		155	150
3	27		44	31
3	26	*	28	29
3	25	*	26	14
3	24		106	101
3	23		62	57
3	21		32	30
3	20		133	134
3	18		68	55
3	17		92	81
3	16		257	264
3	15		86	85
3	14	*	28	23
3	13	*	22	20
3	12		58	58
3	11		46	48
3	10		38	29
3	9		41	45
3	8		40	28
3	7		16	6
3	6		115	112
1	28		52	44
1	27		79	58
1	26		185	192
1	25	*	25	18
1	24		32	4
1	23		54	45
1	22		71	82
1	20		26	44
1	19		106	112
1	18		264	297
1	17		90	92
1	16		133	135
1	15		101	99
1	14		94	94
1	12		424	357
1	11		319	278
1	10		457	448
-1	28		35	43
-1	27	*	26	16
-1	26		121	126
-1	25		127	123
-1	24		61	47
-1	23		64	71
-1	22		167	166
-1	20		139	126
-1	19		140	128
-1	18		464	455
-1	17		282	277
-1	16		189	188
-1	15		60	61
-1	14	*	18	8
-1	12		52	21
-1	11		264	313
-1	10		212	212
-3	28		134	128
-3	27		49	46
-3	26		106	103
-3	24		124	118
-3	23		46	48
-3	22		28	15
-3	20		177	169
-3	19		57	48
-3	18		41	32
-3	17		97	108
-3	16		231	229
-3	15		208	200
-3	14		30	27
-3	13		39	46
-3	12		139	142
-3	11		131	137
-3	10		248	247
-3	9		130	123
-3	8		67	76
-3	7		86	98
-3	6		112	106
-5	28		97	88
-5	26		101	94
-5	25		35	34
-5	24		82	89
-5	22		57	67
-5	21		30	26
-5	20		81	82
-5	18		187	193
-5	17		118	110
-5	15		45	36
-5	14		47	47
-5	13		43	40
-5	12		81	66
-5	11		53	70
-5	10		148	151
-5	9		114	103
-5	8		453	463
-5	7		82	83
-5	6		139	138
-5	5		123	130
-5	4	*	25	16
-5	3		40	43
-5	2		82	75
-5	1		119	117
-7	26		96	96
-7	23		32	30
-7	22		32	37
-7	19		61	59
-7	18		232	225
-7	17		31	30
-7	16		84	80
-7	13		77	66
-7	12		26	34
-7	11		87	72
-7	10		260	246
-7	9		120	119
-7	8		82	82
-7	7		71	60
-7	6		135	138
-7	5		156	158
-7	3		38	24
-7	2		186	192
-9	28		40	47
-9	26		65	63
-9	20		63	59
-9	18		36	47
-9	17		56	58
-9	16		93	94
-9	11		56	61
-9	10		98	98
-9	9		43	48
-9	8		53	73
-9	6		108	100
-9	5		53	65
-9	4		36	25
-9	3		94	88
-9	2		81	82
-9	1		92	79
-9	0		225	230
-11	8		124	121

K = 2

H	L		IF-OI	IF-CI
12	-1		66	71
10	-2		29	39
10	-3		52	54
10	-5		37	46
10	-6		40	40
10	-9		61	60
10	-10		61	61
10	-14		40	46
10	-15		34	25
10	-16		59	57
10	-17		27	30
10	-18		59	58
10	-19		55	63
10	-24		34	31
10	-25		38	39
10	-26		26	30
8	-2		85	99
8	-3		47	39
8	-5		43	60
8	-6		154	153
8	-7		95	94
8	-8		174	180
8	-9		51	48
8	-10		89	94
8	-12		65	56
8	-13		86	87
8	-14		80	74
8	-16		35	31
8	-18		36	42
8	-19		66	68
8	-20		45	43
8	-21		60	67
8	-22		68	67
8	-23		35	38
8	-24		60	58
8	-27		71	64
8	-29		55	55
8	-30		27	23
6	-1		307	333
6	-3		145	146
6	-4		81	66
6	-6		161	164
6	-7		152	144
6	-8		97	106
6	-9		101	107
6	-10		63	76
6	-13		55	54
6	-14		79	63
6	-15		142	141
6	-16		168	162
6	-17		80	92
6	-19		33	36
6	-20		88	82
6	-21		76	75
6	-23		25	27
6	-24		33	29
6	-26		85	85
6	-28		53	55
6	-29		72	65
4	-12		39	74
4	-14		34	43
4	-15	+	24	26
4	-16		133	128
4	-17		107	106
4	-18		230	234
4	-19		124	129
4	-20		40	48
4	-21		38	31
4	-22		54	54
4	-23		46	46
4	-24		23	35
4	-25		68	76
4	-26		56	64
4	-27		39	37
4	-29		25	25
4	-30		26	30
4	-31		26	16
4	-32		45	53
2	-17		156	160
2	-18		102	99
2	-19		109	97
2	-20	+	25	20
2	-21		62	63
2	-22		123	142
2	-24		104	120
2	-25		69	67
2	-26		60	53
2	-27		79	84
2	-28		46	37
2	-29		31	15
2	-30		43	48
2	-31		53	57
2	-33		57	50
2	-34		50	20
0	0		657	696
0	-1		317	328
0	-2		309	307
0	-3		226	219
0	-4		43	33
0	-5		269	267
0	-6		254	239
0	-7		75	70
0	-8		136	136
0	-9		109	118
0	-11		53	49
0	-12		108	113
0	-13		251	268
0	-14		180	175
0	-15		202	206
0	-16		210	212
0	-17		112	117
0	-18	+	34	37
0	-19		50	40
0	-20		137	137
0	-21		61	60
0	-22		62	52
0	-23		91	45
0	-24		82	80
0	-26		81	88
0	-27		72	69
0	-28		108	105
0	-29		68	73
0	-30		40	34
0	-33		54	48
-2	-16		113	107
-2	-20		99	110
-2	-21		109	111
-2	-22		99	109
-2	-23		71	75
-2	-24		44	42
-2	-25		80	83
-2	-26		58	61
-2	-27		24	16
-2	-28		54	53
-2	-29		55	58
-2	-30		25	28
-2	-32		55	64
-2	-34		65	79
-4	-12		79	81
-4	-13		35	34
-4	-14		75	89
-4	-15		124	132
-4	-17		186	183
-4	-18		84	81
-4	-19		72	80
-4	-20		37	50
-4	-21		39	45
-4	-22		43	68
-4	-25		68	71
-4	-26		94	104
-4	-27		73	77
-4	-28		25	20
-4	-30		68	63
-4	-31		67	67
-4	-33		44	39
-6	-1		161	165
-6	-2		213	205
-6	-3		64	59
-6	-4		79	85
-6	-5		101	89
-6	-7		166	169
-6	-8	+	99	87
-6	-9		34	44
-6	-10		51	36
-6	-12		46	39
-6	-13		149	145
-6	-14		79	88
-6	-15		184	179
-6	-16		164	159
-6	-18		23	18
-6	-19		43	45
-6	-20		24	37
-6	-21		36	39
-6	-22		47	47
-6	-23		25	24
-6	-25		43	29
-6	-26		37	52
-6	-27		37	36
-6	-28		80	81
-6	-29		44	45
-6	-30		49	50
-6	-33		41	40
-6	-33		41	40
-8	-1		58	67
-8	-4		29	16
-8	-5		124	119
-8	-6		66	73
-8	-7		124	116
-8	-8		137	137
-8	-9		134	127
-8	-12		66	67
-8	-13		82	83
-8	-14		54	53
-8	-15		40	40
-8	-17		66	78
-8	-18		94	101
-8	-20		64	71
-8	-21		71	70
-8	-23		37	38
-8	-24		34	28
-8	-26		27	25
-8	-27		27	18
-8	-28		41	44
-8	-29		27	26
-10	-1		45	42
-10	-2		39	37
-10	-3		37	27
-10	-4		39	36
-10	-5		42	1
-10	-7		29	27
-10	-8		46	46
-10	-9		41	47
-10	-9		41	47
-10	-10		135	128
-10	-12		57	63
-10	-13		34	38
-10	-14		36	27
-10	-15		38	37
-10	-17		59	59
-10	-18		38	35
-10	-20		27	18
-10	-21		27	33
-10	-24		29	30
-10	-25		33	34
-10	-26		45	53
-12	-2		86	80

K = 4

H	L		IF-OI	IF-CI
0	0		64	66
0	-1		175	180
0	-2		350	341
0	-3		64	74
0	-4		69	64
0	-5		38	36
0	-6		148	148
0	-7		69	80
0	-9		96	67
0	-10		79	87
0	-11		49	44
0	-12		40	39
0	-14		205	195
0	-15		131	132
0	-16		64	63

K = -1

H	L		IF-OI	IF-CI
3	0		995	1069
1	0		149	146

K = -2

H	L		IF-OI	IF-CI
6	0		393	410
2	20		122	110
2	19		138	133
2	18		293	305
2	17		144	146
2	15		112	98
2	14		69	76
2	13		203	200
2	12	*	25	27
2	11		201	205
2	10		33	34
2	9		342	343
2	8		303	300
2	7		509	551
2	6		189	180
2	5		256	275
2	4		204	200
2	2		55	67
2	1	+	104	98
2	0	+	82	70
2	-1		150	152
2	-2		31	60
2	-3		76	74
2	-4		105	109
2	-5		114	99
2	-6		453	469
2	-7		230	237
2	-8		495	498
2	-9		75	64
2	-10		135	136
2	-11		198	211
2	-12		55	52
2	-14		205	193
2	-15	*	25	22
2	-16		73	75

K = -4

H	L		IF-OI	IF-CI
2	18		96	95
2	17		128	117
2	16		188	197
2	15		72	75
2	12		109	107
2	10		139	141
2	9		255	238
2	8		124	122
2	6		172	171
2	4		95	108
2	3		56	50
2	-1		150	153
2	-2		118	126
2	-4		105	98
2	-6		237	233
2	-7		181	177
2	-8		169	166
2	-9		85	92
2	-10		184	187
2	-11		161	161
2	-12		97	93
2	-16		132	135
2	-17		112	99

7.6. Description of the Structure

The structure of sodium pyrophosphate at 410 °C. consists of diphosphate ions formed by a pair of PO_4^{3-} groups sharing a bridging oxygen atom with a P-O-P angle of 132.4(6)°. The P-P vector is at an angle of 12.3° to the c axis in contrast to the room-temperature structure where the angle is only 5°. The oxygen atoms of the anion are in a staggered configuration as viewed down the c axis, Fig. 7.6.1. For a perfect staggered configuration, the dihedral angle between the planes formed by the two phosphorus atoms and two corresponding terminal oxygen atoms on either side of the anion should be 60° while those of a semi-eclipsed and a total eclipsed configuration are 30° and 0° respectively. In the present structure, the average dihedral angle is 65° and that of room temperature is 32°.

The sodium chain which has been a distinctive feature in the room-temperature structure, now becomes a "band" spreading out in the b direction (Figs. 7.6.1 - 2) over a width of about 0.5 Å.

The P-O bridging bond lengths at either end of the anion differ significantly from each other, being 1.577 and 1.644 Å while the individual terminal P-O bond lengths do not differ very much from each other and their averages are 1.485 and 1.477 Å, TABLE VII.3. These figures, although still within the averages of 1.56 - 1.68 (±8) Å for the bridging bond and 1.43 - 1.52 (±8) Å for the terminal bond [39],

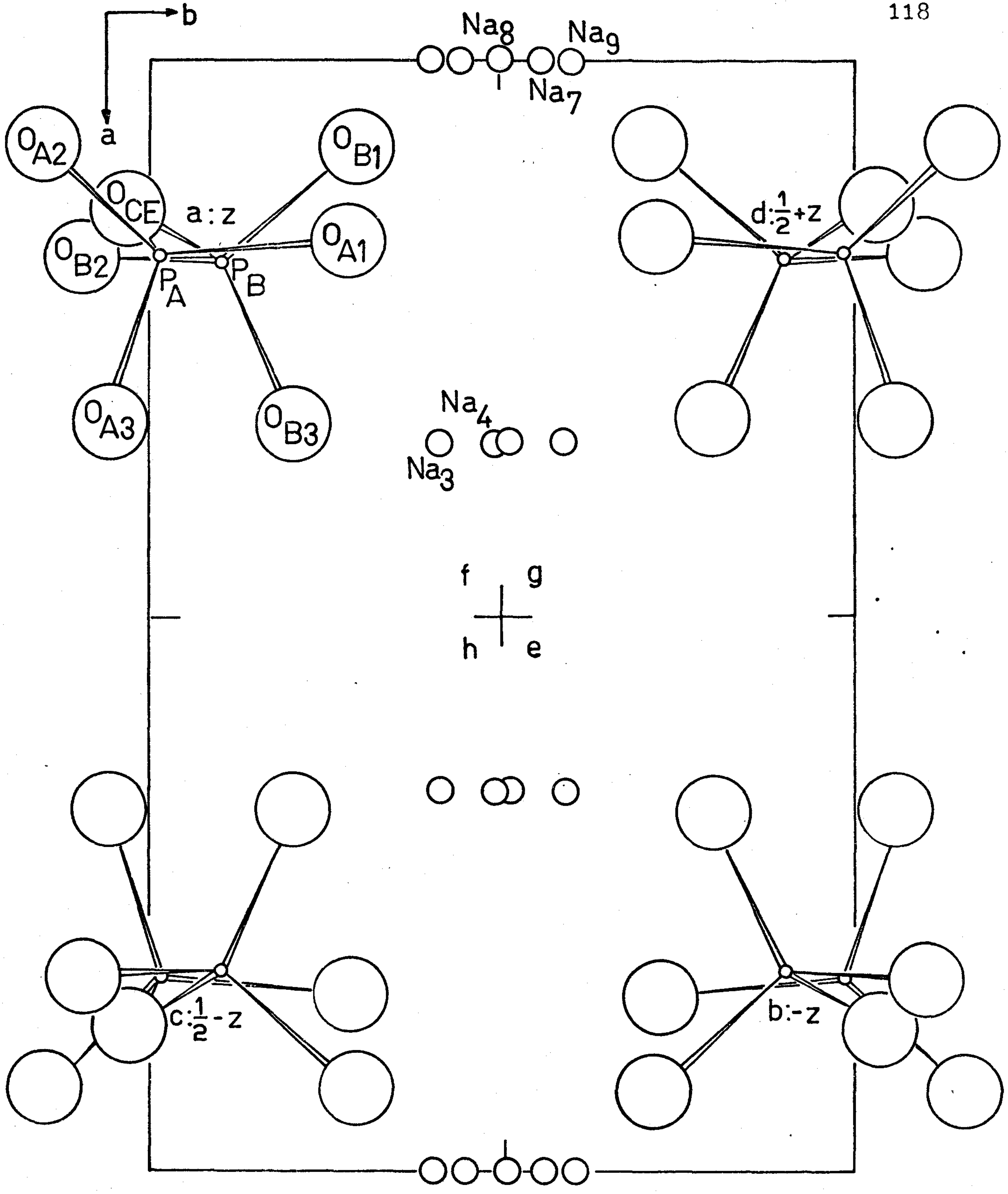

Fig. 7.6.1. The structure of $Na_4P_2O_7$ at 410°C. projected onto the a b plane. Equivalent molecules e, f, g, h corresponding to a, b, c, d by the C-centering operation are omitted for clarity.

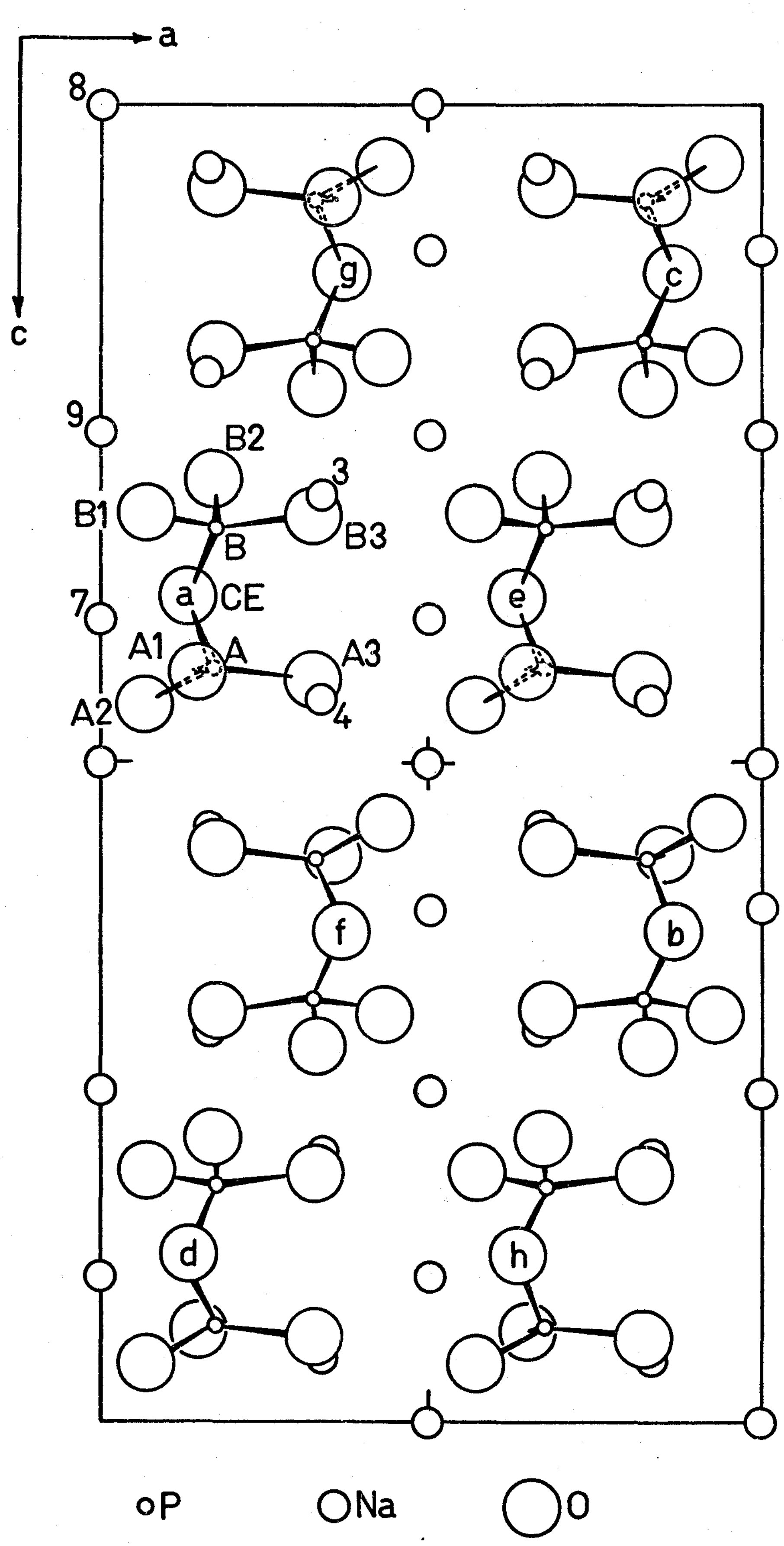

Fig. 7.6.2. Structure of $Na_4P_2O_7$ at 410°C. projected onto the <u>a c</u> plane.

are at variance with the values of the room-temperature structure and it is suspected that some type of thermal motion might be present in the system. For a libration type of motion, Fig. 7.6.3 shows why the apparent (observed) bond lengths are shorter than the actual bond lengths in a simple case where a tetrahedron of the anion undergoes libration about its own phosphorus atom. Fuller discussion of libration of the present system will be given in the next section.

The molecular goemetry of each of the phosphorus and sodium atoms is shown in TABLE VII.3. Na(3) is bonded to four oxygen atoms two of which belong to the same side of the anion while each of the remaining two belongs to a different anion. Na(4) is also bonded to four oxygen atoms belonging to three anions. The sodium band consists of three inequivalent sodium atoms, one of which, Na(7), lies on a general position with the x and y coordinates being close to 0 and $\frac{1}{2}$ respectively. This sodium atom is bonded to six oxygen atoms, four being contributed by a single anion and the remaining two by another. The other two sodium atoms in the band lie in special positions: Na(8) on a centre of symmetry and bonded to six oxygen atoms arising from the terminal oxygen atoms of three different anions, and Na(9) on a two-fold axis and also bonded to six oxygen atoms.

One of the terminal oxygen atoms, O(B2), which is bonded to the phosphorus atom, P(B), has an abnormally high temperature factor while the analogous oxygen atom in the

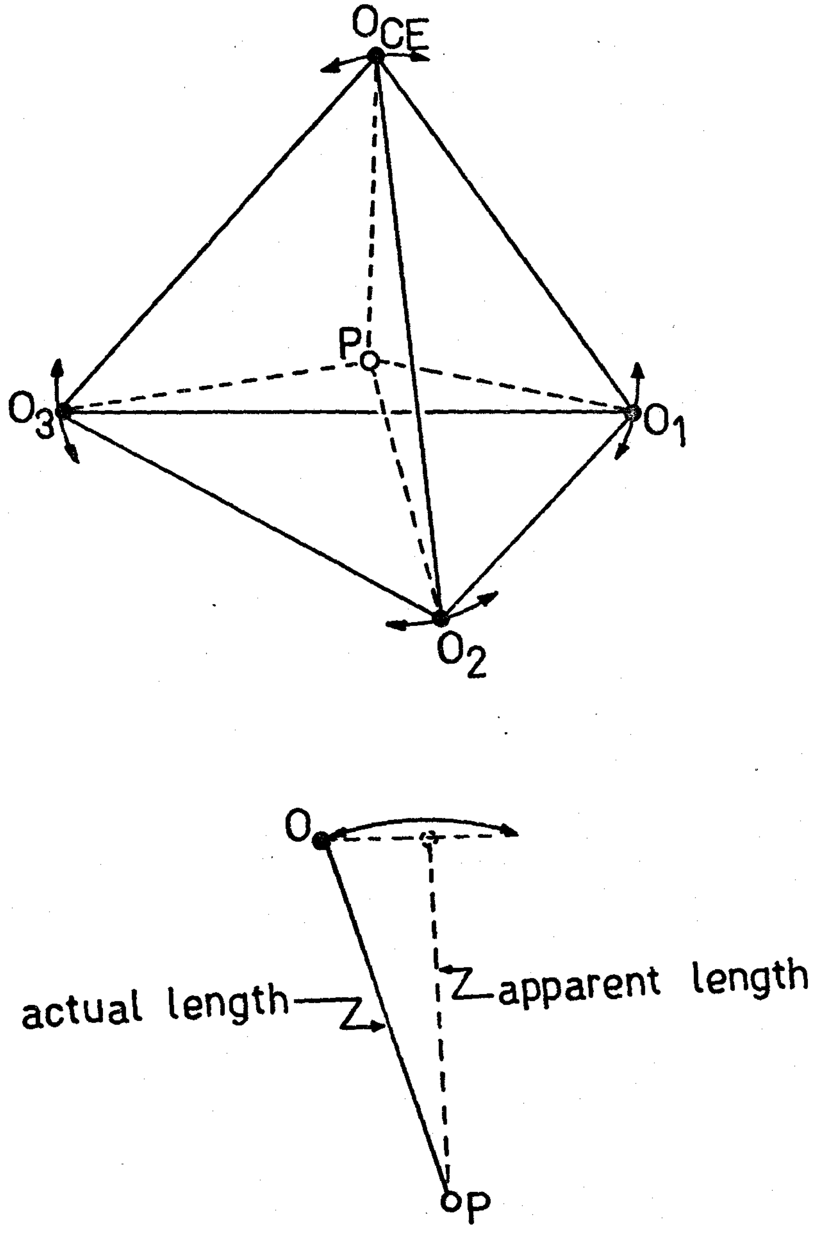

Fig. 7.6.3

Apparent Shortening of Bond Lengths due to Libration

TABLE VII.3

Bond Distances and Angles in $Na_4P_2O_7$ at 410 °C.

Distance*	(Å)	Angle	(°)	Angle	(°)
P(A)-O(CE)	1.577(6)	O(CE)-P(A)-O(A1a)	107.6(6)	O(A1a)-P(A)-O(A2a)	113.8(6)
-O(A1a)	1.507(13)	-O(A2a)	102.7(5)	-O(A3a)	112.6(6)
-O(A2a)	1.473(11)	-O(A3a)	107.1(4)	O(A2a)-P(A)-O(A3a)	112.3(6)
-O(A3a)	1.475(7)				
P(B)-O(CE)	1.644(3)	O(CE)-P(B)-O(B1a)	107.1(5)	O(B1a)-P(B)-O(B2a)	109.9(6)
-O(B1a)	1.468(10)	-O(B2a)	104.1(6)	-O(B3a)	114.1(6)
-O(B2a)	1.486(11)	-O(B3a)	107.7(5)	O(B2a)-P(B)-O(B3a)	113.2(6)
-O(B3a)	1.476(9)				
P(A)-P(B)	2.947(3)	P(A)-O(CE)-P(B)	132.4(6)		
Na(3)-O(B2g)	2.366(11)	O(B2g)-Na(3)-O(B3a)	86.2(4)	O(B3a)-Na(3)-O(B2a)	131.4(4)
-O(B3a)	2.322(13)	-O(B2a)	98.3(4)	-O(B1e)	114.6(4)
-O(B2a)	2.356(13)	-O(B1e)	111.7(4)	O(B2a)-Na(3)-O(B1e)	108.5(5)
-O(B1e)	2.425(10)				
Na(4)-O(A1a)	2.288(13)	O(A1a)-Na(4)-O(A3a)	116.3(4)	O(A3a)-Na(4)-O(A2f)	89.1(4)
-O(A3a)	2.332(14)	-O(A2f)	124.0(4)	-O(A2e)	116.4(4)
-O(A2f)	2.586(10)	-O(A2e)	119.6(6)	O(A2f)-Na(4)-O(A2e)	83.8(3)
-O(A2e)	2.382(11)				
Na(7)-O(A1a)	2.494(12)	O(A1a)-Na(7)-O(A3e)	80.8(3)	O(A3e)-Na(7)-O(B1a)	122.0(4)
-O(A3e)	2.414(8)	-O(B1a)	90.2(4)	-O(CE)	128.9(4)
-O(B1a)	2.451(10)	-O(CE)	108.9(3)	-O(A2a)	80.9(3)
-O(CE)	2.531(11)	-O(A2a)	76.9(4)	-O(B3e)	86.1(3)
-O(A2a)	2.625(11)	-O(B3e)	161.5(4)	O(B1a)-Na(7)-O(CE)	108.4(3)
-O(B3e)	2.339(9)	O(CE) -Na(7)-O(A2a)	55.0(3)	-O(A2a)	80.9(3)
		-O(B3e)	89.5(4)	-O(B3e)	85.7(3)
		O(A2a)-Na(7)-O(B3e)	114.0(4)		

(continued)

TABLE VII.3 (Continued)

Distance*	(Å)	Angle	(°)	Angle	(°)
Na(8)-O(A1c)	2.517(11)	O(A1c)-Na(8)-O(A2d)	99.2(4)	O(A2d)-Na(8)-O(A3g)	93.1(3)
-O(A2d)	2.395(12)	-O(A3g)	81.3(3)	-O(A1d)	80.8(4)
-O(A3g)	2.364(7)	-O(A1d)	180.0(5)	-O(A2c)	86.9(3)
-O(A1d)	2.517(11)	-O(A2c)	80.8(4)	-O(A3h)	180.0(5)
-O(A2c)	2.395(12)	-O(A3h)	98.7(3)	O(A3g)-Na(8)-O(A1d)	98.7(3)
-O(A3h)	2.364(7)	O(A1d)-Na(8)-O(A2c)	99.2(4)	-O(A2c)	86.9(3)
		-O(A3h)	81.3(3)	-O(A3h)	180.0(5)
		O(A2c)-Na(8)-O(A3h)	93.1(3)		
Na(9)-O(B1a)	2.428(12)	O(B1a)-Na(9)-O(B1c)	92.7(5)	O(B1c)-Na(9)-O(B2a)	151.3(3)
-O(B1c)	2.428(12)	-O(B2a)	92.9(3)	-O(B2c)	92.9(3)
-O(B2a)	2.464(14)	-O(B2c)	151.3(3)	-O(B3e)	119.3(3)
-O(B2c)	2.464(14)	-O(B3e)	77.4(3)	-O(B3g)	77.4(3)
-O(B3e)	2.766(9)	-O(B3g)	119.3(3)	O(B2a)-Na(9)-O(B2c)	95.5(5)
-O(B3g)	2.766(9)	O(B2c)-Na(9)-O(B3e)	75.3(3)	-O(B3e)	89.4(4)
		-O(B3g)	89.4(4)	-O(B3g)	75.3(3)
		O(B3e)-Na(9)-O(B3g)	157.3(6)		

Transformations: $a = x, y, z$ $e = \frac{1}{2}+x, \frac{1}{2}+y, z$
$b = \overline{x}, \overline{y}, \overline{z}$ $f = \frac{1}{2}-x, \frac{1}{2}-y, \overline{z}$
$c = \overline{x}, y, \frac{1}{2}-z$ $g = \frac{1}{2}-x, \frac{1}{2}+y, \frac{1}{2}-z$
$d = x, \overline{y}, \frac{1}{2}+z$ $h = \frac{1}{2}+x, \frac{1}{2}-y, \frac{1}{2}+z$

* Includes all interactions less than 3.0 Å.

room-temperature structure vibrates normally. It is of some interest to compare the molecular geometry of this particular oxygen atom in the two structures. Fig. 7.6.4 shows the pyrophosphate groups at similar locations in the two structures (a) at 22°C. and (b) at 410°C. at the same level up the c axis. Although the pyrophosphate groups in each structure are related by different symmetry operations: namely, 2_1 in Case (a) and C-centering in Case (b), it is evident from Fig. 7.6.4 that the gross feature of the pyrophosphate group I' of Case (b) could be obtained from I of Case (a) by translating the tetrahedron of B for about 0.5 Å along the b axis, keeping the tetrahedron of A fixed and then rotating the bridging oxygen atom through 120° about an axis through A parallel to axis c. In this state of rearrangement, terminal oxygen atom O(B2) undergoes great bond geometry changes as shown in Figs. 7.6.5 - 6. The major change is that the bond Na(1)-O(B2) in the room-temperature structure is broken and a new bond Na(3')-O(B2) is formed instead. If we assume that both geometric configurations of O(B2), i.e. one with the Na(1)-O(B2) bond and the other with the Na(3')-O(B2) bond, correspond to local minima of energy, it is highly probable that in the structure at 410°C. O(B2) is resonating between the two configurations, resulting in the large observed amplitude of thermal vibration. An electron difference Fourier for the structure at 410°C. in the final stage showed that there was indeed a residual peak about one-fifth of an oxygen

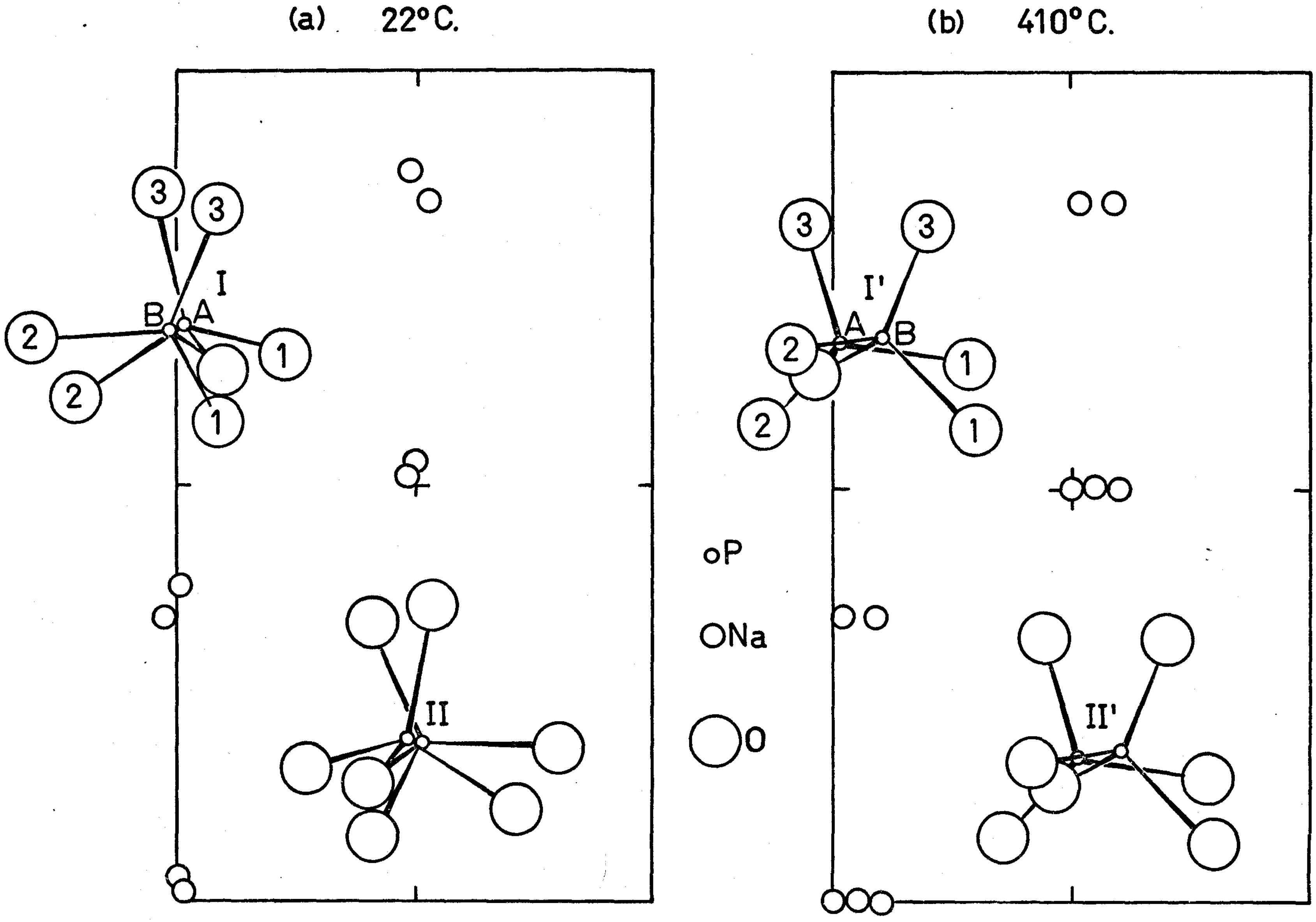

Fig. 7.6.4. Arrangements of pyrophosphate anions of two structures of $Na_4P_2O_7$ at the same level up the c axis.

Fig. 7.6.5

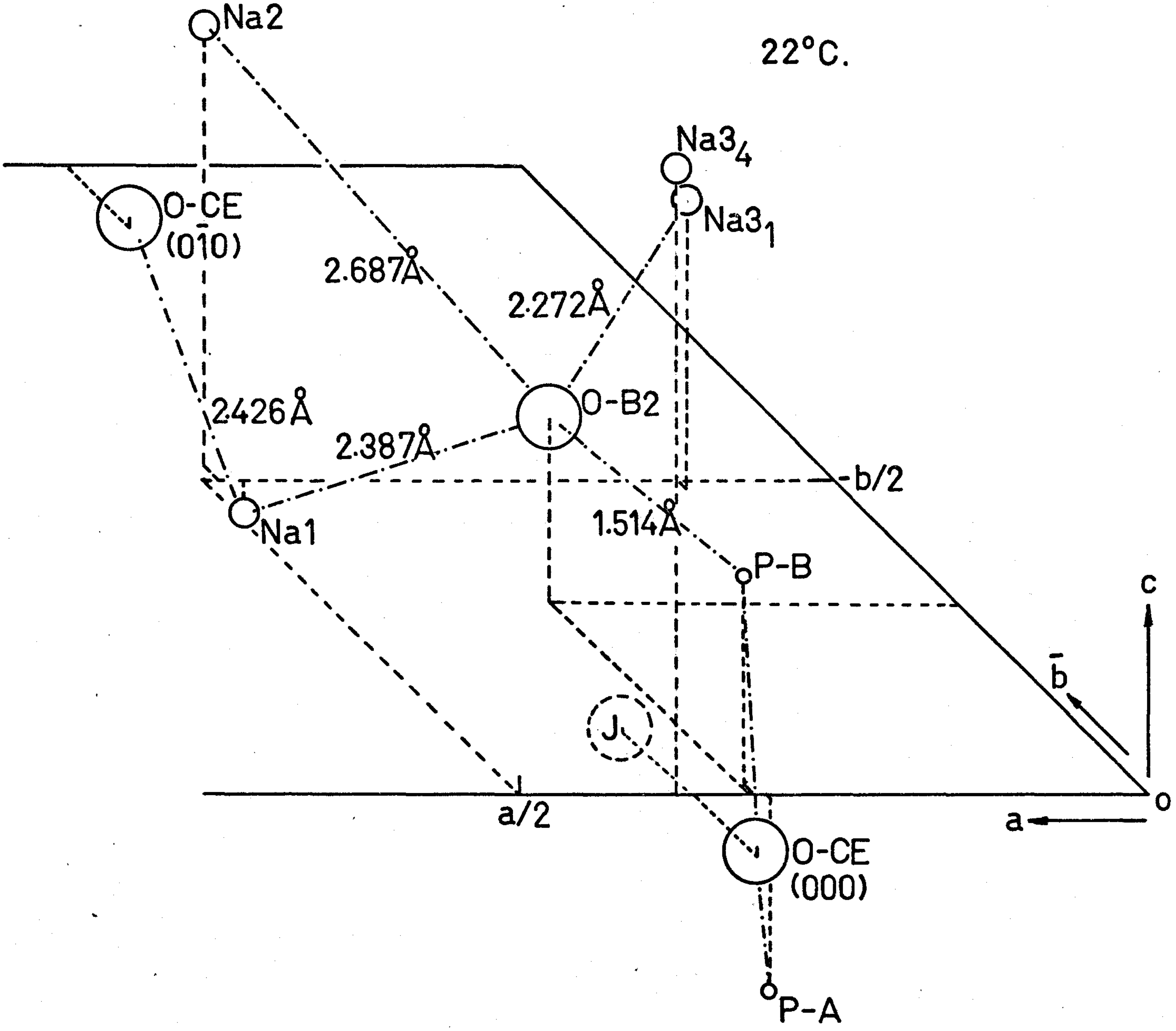

Environment of Oxygen Atom O(B2) at 22°C.

Fig. 7.6.6

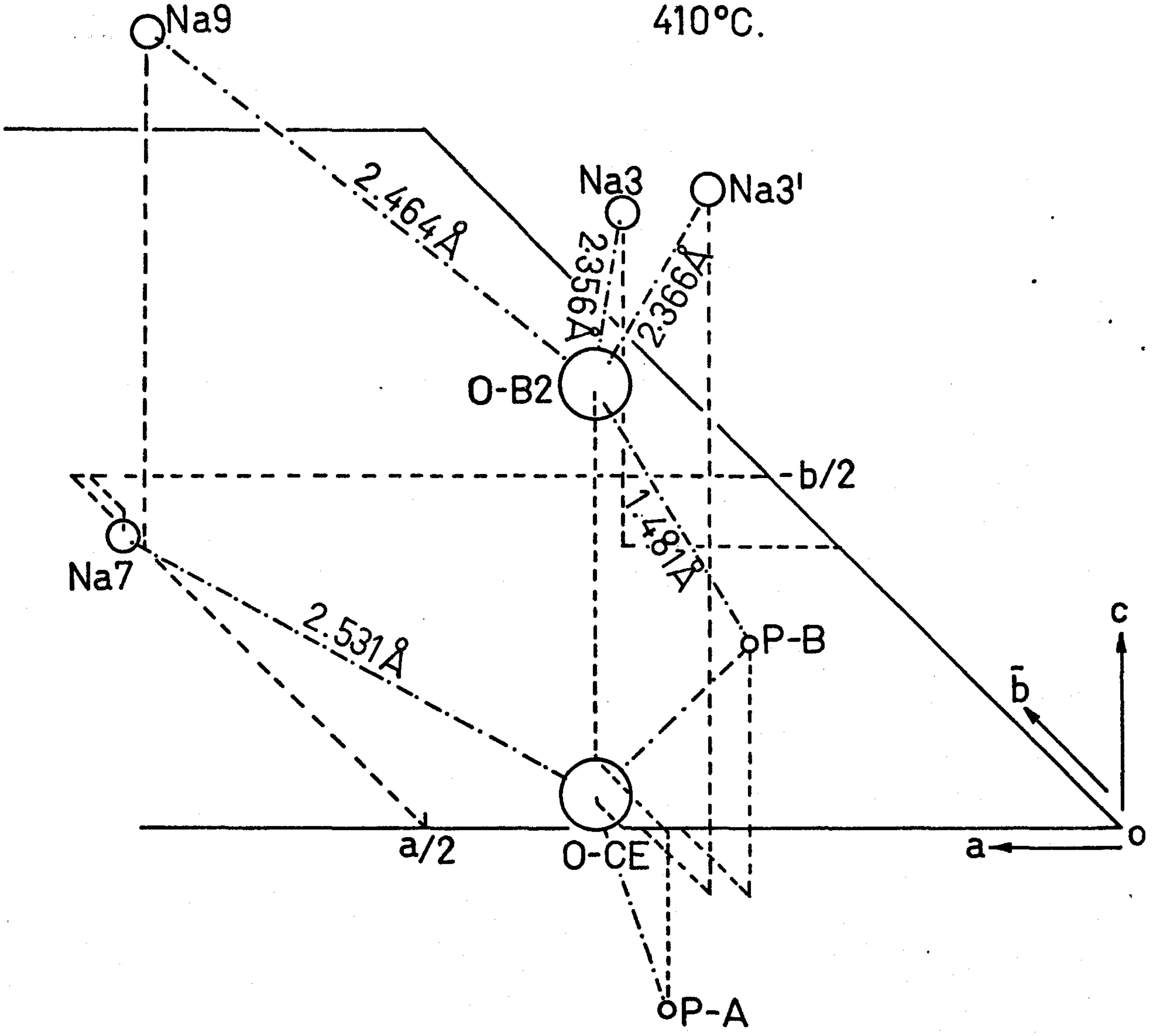

Environment of Oxygen Atom O(B2) at 410°C.

atom at a position corresponding to the configuration with the Na(1)-O(B2) bond. This is then evidence of configurational disorder and further refinement on the structure might be made by using a computer program known as REFINE written by Finger [40] in which the occupancy of a disordered site can be refined along with the rest of the structure.

7.7. Rigid-Body Motion

The effect of thermal motion of atoms on interatomic distances has been discussed by a number of authors: Cruickshank [41] , Busing and Levy [42] , Schomaker and Trueblood [43] , Pawley and Willis [44] , and Johnson [45] . More recently, Scheringer [46] gave a lattice-dynamic treatment of the thermal-motion correction on the bond length. For some known models of thermal motion, he was able to obtain simple expressions in terms of atomic positions, the translational tensor, **T**, and the librational tensor, **L**. A third tensor, **S**, introduced by Schomaker and Trueblood [43] to account for correlationas of libration and translation, is not necessary when the correction is on bond lengths between atoms of the same rigid body. His treatment is as follows.

If **T**, **L**, and **S** are the rigid-body tensors, then the vibration tensor $\mathbf{U}_{\underline{r}}$ of an atom at $\underline{r} = (r_1, r_2, r_3)$ referred to a chosen origin in the system could be expressed as

$$\mathbf{U}_{\underline{r}} = \mathbf{T} + \mathbf{V}_{\underline{r}}\mathbf{L}\mathbf{V}_{\underline{r}}' - \mathbf{V}_{\underline{r}}\mathbf{S} - (\mathbf{V}_{\underline{r}}\mathbf{S})' \tag{7.7.1}$$

where $\mathbf{V}_{\underline{r}}$ is the antisymmetric tensor given by

$$(7.7.2) \qquad \mathbf{V}_{\underline{r}} = \begin{pmatrix} 0 & -r_3 & r_2 \\ r_3 & 0 & -r_1 \\ -r_2 & r_1 & 0 \end{pmatrix}$$

The coupling tensors $\mathbf{U}_{\underline{rs}}$ for the rigid-body motion are now obtained by substituting the atom $\underline{s}$ in Equation (7.7.1) for half the positions of the atom $\underline{r}$. Thus,

$$(7.7.3) \qquad \mathbf{U}_{\underline{rs}} = \mathbf{T} + \mathbf{V}_{\underline{r}}\mathbf{L}\mathbf{V}'_{\underline{s}} - \mathbf{V}_{\underline{r}}\mathbf{S} - (\mathbf{V}_{\underline{s}}\mathbf{S})' .$$

We define

$$(7.7.4) \qquad \mathbf{A}_{\underline{rs}} = \mathbf{U}_{\underline{r}} + \mathbf{U}_{\underline{s}} - \mathbf{U}_{\underline{rs}} - \mathbf{U}'_{\underline{rs}} .$$

From Equations (7.7.1) and (7.7.3), we have, on simplification,

$$(7.7.5) \qquad \mathbf{A}_{\underline{rs}} = (\mathbf{V}_{\underline{r}} - \mathbf{V}_{\underline{s}})\mathbf{L}(\mathbf{V}_{\underline{r}} - \mathbf{V}_{\underline{s}})' .$$

Busing and Levy [42] has shown that the time and lattice average of a bond length in the quadratic approximation is given by

$$(7.7.6) \qquad d_{\text{corrected}} = d + (\overline{r^2} - \overline{z^2})/2d$$

where d is the distance between the mean positions of the atoms, $\overline{r^2}$ is the sum of the relative mean-square displacements of the atoms $\underline{r}$ and $\underline{s}$ along the three axes of the Cartesian reference system, and $\overline{z^2}$ is the relative mean square displacement of the atoms $\underline{r}$ and $\underline{s}$ in the direction of the bond vector $\underline{d}$.

In terms of the matrix elements of $\mathbf{A}_{\underline{rs}}$, Scheringer has shown that

$$(7.7.7) \qquad \overline{r^2} = \text{trace}\ (\mathbf{A}_{\underline{rs}})$$

$$(7.7.8) \qquad \overline{z^2} = \underline{d}'\,\mathbf{A}_{\underline{rs}}\,\underline{d} / d^2$$

For the model of rigid-body motion, $\mathbf{A}_{\underline{rs}}$ is always given by Equation (7.7.5) and as such, Equation(7.7.8) is identically zero since the matrix product $(\mathbf{V}_{\underline{r}} - \mathbf{V}_{\underline{s}})\underline{d}$ corresponds to the vector product $\underline{d} \wedge \underline{d}$. Hence, the correction depends only on the libration tensor **L**, We shall describe below how **L** is determined.

7.8. Evaluation of **L**

Determination of the tensor **L** depends on a proper choice of the position of the centre of libration for the molecule in motion. In the present case, the librating group is the pyrophosphate anion, P_2O_7 and the centre of libration is chosen to coincide with its centre of mass. Cruickshank [47] has given equations for the evaluation of the components L_{ij} of **L** and the components T_{ij} of the translational vibration tensor **T** of the centre of mass in terms of the coordinates (x,y,z) of each atom in the molecule and its thermal parameters (U_{ij}).

Since the angle β of the system is 93°, it could be taken as close to 90° so that the atomic coordinates and thermal parameters in TABLE VI.1 could be used directly after a translation to an orthogonal coordinate system at the centre of libration. Components of the tensors **T** and **L** are shown in TABLE VII.4, and the corrected P-O bond lengths of the pyrophosphate anion in TABLE VII.5.

TABLE VII.4

Components of Tensors **T** and **L**

T_{11}	T_{22}	T_{33}	T_{12}	T_{23}	T_{13}
0.0269	0.0276	0.0490	-.0078	0.0017	-.0024

L_{11}	L_{22}	L_{33}	L_{12}	L_{23}	L_{13}
0.0039	0.0064	0.0219	-.0015	-.0055	0.0029

TABLE VII.5

Corrected and Uncorrected Bond Lengths of the P_2O_7 Group

Distance	Uncorrected	Corrected
P(A)-O(CE)	1.577 Å	1.592 Å
-O(A1)	1.507	1.524
-O(A2)	1.473	1.489
-O(A3)	1.475	1.480
P(B)-O(CE)	1.644	1.679
-O(B1)	1.468	1.477
-O(B2)	1.486	1.507
-O(B3)	1.476	1.487

7.9. Rigid Group Refinement

It is evident from TABLE VII.5 that the corrections on the P-O bond lengths based on the libration of the rigid-body, P_2O_7, about its centre of mass, are not sufficient to bring the bond lengths to their usual accepted values, i.e. 1.515 Å for terminal and 1.630 Å for bridging P-O bonds. Another rigid group refinement based upon the room-temperature structure was carried out. In this case, the P_2O_7 anion was treated as a rigid group with the P-O bond lengths adjusted to the room-temperature values, i.e. 1.513 Å for the terminal and 1.635 Å for the bridging bonds. Phosphorus atom P(A) was chosen arbitrarily as the origin of the group. The refinement was carried out in such a way that the group was allowed to find its optimum position as well as its orientation with respect to a coordinate system parallel to the crystal axes. The parameters of the group which could be varied were the three positional coordinates of the origin, three angles defining the orientation of the group and the isotropic temperature factors of each atom in the group. All the sodium atoms were treated as independent atoms and were refined along with the group. The atomic and thermal parameters of the system after the rigid group refinement are shown in TABLE VII.6. The temperature factors are now more meaningful. The final R value is 0.074.

TABLE VII.6. Atomic and Thermal Parameters of $Na_4P_2O_7$ at 410°C. obtained under Rigid Group Refinement

Rigid Group

Atom	x	y	z	U
P-A	0.1759	0.0141	0.4296	0.028(1)
P-B	0.1817	0.1037	0.3209	0.028(1)
O-CE	0.1367	-.0352	0.3713	0.052(3)
O-A1	0.1483	0.2864	0.4380	0.068(3)
O-A2	0.0749	-.1548	0.4555	0.055(3)
O-A3	0.3316	-.0571	0.4363	0.051(3)
O-B1	0.0699	0.3002	0.3196	0.052(3)
O-B2	0.1716	-.1009	0.2826	0.081(4)
O-B3	0.3319	0.2039	0.3282	0.063(3)

Independent

Atom	x	y	z	U_{11}	U_{22}	U_{33}	U_{12}	U_{13}	U_{23}
Na-3	0.3455(6)	0.5995(15)	0.2963(2)	0.059(3)	0.047(5)	0.065(3)	0.007(4)	-.008(3)	0.000(3)
Na-4	0.3458(6)	0.5226(17)	0.4567(2)	0.059(3)	0.069(6)	0.072(3)	0.001(4)	-.002(3)	-.003(4)
Na-7	0.0097(5)	0.5546(13)	0.3802(2)	0.045(3)	0.043(5)	0.047(3)	-.000(4)	-.005(2)	0.001(3)
Na-8	0	$\frac{1}{2}$	0	0.049(4)	0.039(6)	0.036(3)	-	-.008(3)	-
Na-9	0	0.6035(21)	$\frac{1}{4}$	0.071(5)	0.047(8)	0.065(5)	-	-.012(4)	-

7.10. Discussion

It is now evident that the structure of sodium pyrophsophate at 410°C. is more complex than it was first believed to be. This is not surprising if we recall the twinning phenomenon (Section 4.3) which nearly always accompanied this transformation. The presence of residual peaks in the electron difference Fourier in the final stage suggest configurational disorder which requires further investigation.

It is of some interest to carry out a significance test (Hamilton [48]) on the two models used in the refinement of this structure. In the unrestrained model (a), there are 119 parameters based on 580 reflections and the R factor (R_a) is 0.054. In the rigid-group model (b), there are 92 parameters with the same number of reflections and the R factor (R_b) is 0.073. The hypothesis to be tested may be formulated

H_o: The rigid-group model is a better description of the structure.

The Hamilton R-factor ratio is then

$$R = \frac{R_b}{R_a} = \frac{0.073}{0.054} = 1.331. \tag{7.10.1}$$

The dimension of the hypothesis is 119 - 92 = 27 and the number of degrees of freedom for the refinement is 580 - 27 = 553. At a rejection level of 5%, a pertinent tabular value of R, obtained by interpolation from Table 1 of Hamilton's paper gives

$$R_{27,553,0.05} = 1.015. \tag{7.10.2}$$

Since $R > R_{27,553,0.05}$ we conclude that the probability of error if the hypothesis H_o is rejected does not exceed 5%. In other words, the rigid-group model is not a satisfactory model either.

It seems therefore we are left with only a disordered model. As pointed out previously, the Finger program might be used to refine the occupancy of the disordered sites. In addition, it might be fruitful, though very much more complicated, to carry out the analysis further by using a set of reflection data corresponding to a twinned crystal rather than using only the apparently "untwinned" crystal data as in the present case.

CHAPTER VIII

STRUCTURE OF $Na_4P_2O_7$ BETWEEN 500° AND 600°C.

Between 500° and 600°C. the system of sodium pyrophosphate undergoes a series of phase transformations which can be grossly divided into two regions: a first region from 500° to 540°C and a second one from 540° to 600°C. Each region has distinctive features of its own which will be described below. However, since each region consists of transformations which are very close together, no attempt was made to determine the structure of each phase; rather, an overall structure determination within each region has been carried out.

REGION I: $Na_4P_2O_7$ between 500° and 540°C.

8.1. Introduction

The D.T.A trace in Fig. 4.1.1 (p. 43) showed that in this temperature region, there are two main phases at 517° and 522°C. The resulting phases have been labelled as III and IV. The separation of these two phases corresponds to only 5 degrees. Immediately below the transition temperature 517°C. the crystal is invariably twinned while immediately above, twinning disappears. As the furnace (Section 7.3) which was used to heat the crystal was unable to hold temperatures within a stability of ± $5^oC.$, reflection data collected within this region were at a temperature of $525 \pm 5^oC.$, i.e. the data corresponded to phase III and phase IV. This means that the data would correspond to an average of at least two phases and this might cause a serious refinement problem if the two phases have different structural symmetries. This point will be discussed further below.

8.2. Space Group Determination

Sodium pyrophosphate at room temperature is orthorhombic in space group $P2_12_12_1$ with $\underline{a} = a_o = 9.37$, $\underline{b} = b_o = 5.39$, $\underline{c} = c_o = 13.48$ Å and z = 4. The structure consists of a repeat of a two-layer arrangement with pyrophosphate groups related by a two-fold screw axis parallel to the $\underline{a}$ axis in the layer and the adjacent layer generated by two-fold screw axes parallel to the $\underline{b}$ axis between layers. The structure between 405^o and $515^oC.$ has $\underline{a} \approx a_o$, $\underline{b} \approx b_o$, $\underline{c} \approx 2c_o$, $\beta = 93^o$ and z = 8. Here adjacent layers are related to each other by centres of symmetry or by two-fold screw axes parallel to $\underline{b}$.

The situation in Region I is not at all clear. The cell has axes lengths $\underline{a} \approx a_o$, $\underline{b} \approx b_o$, $\underline{c} \approx 3c_o$ and z = 12. All the angles are 90^o. By considering all the would-be equivalent reflections, the crystal appears to be monoclinic but with almost orthorhombic symmetry. The observed extinction is consistent with C-centering in the ab plane. In addition, 0kl reflections appear only when l is even implying a glide plane. If we assume that the pyrophosphate groups of the structure at this temperature occupy positions similar to the room-temperature structure, differing perhaps by small translations of the centre of mass of the group and fine details of the bridging and terminal oxygen atoms, then the glide planes are consistent only if they are perpendicular to the a axis and at 0 and ½. In other words, the unique axis of the monoclinic system is the longer axis, a_o rather than b_o as in the previous structure at 410°C. Since there are only two space groups in the monoclinic system with a C-centering and a c-glide, namely: C2/c and Cc, a choice must be made between the two. Fig. 8.2.1(a) and (b) show that with a proper choice of origin, both space groups satisfy the condition that each must generate pyrophosphate groups at positions similar to the room-temperature structure. The difference is, in C2/c there are one and a half independent molecules in the asymmetric unit while in Cc there are three. The correct choice of the space group for the system depends then on a calculation of structure factors.

8.3. Refinement with Space Group Cc

The cell dimensions used in this refinement were obtained from the curves in Figs. 4.6.1 - 3 (pp. 53-55) which recorded the linear expansion of the three axes.

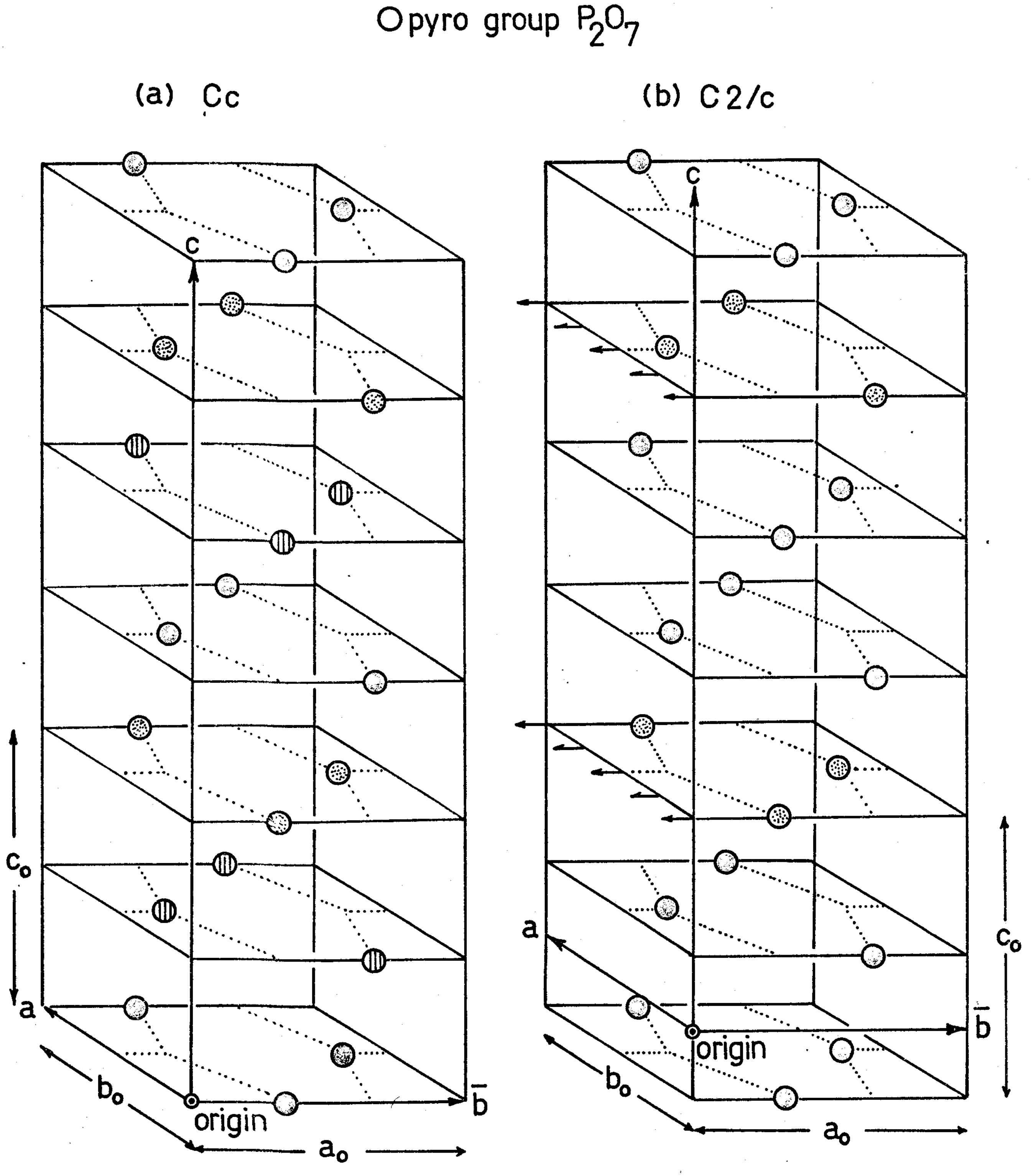

Fig. 8.2.1. Choice of Origins in space groups Cc and C2/c for $Na_4P_2O_7$ in Region I. The structure is formed by stacking three unit cells of the room-temperature structure up the <u>c</u> axis. All equivalent pyro groups are shaded in the same way.

Refinement under Cc required three independent molecules in the asymmetric unit. Although the atomic parameters from the structure at 410°C. could be used as a guide, the refinement developed in such a way that the molecular geometry of each pyrophosphate group bore no immediate resemblance to its counterpart at 410°C. Since there were 39 independent atoms with 163 parameters using isotropic temperature factors, and there were only 788 reflections, 159 and 38 of which are unobserved and unreliable respectively, not much could be expected towards an accurate structure determination. The R value obtained so far is 25%.

The batch with the 0kl data was always the best in R value, being 16% compared to an overall 25%. This could be attributed to the fact that this batch was more accurate than the others. We recall $\underline{c} = 3c_o = 40.44$ Å. With only l = even appearing, the integrated areas on an 0kl photograph were still well separated along $\underline{c}$; but for other projections, the areas along $\underline{c}$ were so close together that there was only a slit for separation using Mo-radiation. With Cu-radiation, the separation was satisfactory along $\underline{c}$ but not along $\underline{a}$ and $\underline{b}$ where the lengths are 5.39 and 9.37 Å respectively. The set of data used here was collected with Mo-radiation.

The atomic and thermal parameters were shown in TABLE VIII.1 and the observed and calculated structure factors in TABLE VIII.2. Fig. 8.3.1 shows the molecular geometry of pyrophosphate anions at three different levels up the $\underline{c}$ axis.

TABLE VIII.1

Atomic and Thermal Parameters of $Na_4P_2O_7$ at 525 ± $5^{o}C$.*

Atom	x	y	z	U
1-P1	-.1186	0.3178	0.1305	0.0621
1-P2	-.0251	0.3175	0.2000	0.0221
1-OCE	-.2318	0.3497	0.1671	0.0771
1-O1A	-.1624	0.1785	0.1250	0.0559
1-O1B	-.2987	0.4065	0.1092	0.0530
1-O1C	0.1166	0.3681	0.1256	0.0747
1-O2A	0.1753	0.4568	0.2057	0.0530
1-O2B	-.1815	0.3329	0.2296	0.0784
1-O2C	0.0470	0.1745	0.1988	0.0445
1-Na3	-.0601	0.3434	0.0467	0.0670
1-Na4	-.0438	0.3491	0.2795	0.0476
2-P1	-.1053	0.3214	0.4631	0.0300
2-P2	-.0893	0.3274	0.5341	0.0432
2-OCE	-.1051	0.3690	0.5001	0.0635
2-O1A	-.0172	0.1700	0.4582	0.1349
2-O1B	-.3498	0.2944	0.4528	0.1176
2-O1C	0.0567	0.4035	0.4375	0.0486
2-O2A	-.1780	0.1779	0.5338	0.0499
2-O2B	-.2538	0.4076	0.5542	0.0974
2-O2C	0.1692	0.3573	0.5401	0.0756
2-Na3	-.1663	0.3657	0.3857	0.0663
2-Na4	-.1732	0.3308	0.6104	0.0644
3-P1	-.0278	0.3284	0.7966	0.0333
3-P2	-.1269	0.3082	0.8676	0.0387
3-OCE	-.0163	0.3379	0.8358	0.0585
3-O1A	0.0208	0.1535	0.7920	0.0491
3-O1B	0.1487	0.4478	0.7853	0.0318
3-O1C	-.2805	0.3686	0.7896	0.0721
3-O2A	-.3506	0.4185	0.8783	0.0648
3-O2B	0.1003	0.3015	0.8922	0.0571
3-O2C	-.2508	0.1693	0.8587	0.0670
3-Na3	-.0673	0.3476	0.7205	0.0861
3-Na4	-.1319	0.3384	0.9419	0.0636
4-Na5	0.3965	0.5189	0.0002	0.0482
5-Na5	0.4618	0.5129	0.0793	0.0803
6-Na5	0.4665	0.5085	0.1653	0.0720
7-Na5	0.4546	0.5029	0.2467	0.0548
8-Na5	0.3833	0.5056	0.3352	0.0377
9-Na5	0.3647	0.5115	0.4140	0.0163

* Refined in Space Group Cc to an R value of 25%.

TABLE VIII.2

TABLE OF OBSERVED AND CALCULATED STRUCTURE FACTORS OF NA4P2O7 AT 525 DEGREES C.

UNOBSERVED REFLECTIONS ARE MARKED WITH * AND UNRELIABLE REFLECTIONS WITH + .

K = 0

H	L		|F-O|	|F-C|
0	12	+	930	925
0	18		232	232
0	24		483	539
0	30		249	211
0	36		125	136
0	42		191	169
2	2		352	284
2	4		214	292
2	6		164	169
2	8		239	329
2	10		157	235
2	12		73	60
2	14		64	81
2	16		67	181
2	18		69	77
2	20		257	136
2	22		222	145
2	24		275	256
2	26		78	71
2	28		80	29
2	30		195	185
2	32		84	74
2	34		85	27
2	36		98	109
2	38		86	91
2	40		95	51
2	42		145	123
2	-2		314	228
2	-4		249	261
2	-6		65	33
2	-8		202	232
2	-10		223	222
2	-12		109	43
2	-14		79	113
2	-16		67	121
2	-18		82	135
2	-20		216	207
2	-22		268	176
2	-24		274	251
2	-26		82	158
2	-28		80	62
2	-30		155	148
2	-32		70	61
2	-34		51	60
2	-36		112	108
2	-38		59	13
2	-40		103	105
2	-42		113	114
4	0		192	252
4	2		310	233
4	4		151	202
4	6		76	35
4	8		123	166
4	10		138	84
4	12		78	79
4	14		125	35
4	16		80	43
4	18		81	25
4	20		141	110
4	22		145	106
4	24		107	143
4	-2		274	264
4	-4		229	220
4	-6		76	53
4	-8		76	175
4	-10		187	159
4	-12		78	59
4	-14		87	77
4	-16		80	108
4	-18		81	36
4	-20		120	123
4	-22		180	161
4	-24		107	111

K = 1

H	L		|F-O|	|F-C|
1	7	+	101	164
1	8		82	82
1	9	+	18	89
1	10		161	192
1	11		93	133
1	12		569	592
1	13		175	242
1	13		304	242
1	14		284	240
1	15		457	433
1	16		157	116
1	17		226	150
1	18		192	210
1	19		85	111
1	20		68	76
1	21	+	38	99
1	22	+	29	66
1	23		75	96
1	24		166	157
1	25		158	102
1	26		95	48
1	27		407	377
1	28	+	33	46
1	29	+	70	53
1	30	+	101	51
1	31	*	34	25
1	32	*	35	19
1	33		119	113
1	34	*	36	35
1	35	*	36	28
1	36	*	36	74
1	37		52	41
1	38	*	37	34
1	39		163	153
1	40	*	37	4
1	41	*	39	11
1	42		69	60
1	43	*	38	12
1	44	+	38	17
1	45		68	68
3	0		85	76
3	1		62	73
3	2		79	115
3	3		62	121
3	4		44	21
3	5		95	259
3	6	*	25	95
3	7		55	89
3	8		69	72
3	9		96	80
3	10		189	124
3	11		137	163
3	12		249	279
3	13		212	184
3	14		144	127
3	15		184	238
3	16	*	30	22
3	17		221	193
3	18		55	80
3	19		65	66
3	20		47	20

K = 1

H	L		|F-O|	|F-C|
3	21	*	32	24
3	22	*	33	13
3	23		147	134
3	24		65	59
3	25		184	158
3	26		106	105
3	27		166	141
3	28		56	62
3	29		98	126
3	30		40	24
3	31		43	41
3	32	*	36	10
3	33	*	37	48
3	34		41	36
3	35		65	82
3	37		96	66
3	38	*	38	10
3	39		67	64
5	0		38	44
5	1	*	34	19
5	2		39	48
5	3		34	27
5	4	*	34	45
5	5		75	118
5	6		44	25
5	7		69	71
5	8		67	62
5	9	*	35	31
5	10		116	101
5	11	*	35	50
5	12		49	68
5	13		76	45
5	14		109	91
5	15	*	36	32
5	16		42	84
5	17		86	92
5	18	*	35	33
5	19		37	46
5	20	*	37	34
5	21	*	37	6
5	22	+	37	25
5	23		53	67
5	24	*	37	35
5	25		59	92
5	29		46	49
-1	0		12	115
-1	7		101	121
-1	8		82	110
-1	9		29	40
-1	10		161	193
-1	11		115	97
-1	12		568	459
-1	13		344	215
-1	14		273	190
-1	15		457	483
-1	16	*	25	81
-1	17		235	167
-1	18		171	124
-1	19	+	78	122
-1	20		44	101
-1	21	*	29	119
-1	22	*	29	54
-1	23		74	76
-1	24		189	186
-1	25		177	93
-1	26		98	78
-1	27		426	408
-1	28	+	33	45
-1	29	+	75	39
-1	30		108	71
-1	31	*	34	51
-1	32	+	35	27
-1	33		123	126
-1	34	*	36	66
-1	35	*	36	44
-1	36		41	38
-1	37		61	30
-1	38	+	41	75
-1	39		154	149
-1	40	*	37	18
-1	41	*	38	25
-1	42		64	53
-1	43	*	38	18
-1	44	*	38	3
-1	45		60	75
-3	0		85	77
-3	1		60	75
-3	2		85	121
-3	3		62	65
-3	4		40	104
-3	5		81	84
-3	6	*	26	39
-3	7		60	116
-3	8		62	36
-3	9		95	70
-3	10		191	121
-3	11		127	94
-3	12		256	224
-3	13		231	144
-3	14		144	108
-3	15		199	143
-3	16	*	30	78
-3	17		204	88
-3	18		78	98
-3	19		90	167
-3	20		57	14
-3	21	*	32	66
-3	22	*	33	109
-3	23		140	127
-3	24		75	27
-3	25		188	151
-3	26		99	67
-3	27		162	164
-3	28		69	67
-3	29		86	33
-3	30		46	60
-3	31		40	56
-3	32	*	36	4
-3	33	*	37	39
-3	34		41	42
-3	35		59	95
-3	36		51	47
-3	37		105	60
-3	38	*	39	46
-3	39		67	57
-5	0		39	44
-5	1	*	34	25
-5	2	*	34	68
-5	3	+	44	35
-5	4		39	44
-5	5		73	121
-5	6	*	35	43
-5	7		68	76
-5	8		67	102
-5	9	*	35	39
-5	10		129	89
-5	11		41	53

K = 1

H	L		|F-O|	|F-C|
-5	12		35	60
-5	13		86	52
-5	14		109	117
-5	15	*	36	16
-5	16		57	58
-5	17		77	83
-5	18	*	36	16
-5	19		41	60
-5	20	*	37	34
-5	21	*	37	16
-5	22		37	68
-5	23		49	43
-5	24		37	48
-5	25		73	72

K = 2

H	L		|F-O|	|F-C|
0	0		278	260
0	15	+	213	150
0	16	+	34	19
0	17	*	38	29
0	18		102	108
0	19		43	18
0	20		46	36
0	21		77	50
0	22		59	94
0	23		52	37
0	24		108	105
0	25		55	63
0	26		57	47
0	27		365	316
0	28		60	40
0	29		61	28
0	30		196	181
0	31		64	41
0	32		65	45
0	33		103	87
0	34		67	27
0	35		68	10
0	36		101	84
0	37		70	21
0	38		70	33
0	39		111	113
0	40		72	33
0	41		72	16
0	42		110	95
0	-3		449	411
0	-6		109	108
0	-9		74	89
0	-12		575	735
0	-15		206	150
0	-18		97	108
0	-21		103	50
0	-24		109	105
0	-27		372	316
0	-30		186	181
0	-33		123	87
0	-36		125	84
0	-39		127	113
2	0		98	125
2	1		94	48
2	2	*	31	68
2	3	*	32	79
2	4	*	32	100
2	5		118	145
2	6	*	35	28
2	7		170	161
2	8		164	160
2	9	+	438	276
2	10	+	339	177
2	11		181	133
2	12		593	479
2	13		149	242
2	14		190	184
2	15		124	184
2	16		48	108
2	17		122	81
2	18		51	84
2	19		52	77
2	20		119	98
2	21		150	117
2	22		60	94
2	23		92	110
2	24		59	60
2	25		156	111
2	26		61	56
2	27		216	207
2	28		63	51
2	29		64	63
2	30		92	90
2	30		70	90
2	31		66	58
2	32		67	51
2	33		96	96
2	-25		154	107
2	-26		77	63
2	-27		209	233
2	-28		82	63
2	-29		54	66
2	-30		85	77
2	-31		48	75
2	-32		53	45
2	-33		106	95
2	-34		67	90
2	-36		74	59
2	-37		79	45
2	-39		79	76
4	0		74	43
4	1		56	29
4	2		60	161
4	3		57	134
4	4		57	37
4	5		102	92
4	6		57	25
4	7		62	54
4	8		110	104
4	9		58	62
4	10		166	157
4	11		71	93
4	12		79	121
4	13		140	91
4	14		197	116
4	15		93	138
4	16		62	58
4	17		126	51
4	18		64	48
4	19		64	61
4	20		65	67
4	21		65	33
4	22		65	41
4	23		67	101
4	24		67	56
4	25		126	110
-2	7	+	193	117
-2	8		137	127
-2	9		426	401
-2	10	+	338	182

K = 2

H	L		|F-O|	|F-C|
-2	11		164	74
-2	12		562	545
-2	13		149	196
-2	14		175	135
-2	15		120	143
-2	16		48	67
-2	17		125	76
-2	18		51	79
-2	19		52	90
-2	20		111	131
-2	21		162	202
-2	22		69	96
-2	23		81	52
-2	24		59	36
-2	25		165	109
-2	26		61	63
-2	27		230	234
-2	28		63	63
-2	29		64	64
-2	31		65	76
-2	32		67	45
-2	33		96	95
-4	8		98	112
-4	9		58	24
-4	10		181	117
-4	11		59	70
-4	12		79	98
-4	13		157	122
-4	14		145	135
-4	15		99	131
-4	16		62	58
-4	17		112	63
-4	18		64	40
-4	19		64	110
-4	20		65	61
-4	21		65	13
-4	22		66	102
-4	23		67	88
-4	24		67	26
-4	25		126	106

K = 3

H	L		|F-O|	|F-C|
1	3		79	91
1	4		43	126
1	5		69	38
1	6		64	150
1	7		45	71
1	8		74	64
1	9		111	93
1	10	+	41	73
1	11		79	79
1	12	*	26	8
1	13		59	145
1	14		79	73
1	15		104	56
1	16		54	44
1	17		95	94
1	18		96	135
1	19	*	30	28
1	20		51	83
1	21	*	19	23
1	22		114	120
1	23		65	45
1	24		292	246
1	25	+	58	15
1	26	*	35	16
1	27		45	48
1	27		45	46
1	28	*	36	32
1	29	*	36	52
1	30		177	171
1	31	*	25	16
1	32	*	27	25
1	33	*	27	22
1	34	+	28	68
1	35		29	49
1	36		112	131
1	37	*	29	21
1	38	*	30	84
1	39	*	30	27
1	40		45	23
1	41	*	31	7
1	42		136	118
3	0		477	452
3	1	+	64	78
3	2		338	237
3	3	+	53	111
3	4		169	181
3	5		172	112
3	6		64	91
3	7		93	104
3	8		114	164
3	9		62	78
3	10		152	68
3	11	+	20	91
3	12		81	105
3	13	+	20	47
3	14		72	48
3	15	+	21	39
3	16	*	22	80
3	17	+	41	72
3	18	+	63	81
3	19	+	22	45
3	20		127	87
3	21	*	24	31
3	22		154	111
3	23	*	25	57
3	24		169	187
3	25	*	26	51
3	26		53	54
3	27	+	27	45
3	28	*	27	38
3	29	*	28	21
3	30		85	105
3	31	*	28	22
3	32		55	46
3	33	*	29	15
3	34		30	11
3	35	*	30	21
3	36	*	30	37
3	37	*	30	37
3	38		36	77
3	39	*	31	15
3	40		61	68
3	41	*	32	15
3	42		59	63
3	44		46	25
5	0	*	26	100
5	1	*	26	32
5	2		173	115
5	3	*	25	18
5	4		84	98
5	5	*	26	35
5	6	*	26	11
5	7	*	26	14
5	8		51	56

K = 3

H	L		|F-O|	|F-C|
5	9	*	26	4
5	10		66	72
5	11	*	27	2
5	12	*	27	51
5	13	*	27	34
5	14		44	28
5	15	*	28	2
5	16	*	28	28
5	17	*	28	9
5	18	*	28	7
5	19	*	29	12
5	20		57	50
5	21	*	29	6
5	22		66	104
-1	17		78	41
-1	18		86	116
-1	19	*	16	75
-1	20		44	56
-1	21	*	19	24
-1	22		101	112
-1	23		76	57
-1	24		300	279
-1	27		46	61
-1	28	*	24	25
-1	30		183	133
-1	31	*	26	35
-1	32	*	27	11
-1	33	*	27	22
-1	34	*	28	27
-1	35		29	11
-1	36		105	113
-1	37	*	29	15
-1	38	*	30	18
-1	39	*	30	21
-1	40		53	63
-1	41	*	31	18
-1	42		133	114
-3	0		477	452
-3	1	+	72	52
-3	2		317	202
-3	3	+	53	72
-3	4		169	227
-3	5		107	128
-3	6		74	72
-3	7		118	56
-3	8		110	108
-3	9		67	80
-3	10		152	113
-3	11	*	20	42
-3	12		82	94
-3	13	*	20	13
-3	14		75	96
-3	19	+	52	33
-3	20		109	84
-3	21	*	24	22
-3	22		150	142
-3	23	*	25	14
-3	24		176	145
-3	25	*	26	21
-3	26		53	99
-3	27	*	27	6
-3	28	*	27	22
-3	29	*	28	34
-3	30		84	84
-3	31	*	28	10
-3	32		53	44
-3	33	*	29	36
-3	34	*	30	17
-3	35	*	30	4
-3	36	*	30	63
-3	37	*	31	28
-3	38		31	17
-3	39	*	31	4
-3	40		67	73
-3	41	*	32	12
-3	42		59	61
-3	44		46	24
-5	0	*	26	100
-5	1	*	26	10
-5	2		137	196
-5	3	*	26	27
-5	4		106	107
-5	5	*	25	7
-5	6		37	49
-5	7	*	26	17
-5	8		48	99
-5	9	*	26	17
-5	10		84	78
-5	11	*	27	8
-5	12	*	27	49
-5	13	*	27	13
-5	14	*	32	28
-5	15	*	28	22
-5	16	*	28	30
-5	17	*	28	8
-5	18	*	28	34
-5	19	*	29	13
-5	20		77	95
-5	21	*	29	17
-5	22		79	73

K = 4

H	L		|F-O|	|F-C|
0	0		341	314
0	-3		83	90
0	-6		85	66
0	-9		216	186
0	-12		422	508
0	-13		143	87
0	-15		269	246
0	-18		170	160
0	-21		182	168
0	-24		114	101
0	-27		290	245
0	-30		122	45
0	-33		125	97
0	-36		127	45
0	-39		128	115
2	-20	*	36	49
2	-21		46	65
2	-23		76	60
2	-24		96	86
2	-25		131	106
2	-26	+	78	51
2	-27		180	170

K = 5

H	L		|F-O|	|F-C|
1	0		48	65
1	1		43	42
1	2		59	18
1	3		183	198
1	4		68	108
1	5	*	32	72
1	6	*	32	47
1	7		46	53
1	8	*	37	60

K = 5

H	L		|F-O|	|F-C|
1	9		161	152
1	10		102	67
1	11		38	115
1	12		393	327
1	13		123	128
1	14	+	65	41
1	15		180	172
1	16	*	35	22
1	17	*	35	44
1	18		156	99
1	19	*	35	23
1	20	*	36	53
1	21	*	37	61
1	22	*	37	27
1	23		51	87
1	24		48	65
1	25		100	52
1	26	*	39	37
1	27		250	212
1	28	*	40	32
1	29	*	40	47
1	30		131	127
1	36		81	78
1	39		80	62
1	42		94	81

K = 6

H	L		|F-O|	|F-C|
0	0		581	719
0	-1		170	99
0	-3		132	162
0	-6		103	63
0	-9		132	136
0	-12		204	141
0	-14		132	51
0	-18		139	110
0	-21		118	35
0	-24		249	239
0	-27		174	48
0	-30		178	132
2	0	+	297	467
2	-1	+	111	8
2	-2	+	169	119
2	-3		109	83
2	-4		125	114
2	-5		101	111
2	-6	*	36	43
2	-7		77	59
2	-8		88	95
2	-9		86	64
2	-10		122	96
2	-11		40	21
2	-12		133	137
2	-13		41	30
2	-14		42	56
2	-15		51	55
2	-16		44	7
2	-17		45	28
2	-18		45	55
2	-19		46	59
2	-20		84	109
2	-21		49	28
2	-22		115	118
2	-23		50	33
2	-24		174	158

K = 7

H	L		|F-O|	|F-C|
1	0		47	42
1	1		39	73
1	2		72	76
1	3		165	178
1	4	*	39	27
1	5		63	95
1	6		68	31
1	7		71	73
1	8		47	51
1	9		120	67
1	10		40	44
1	11		40	17
1	12		121	136
1	13		81	42
1	14	+	85	34
1	15		288	265
1	16		41	10
1	17		71	54
1	18		93	106
1	19		41	81
1	20		41	69
1	21		42	67
1	22		42	11
1	23		60	57
1	24		75	85
1	25		56	79
1	26		86	65
1	27		174	165
1	39		104	88

K = 8

H	L		|F-O|	|F-C|
0	0		153	110
0	-3		119	45
0	-6		119	45
0	-9		127	119
0	-12		359	273
0	-15		123	52
0	-18		132	107
2	-8		99	38
2	-9		65	54
2	-10		101	93
2	-11		50	49
2	-12		167	182
2	-13		51	15
2	-14		71	63

K = 9

H	L		|F-O|	|F-C|
1	0		198	202
1	1		44	24
1	2		44	49
1	3		123	118
1	4		44	24
1	5		58	60
1	6		44	10
1	7		44	28
1	8		44	55
1	9		75	81
1	10		44	44
1	11		44	33
1	12		53	41
1	13		44	34
1	14		44	21
1	15		79	75
1	24		69	85

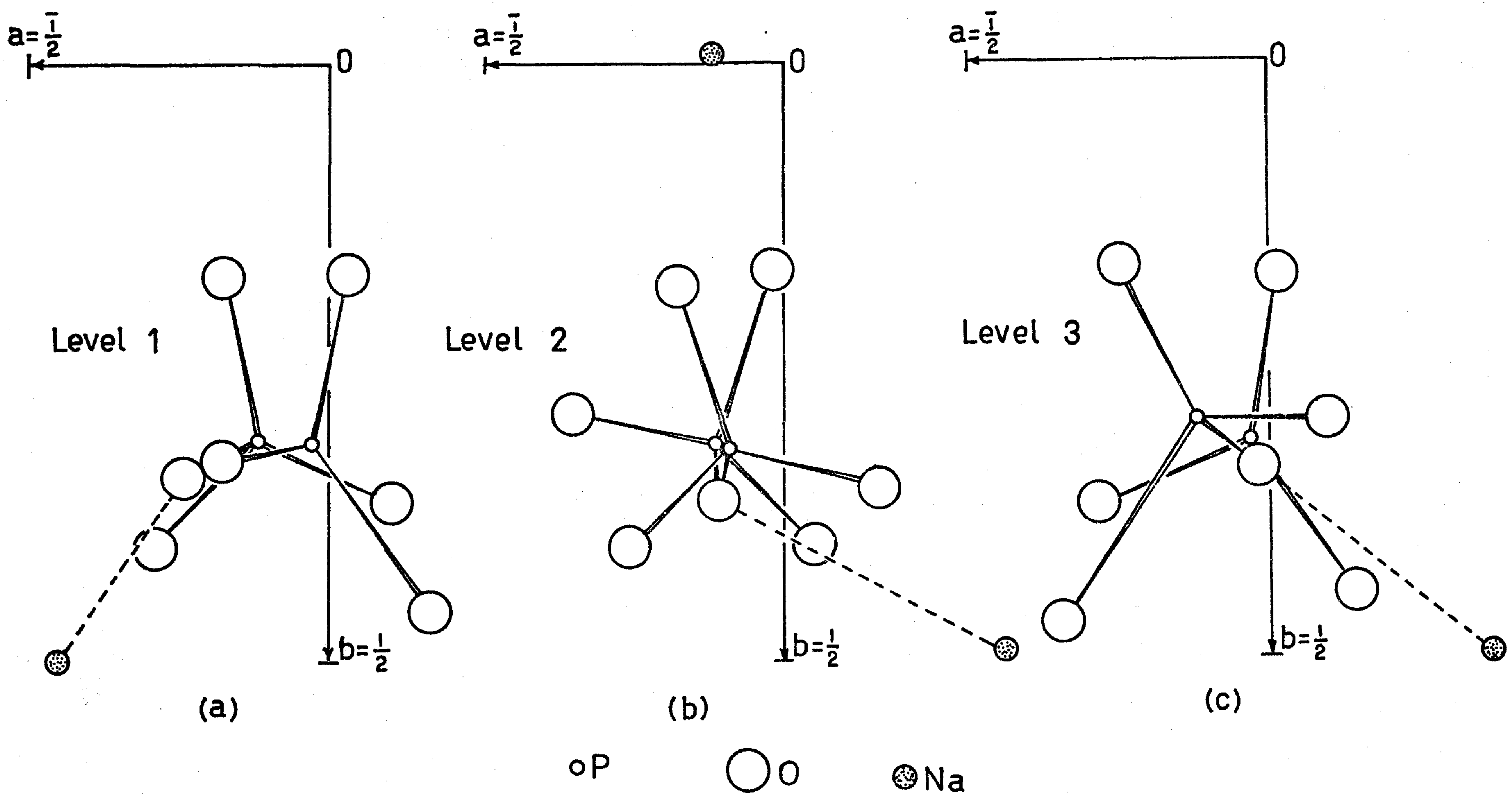

Fig. 8.3.1. Bond Geometry of the Pyrophosphate Anion at three different levels separated by 1/3 c axis. Note the orientations of the bridging oxygen atoms in the three cases.

As discussed in connection with the room-temperature structure (Chapter V) there could be three basic configurations of the pyrophosphate anions in a layer (Cf. Fig. 5.6.3, p. 72) and it is interesting to note that the configuration (c) in Fig. 5.6.3 with the bridging oxygen atom parallel to the longer axis exists in the present structure (Fig. 8.3.1(b)). However the oxygen atom is not bonded to the sodium atom at the origin. The reason for this configuration is not clear but is probably due to the fact that the structure is not yet fully refined (R value still 25%).

8.4. Refinement with Space Group C2/c

Refinement under C2/c requires one and a half independent molecules in the asymmetric unit. The bridging oxygen atom of one of the pyrophosphate anions must lie in a special position so that the tetrahedron on one side generates an equivalent one on the other side. Because of the higher symmetry compared to space group Cc, the orientations of the bridging oxygen atoms in C2/c are more restricted. An attempt was initially made to use the atomic parameters adapted from the previous refinement with space group Cc; but the changes required to allow for the higher symmetry soon made it necessary to abandon many of the coordinates. At the time of writing of this thesis, a structure factor calculation with three phosphorus atoms, one bridging oxygen atom (in special position) and the sodium atoms which had been in the "chain" in the room-temperature structure (Chapter V), gave an R value of 40%. Further electron density analyses might locate the other sodium and oxygen atoms; but, as in the case of space group Cc, the quality of the data coupled with a low reflection-to-parameter ratio, might not have much to offer towards a good structure determination.

REGION II: $Na_4P_2O_7$ between 540° and 600°C.

8.5. Introduction

The D.T.A. trace in Fig. 4.1.1 (p. 43) showed that in this temperature region, there are three main phase transformations at 542°, 547° and 554°C. and the resulting phases have been labelled as V, VI, and VII. Once again, these phases are very close together and so only reflection data were collected at 575 ± 5°C. which was inside phase VII.

8.6. Space Group Determination

In this temperature region, all the layers normal to the c axis show apparent hexagonal symmetry. In addition, in l = odd layers, reflections with indices h and k satisfying h - k = 3n develop into diffuse streaks (Cf. Fig. 4.5.1, p. 51). In order to arrive at the proper space group for the structure, it is convenient to consider once again the idealized structure discussed in Chapter V (Section 5.6).

The proposed idealized structure is based upon pyrophosphate groups showing D_{3h} (or $\bar{6}m2$) symmetry. Alternatively, if the terminal oxygen atoms at either end are rotated by 30° in opposite directions about the P-P vectors, assumed parallel to the c axis, the symmetry of the idealized anions is D_3 (or 32). At 600°C. the only extinctions are 00l reflections with l = odd, consistent with a 6_3 axis. However, $hh\overline{2h}l$ reflections with l = odd have developed streaks and have begun to fade into the background. We have attributed this phenomenon to some structural disorder and the disorder will be complete when all such reflections with l = odd disappear. In other words, when disorder is complete, a c-glide plane will relate anion groups in adjacent layers. The space group when disorder is complete is $P6_3/mmc$. However, the structure is not hexagonal prior to this but only nearly so.

The question of the space group of the low symmetry phase prior to the disordering, and the order parameter - the deviation in electron density from the c-glide symmetry - must be considered. In the room-temperature structure, the top half of a layer, i.e. the ab plane with one molecule thick, is related to the bottom half by a two-fold screw-axis while two molecules in the same layer are also related by a two-fold screw axis (Fig. 8.6.1). A disorder which sets in at high temperatures, tries to randomize the direction of the sodium-bridging oxygen atom interaction among the three alternatives (Fig. 8.6.2) and the resulting structure can be thought of as a superposition of the three structures derived from the room-temperature structure by a rotation of 120° about the screw axis parallel to the c axis. However, this does not generate the hexagonal cell of the high-temperature phase because the disordered groupings are not translationally equivalent unless the original structure also contains a C-centering operation. Alternatively, the C-centering plus the proposed disordering can yield the hexagonal translational

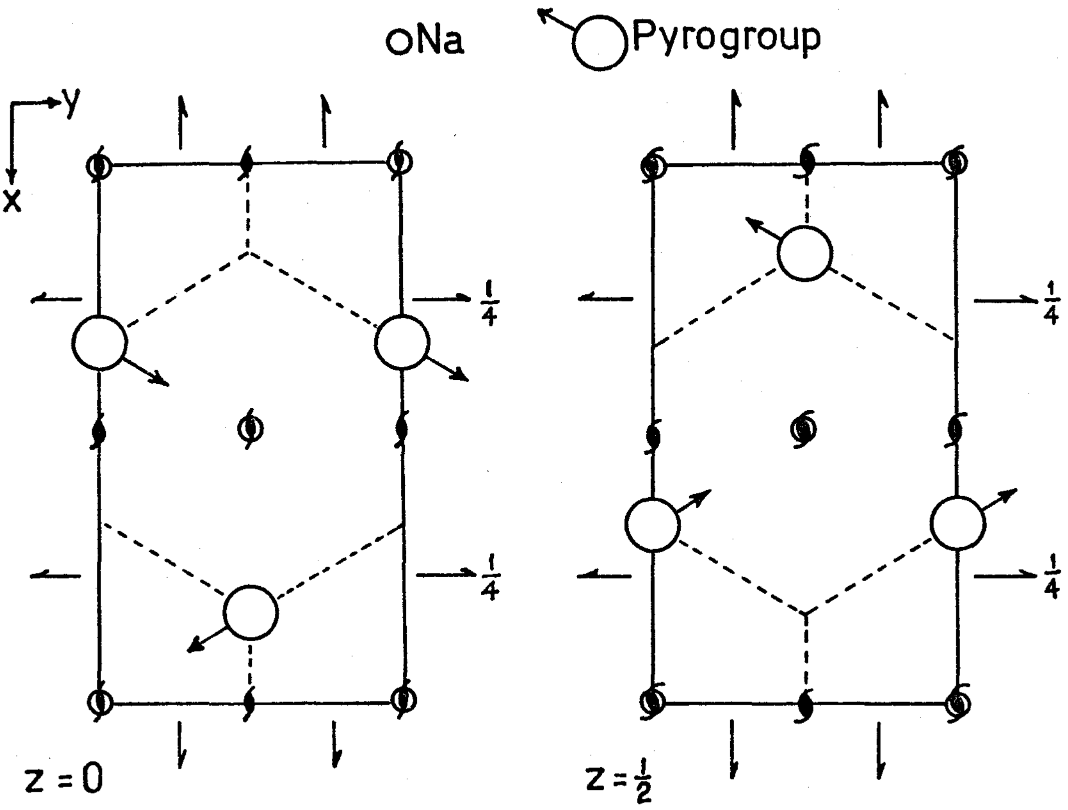

Fig. 8.6.1. The simplified room-temperature structure. Arrow on pyrogroup indicates the direction of the Na-O(bridging) interaction.

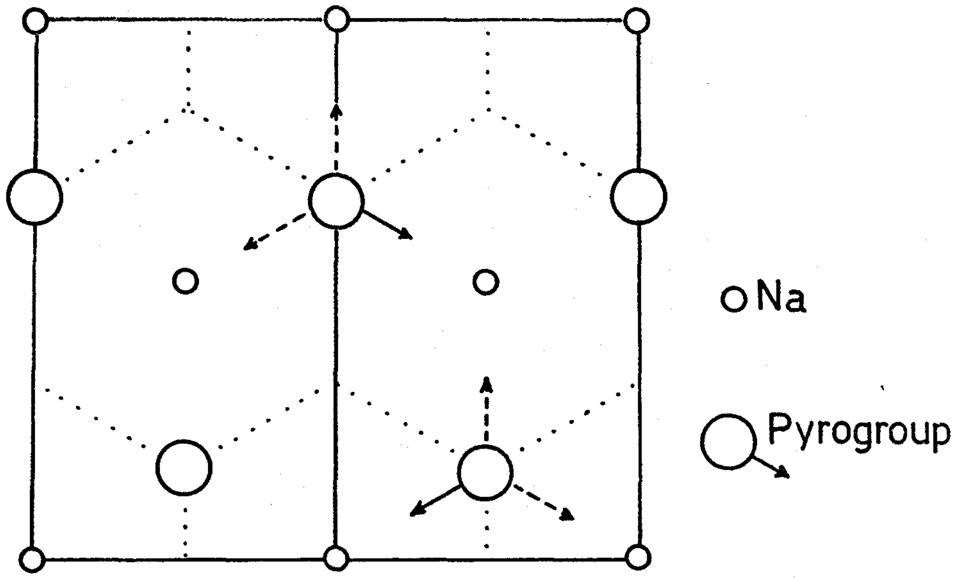

Fig. 8.6.2. The three alternative directions of the Na-O(bridging) interaction.

symmetry. Since all the phases identified between room temperature and 600°C. have two-fold and/or two-fold screw axes in the layer it seems reasonable to assume that the disorder will be based upon a structure with a screw-axis relationship between the pyrophosphate anions in the layer. However, this plus a C-centering, possibly derived by disordering, leads to an anion or a disordered pair with a two-fold screw axis. The "hexagonal" disordering would then generate a structure showing apparent $P6_322$ symmetry.

This however implies that the disordering is one between space groups $P6_322$ and $P6_3/mmc$ which does not appear to be consistent with the observation that the structure deviates slightly but significantly from hexagonal symmetry while the streaks are present. (A closer look at the photograph in Fig. 4.5.1, p.51, shows that the intensities are nearly but not exactly hexagonally equivalent.) It is apparent that the structure beyond 400°C. develops a centre of symmetry which is preserved as the structure disorders from the $3c_o$ (Region I) to the hexagonal cell. The crystal prior to the disappearance of the streaks must be orthorhombic with space group Cc2m with the longer axis in the <u>ab</u> plane as the "unique" axis.

8.7. Structure Determination

Earlier in the analysis of the reflection data in this temperature region, the complications of the space group problem discussed above were not fully recognized. An initial attempt was made with an ordered model in space group $P6_322$ with the atoms shown in TABLE VIII. 3. The R value was 36%. Electron density difference maps showed the presence of significant peaks and this, together with the abnormal temperature factor of the bridging oxygen atom OCE indicated strong evidence of disorder in the system.

A disordered model with the space group $P6_3/mmc$ was subsequently tried. The R value of 9.5% showed that this space group probably contained all the essential symmetries of the system in this temperature region. The atomic and thermal parameters are shown in TABLE VIII.4 and the observed and calculated structure factors are shown in TABLE VIII.5.

8.8. Discussion

Although the R value corresponding to $P6_3/mmc$ is 9.5%, that this is the proper space group already could not be accepted because the extinction condition: $hh2\bar{h}l$: l = odd does not hold. The present result, however, does not contradict our discussion in Section 8.6. The present system was probably not yet completely disordered and all the twenty-four equivalent sites allowed by the space group did not have equal occupancy.

TABLE VIII.3. Atomic and Thermal Parameters of $Na_4P_2O_7$ at 575°C. refined in Space Group $P6_322$

Atom	Multi-plicity	x	y	z	U
P	1/3	1/3	2/3	0.3581	0.0710
O-1	1	0.5657	0.9158	0.3885	0.0389
O-CE	1/6	0.2600	0.5200	1/4	0.1509
Na-1	1/6	0	0	0	0.0335
Na-2	1/6	0	0	1/4	0.0758
Na-3	1/3	1/3	2/3	0.5815	0.0582

R value = 36%

TABLE VIII.4. Atomic and Thermal Parameters of $Na_4P_2O_7$ at 575°C. refined in Space Group $P6_3/mmc$

Atom	Multi-plicity	x	y	z	U
P-1	1/12	0.6058	0.3314	0.1433	0.0573
P-2	1/12	0.6254	0.3032	0.3571	0.0261
O-CE	1/12	0.7327	0.4785	0.2499	0.0444
O1-A	1/12	0.3277	0.1388	0.1504	0.0372
O1-B	1/12	0.7932	0.2235	0.1122	0.0551
O1-C	1/12	0.7226	0.5940	0.0822	0.0694
O2-A	1/12	0.6142	0.0172	0.3374	0.0294
O2-B	1/12	0.8278	0.4818	0.4290	0.0862
O2-C	1/12	0.3279	0.2497	0.3822	0.0211
Na-1	1/12	0.9479	0.9731	0.2292	0.0442
Na-2	1/12	0.9870	0.9783	0.4820	0.0592
Na-3	1/12	0.7553	0.4028	0.5917	0.0779
Na-4	1/12	0.6446	0.3575	-.0855	0.0679

R value = 9.5%

TABLE VIII. 5.

TABLE OF OBSERVED AND CALCULATED STRUCTURE FACTORS OF NA4P207 AT 575 DEGREES C. UNOBSERVED REFLECTIONS ARE MARKED WITH * AND UNRELIABLE REFLECTIONS WITH +

L = 0

H	K		|F-O|	|F-C|
0	1		171	162
1	1		873	804
0	2		126	111
1	2		57	95
2	2		321	330
0	3		441	424
1	3	*	25	3
2	3	*	30	23
3	3		61	65
0	4	*	16	15
1	4		95	105

L = 1

H	K		|F-O|	|F-C|
0	1		433	432
0	2		34	28
1	2		94	103
0	3		62	63
1	3		73	63
0	4		50	41

L = 2

H	K		|F-O|	|F-C|
1	0	*	12	1
2	0	*	16	4
3	0		19	5
4	0		21	12
1	1		14	10
2	1	*	22	7
3	1		28	32

L = 3

H	K		|F-O|	|F-C|
1	0		26	43
2	1		42	33
0	2		225	208
1	2		41	33
0	3		26	21
1	3		35	30
2	3		15	15
0	4		20	16
1	4		15	15

L = 4

H	K		|F-O|	|F-C|
2	0		397	403
5	1		32	33
1	2		231	229
2	2		109	96
0	3		106	91
1	3		125	132
2	3		95	91
0	4		137	139
1	4		26	22
0	5		34	34
2	6		95	39

L = 5

H	K		|F-O|	|F-C|
2	0		152	153
0	1		280	296
5	1	*	25	7
1	2		209	206
5	2		65	70
0	3		40	22
1	3		136	140
0	4		75	70

L = 6

H	K		|F-O|	|F-C|
0	0		164	163
2	0		20	45
3	0		64	71
4	0		22	39
0	1		52	71
1	1		41	55
2	1		46	38
3	1		29	19

L = 7

H	K		|F-O|	|F-C|
2	0		103	103
3	0		34	51
4	0	*	22	9
0	1	*	20	9
2	1		26	35
3	1		29	26

L = 8

H	K		|F-O|	|F-C|
0	0		387	334
2	0		19	24
3	0		123	103
4	0		22	32
0	1		90	49
1	1		206	175
2	1		49	37
3	1	*	30	6

L = 9

H	K		|F-O|	|F-C|
2	0		177	185
3	0	*	21	5
4	0		46	52
0	1		289	301
2	1		166	166
1	3		96	85

L = 10

H	K		|F-O|	|F-C|
0	0		167	162
1	0		79	71
2	0		53	51
3	0		69	69
1	1		131	92
2	1		46	47

It is worth mentioning here that at one stage of structure trials, in spite of the apparent incompatibility of an orthorhombic space group for Region I due to the presence of some visually inequivalent reflections, a trial model was made with the space group C2cm on the data in Region I. The resulting R value was 31%. This seems to be consistent with our speculation in Section 8.6 that the space group prior to the completely disordered state should be C2cm. However, no attempt has yet been made to test the present hexagonal data against this space group.

CHAPTER IX

CONFIGURATIONAL ENTROPY CHANGE OF $Na_4P_2O_7$

In this Chapter a discussion of the configurational entropy change of sodium pyrophosphate when the system changes from the room-temperature ordered phase to the highly disordered phase above 600°C. will be given. The discussion will be purely theoretical because no measurement has yet been obtained on the system at the time of this thesis. A suggestion on how such measurements could be carried out will be given, however.

9.1. Equivalent Model for the Calculation of Entropy

We first review on the general features of the system of sodium pyrophosphate. Both the room-temperature phase and the disordered hexagonal phase above 600°C. have a c axis equal to about 13.5 Å. The general locations of the pyrophosphate groups are not changed, the major difference being in the orientations of the bridging oxygen atoms.

The pyrophosphate groups in both phases are not linear; but each is bent by an angle of the order of 130°. In the room-temperature phase, the orientation of a pyrophosphate group is fixed by the symmetry of the space group

$P2_12_12_1$. In the disordered phase, the structure refined by using the hexagonal space group $P6_3/mmc$ gave an R value of 10%. Although it is not yet certain that this is the proper space group for the disordered phase, it is definitely not far from the true picture.

Since hexagonal systems are usually describable in terms of an orthorhombic system, we shall keep using an orthorhombic system to describe the disordered phase. In arriving at a model for the calculation of the entropy, it is convenient to make some postulates regarding the environment of the sodium atoms which are coplanar with the bridging oxygen atoms of the pyrophosphate groups.

POSTULATE I. The bridging oxygen atom of each pyrophosphate group must be directed towards one of the three nearest coplanar sodium atoms.

POSTULATE II. Each of the sodium atoms coplanar with the bridging oxygen atom must have one and only one pyrophosphate groups directed towards it.

The two terminal sodium atoms at the ends of each pyrophosphate group are considered to have only interlayer but no intralayer effect on the building of the crystal structure.

There are altogether twelve configurations which satisfy the above postulates. They are shown in Fig. 9.1.1. It is seen that some of them can repeat themselves; while

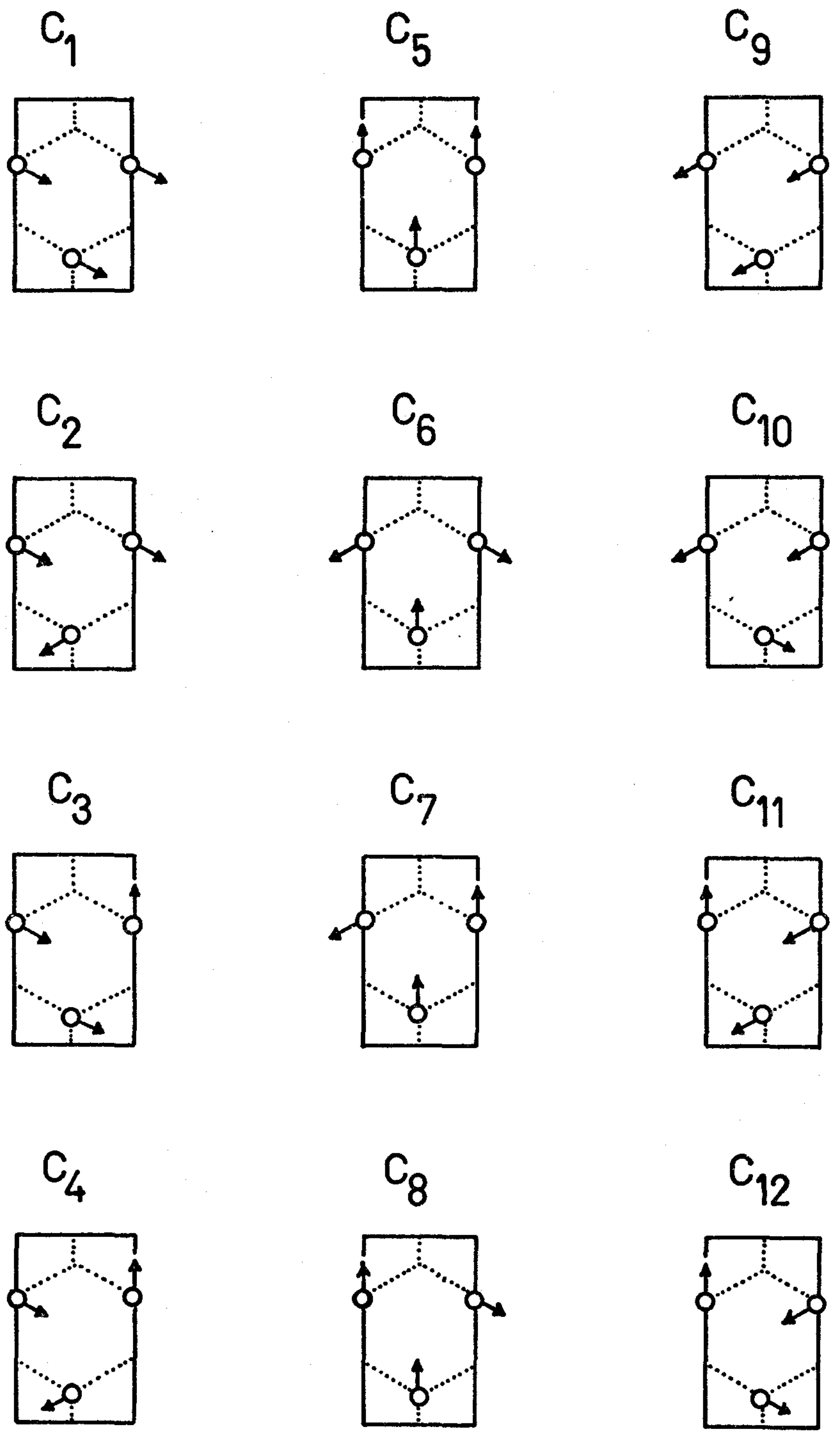

The 12 possible Configurations

Fig. 9.1.1

others cannot. Those which can repeat themselves are called the ordered types while the others are called the disordered types. Ordered types are C_1, C_2, C_5, C_9 and C_{10}. Disordered types may result from an ordered type by making a "mistake". The mistake may bring an ordered type to another ordered type as, for example, from C_1 to C_2, or to a disordered type as from C_1 to C_3. When a disordered type has occurred, another mistake must follow which may bring the disordered type to yet another disordered type as from C_3 to C_8; but it may also bring it to an ordered type as from C_3 to C_5. Although it might appear intuitively that there would be a higher probability for an ordered type to generate another ordered type of the same configuration, there is in reality no a priori reason why one configuration is preferred to another in a completely disordered state of the system. Hence, we could make a third postulate on the equal probability of the configurations.

POSTULATE III. Each configuration satisfying Postulates I and II has an equal probability in the disordered state of the system.

With the three postulates on the configurations we can proceed to formulate the problem on the entropy as described in the subsequent sections.

9.2. One-Dimensional Checkerboard

Following the treatment of Copper Formate Tetrahydrate by Okada [49], we first consider a one-dimensional array of n unit cells along the b axis, a one-dimensional checkerboard. Let P(n) be the number of configurations of this one-dimensional model. Then P(n) is divided into twelve terms as

$$P(n) = \sum_{i=1}^{12} C_i(n) \tag{9.2.1}$$

corresponding to the twelve possible configurations of the pyrophosphate groups in the n-th cell. For example, $C_1(n)$ is the number of arrangements when all the three pyrophosphate groups point towards the lower right in the n-th cell, Fig. 9.1.1. For the case of (n+1) cells built by adding one cell to the n-th, we have

$$C_1(n+1) = C_1(n) + C_2(n) + C_6(n) + C_8(n) \tag{9.2.2}$$

because the left-hand edge of the (n+1)-th cell with configuration C_1 can only match the right-hand edge of the n-th cell with configuration C_1, C_2, C_6 or C_8. Similarly, we have

$$C_2(n+1) = C_2(n) + C_6(n) + C_8(n)$$

$$C_3(n+1) = C_1(n) + C_2(n) + C_6(n) + C_8(n)$$

$$C_4(n+1) = C_2(n) + C_6(n) + C_8(n)$$

$$C_5(n+1) = C_3(n) + C_4(n) + C_5(n) + C_7(n)$$

$$\begin{aligned}
C_6(n+1) &= C_9(n) + C_{10}(n) + C_{11}(n) + C_{12}(n) \\
C_7(n+1) &= C_9(n) + C_{10}(n) + C_{11}(n) + C_{12}(n) \\
C_8(n+1) &= C_3(n) + C_4(n) + C_5(n) + C_7(n) \\
C_9(n+1) &= C_9(n) + C_{10}(n) + C_{11}(n) \\
C_{10}(n+1) &= C_9(n) + C_{10}(n) + C_{11}(n) + C_{12}(n) \\
C_{11}(n+1) &= C_4(n) + C_5(n) + C_7(n) \\
C_{12}(n+1) &= C_3(n) + C_4(n) + C_5(n) + C_7(n)
\end{aligned}$$

It is to be noted that most of the equations for $C_i(n+1)$ have four terms. Some of them have only three terms because of Postulate II which does not allow more than one pyrophosphate groups being directed towards a sodium atom. From Postulate III we have $C_i(n) = C_j(n)$ for all i, j = 1, 2, ... , 12. Hence, from the above equations, it is obvious that

$$(9.2.3) \qquad P(n+1) = \sum_{i=1}^{12} C_i(n+1) = \frac{44}{12} P(n)$$

which, on simplification, gives $P(n) = (11/3)^{n-1}P(1)$.

Since $P(1) = 12$, we have

$$(9.2.4) \qquad P(n) = 12 \times (11/3)^{n-1}.$$

9.3. Two-Dimensional Checkerboard

We next consider a two-dimensional checkerboard formed by putting two one-dimensional checkerboards alongside each other. Postulates I and II impose certain restrictions on the matching of the upper and lower sides of the two adjacent one-dimensional checkerboards. We first work out the matching probability of the one-dimensional checkerboards. Consider the corner A in Fig. 9.3.1. The probability of having a pyrophosphate group being directed towards it is 4/12. A cell with this configuration can be matched with a cell in the lower checkerboard when the latter cell does not have a pyrophosphate group being directed towards the corner B. This probability is 8/12. The joint probability for the matching is then $(4/12) \times (8/12) = 2/9$. However, matching is also possible when A does not have any pyrophosphate group being directed towards it while B does; and the joint probability is again 2/9. Hence, the total probability for matching two adjacent unit cells is $(2/9) + (2/9) = 4/9$. If there are n unit cells in each one-dimensional checkerboard, the matching probability is then $(4/9)^n$.

Let there be m one-dimensional checkerboards each of n unit cells. If we write $Q(n,m)$ as the number of arrangements that the m one-dimensional checkerboards can be placed alongside each other without violating Postulates I and II, we have, for a general value of $m = i$ with $i \geqslant 2$

$$Q(n,i) = Q(n,i-1)Q(n,1)\cdot(4/9)^n \tag{9.3.1}$$

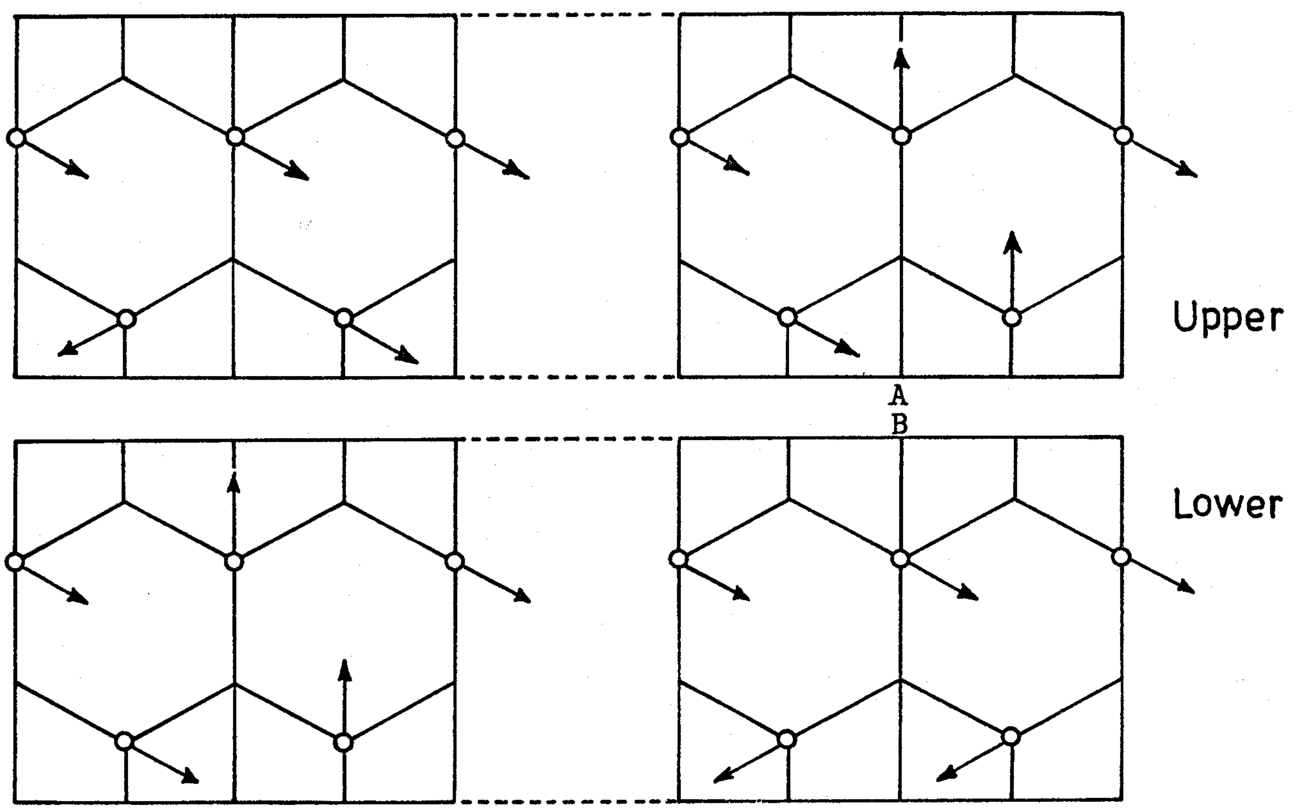

Fig. 9.3.1. Two 1-Dimensional Checkerboards placed alongside each other.

which reduces to

$$Q(n,m) = Q(n,1)^m(4/9)^n \tag{9.3.2}$$

when i = m. By definition, Q(n,1) = P(n). Substituting Q(n,1) by P(n) and taking logarithms, we have

$$\ln Q(n,m) = m \ln P(n) + n \ln (4/9) \tag{9.3.3}$$

From Equation (9.2.4), $P(n) = 12 \times (11/3)^{n-1}$ so that

$$\ln Q(n,m) = m \ln (12) + m(n-1) \ln (11/3) + n \ln (4/9) \tag{9.3.4}$$

For an actual crystal, both m and n have very large values and ln Q(n,m) can be approximated as

$$\ln Q(n,m) = mn \ln (11/3) \tag{9.3.5}$$

Since the number of cells is equal to half the number of molecules in the crystal, N, we can put mn = N/2. Multiplying by the Boltzmann constant, k, the configurational entropy of the disordered state is given by

$$\begin{aligned} k \ln Q(n,m) &= k\cdot(N/2)\cdot\ln (11/3) \\ &= R \ln (11/3)^{\frac{1}{2}} \end{aligned} \tag{9.3.6}$$

where R is the gas constant. Actually, two-dimensional checkerboards themselves are stacked to form a three-dimensional crystal. When the crystal is large and interactions between adjacent layers are weak, no modification is necessary and the above result holds.

9.4. Discussion

As noted above, we have not yet obtained any experimental data on the entropy change of sodium pyrophosphate so that it is rather difficult to judge the accuracy of the calculation. The following method is suggested for a measurement of the entropy change. By definition

$$\text{Entropy change} = \Sigma \, \frac{\text{Heat change}}{\text{Temperature}}$$

where the summation goes over all the transitions from room temperature to 600°C. A differential thermal analyser may be used to measure both the heat change and the temperature corresponding to each transition.

CHAPTER X

A MODEL FOR THE DISORDER OF $Na_4P_2O_7$

A model for the disorder observed in the high-temperature phases of sodium pyrophosphate is described. Because of the possible existence of the twelve configurations as discussed in Chapter IX, the problem is rather involved and it is necessary to make further simplications. The justification of these simplications will be discussed as we proceed.

10.1. Intensity in Reciprocal Space

A perfect crystal consists of identical unit cells arranged at the points of a lattice defined by the axes $\underline{a}$, $\underline{b}$ and $\underline{c}$. With an arbitrary cell chosen as the origin, the position of the n-th cell is given by

$$\underline{r}_n = n_1\underline{a} + n_2\underline{b} + n_3\underline{c} \tag{10.1.1}$$

where n_1, n_2, n_3 are three integers defining $n = (n_1,n_2,n_3)$. The lattice cells are therefore arranged in rows, columns, and layers in such a way that $\underline{r}_n$ terminates on the point in the n_1-th row, the n_2-th column and the n_3-th layer. The ranges over which n_1, n_2, and n_3 can vary depend on the size and shape of the crystal. This lattice-cell model is particularly useful in describing systems where there is a possibility of non-uniformity in the contents of the unit cells. In disordered systems, non-uniformity of some quantity is invariably present. In the present case, the quantity of interest is the structure factor F.

In order to allow for its change, we write the scatttering factor of the n-th cell as F_n. It is convenient to consider continuous variables (H,K,L) in reciprocal space in addition to the familiar integer variables (h,k,l). Thus, any point $\underline{S}$ in reciprocal space can be written as

$$\underline{S} = H\underline{a}^* + K\underline{b}^* + L\underline{c}^* \tag{10.1.2}$$

where $\underline{a}^*$, $\underline{b}^*$, and $\underline{c}^*$ are the reciprocal lattice vectors. The X-rays scattered by the n-th cell at $\underline{r}_n$ are advanced in phase with respect to those scattered at the origin by an amount D_n given by

$$D_n = 2\pi(\underline{S}\cdot\underline{r}_n)$$

and their contribution to the total amplitude scattered by the crystal is

$$F_n\, e^{iD_n} = F_n \exp[2\pi i(\underline{S}\cdot\underline{r}_n)]$$

The total amplitude scattered by all n cells in the crystal is then

$$G(H,K,L) = F_n \exp[2\pi i(\underline{S}\cdot\underline{r}_n)]\,. \tag{10.1.3}$$

The intensity of scattering at (H,K,L) is

$$(10.1.4) \qquad I(H,K,L) = G(H,K,L)G^*(H,K,L)$$

$$= \sum_n \sum_{n'} F_n F^*_{n'} \exp[2\pi i(\underline{S}\cdot\{\underline{r}_n - \underline{r}_{n'}\})]$$

The evaluation of the summations depends on a knowledge of F_n and the limits of n. If $\underline{h} = (h,k,l)$ is a reciprocal lattice vector so chosen that in

$$(10.1.5) \qquad \underline{S} = \underline{S}_{\underline{h}} + \underline{s}$$

$|\underline{s}|$ is smallest, then $(\underline{S}_h\cdot\underline{r}_n)$ and $(\underline{S}_h\cdot\underline{r}_{n'})$ are integers and may be dropped out of the exponents, giving

$$(10.1.6) \qquad I(\underline{s}) = \sum_n \sum_{n'} F_n F^*_{n'} \exp[2\pi i(\underline{s}\cdot\{\underline{r}_n - \underline{r}_{n'}\})]$$

If $(\underline{s}\cdot\underline{r}_n)$ and $(\underline{s}\cdot\underline{r}_{n'})$ change only slightly in going from one unit cell to another, the summations can be replaced by integrations over the volume of the crystal. Thus, we have

$$(10.1.7) \qquad I(\underline{s}) = V^{-2}\int d\underline{r}\int d\underline{r}'\; F_n F^*{}_{n'} \exp[2\pi i(\underline{s}\cdot\{\underline{r}_n - \underline{r}_{n'}\})]$$

For a particular type of imperfection of the crystal, we are interested in exploring the way in which the intensity varies with the distance s from the reciprocal lattice point (h,k,l) in the direction $\underline{s}$. Non-zero values of $I(\underline{s})$ for some $\underline{s}$ give rise to the phenomenon of streaks. We shall go into more detail on this problem of streaks below.

10.2. General Treatment of Mistakes

Wilson [50] has given a general treatment of mistakes in crystals. Following his treatment, if we write

$$n'_i = n_i + m_i \qquad (i = 1, 2, 3)$$

and

$$\underline{s} = (u,v,w)$$

we have, from (10.1.6)

$$I(u,v,w) = \sum_n \sum_m F_n F^*_{n+m} \exp\left[-2\pi i(m_1 u + m_2 v + m_3 w)\right] \tag{10.2.1}$$

$$= \sum_m \left[\sum_n F_n F^*_{n+m}\right] \exp\left[-2\pi i(m_1 u + m_2 v + m_3 w)\right]$$

The summation within the bracket contains no exponential factors and can be evaluated for postulated models of how the mistakes occur. Its physical interpretation is the following. Starting with the cell defined by $n = (n_1,n_2,n_3)$ we find the cell which is $m_1 a$, $m_2 b$, $m_3 c$ away in the directions $\underline{a}$, $\underline{b}$, $\underline{c}$ respectively. Having found it, we multiply together the structure factor of the first cell and the complext conjugate of the structure factor of the second and add these products together for all pairs of cells having the same separation. Obviously, for cells near the surface and for a fixed $m = (m_1,m_2,m_3)$ it may happen that is is not possible to find the second cell as it would be outside the crystal boundary. The number of such possible pairs depends therefore on m and we may denote this number by W(m). For a given m, W(m) is a large number and each product $F_n F^*_{n+m}$ may take up values depending on the distribution of the mistakes. If we write the average value of the products $F_n F^*_{n+m}$ over this range as

$$Y(m) = \langle F_n F^*_{n+m} \rangle \tag{10.2.2}$$

we have, from Equation (10.2.1)

$$I(u,v,w) = \sum_m W(m)\, Y(m) \exp\left[-2\pi i(m_1 u + m_2 v + m_3 w)\right] \tag{10.2.3}$$

Since W(m) is purely geometrical, it is independent of the nature of the mistakes. Y(m), on the other hand, depends on the distribution and nature of the mistakes and can only be estimated by postulating some statistical models of how the changes in the atomic arrangement in the unit cell occur and how the affected unit cells are distributed throughout the crystal. A model to account for the observed streaks in sodium pyrophosphate is described below.

10.3. Model for the Streaks of Sodium Pyrophosphate

In Chapter IX, we introduced the twelve possible configurations of each cell in the disordered phase. Suppose now we label these cells by the numbers (m,n,p). Then, we could ask the following question: What is the probability of having one of the twelve configurations at the cell which is m column, n rows, and p layers away from the origin? This question cannot be answered precisely because it involves twelve configurations with varying degrees of probability at each cell. We shall attempt, instead, to simplify the system by introducing zones or domains within which every cell will have the same configuration. In other words, we introduce a certain amount of local short-range order.

The thickness of each domain is $\frac{1}{2}\underline{c}$ and its extent in the $\underline{a}\,\underline{b}$ plane may in general vary with the domains. Of the twelve configurations only five can repeat themselves, Fig. 9.1.1, p. 157. The other seven may be regarded as transitional units forming the boundary between the domains. These units are small in number compared to the five repeatible units so that their contributions to the structure factor calculation for the entire crystal might be neglected. Since the structure of the disordered phase refined by using the hexagonal space group $P6_3/mmc$ gave an R value of 10%, it seems legitimate to assume further that the bridging oxygen atoms of the pyrophosphate groups within a unit cell all point in the same direction. This eliminates two more configurations out of the repeatible five, i.e. C_2 and C_{10} of Fig. 9.1.1. We are then left with three configurations A, B, and C which can form a domain, Fig. 10.3.1. A direct transition among three configurations is impossible and is brought about only through the other transitional units.

In order that we may label the domains in the same way as the cell, we shall make a further minor assumption:

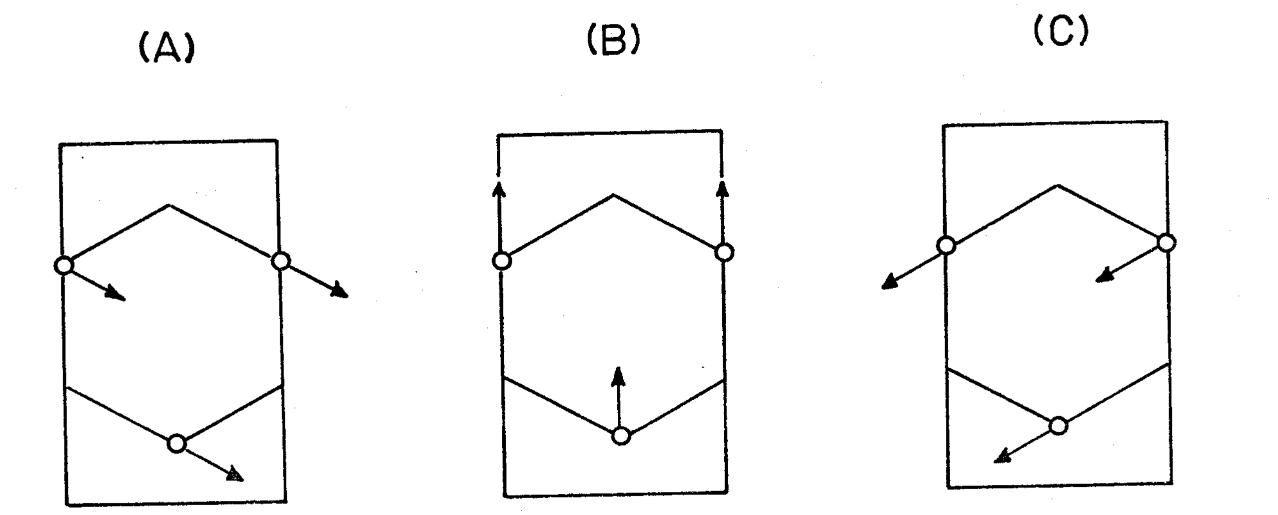

Fig. 10.3.1. The three basic configurations in a domain. Circle stands for a pyrophosphate group with arrow showing Na-O(bridging) interaction.

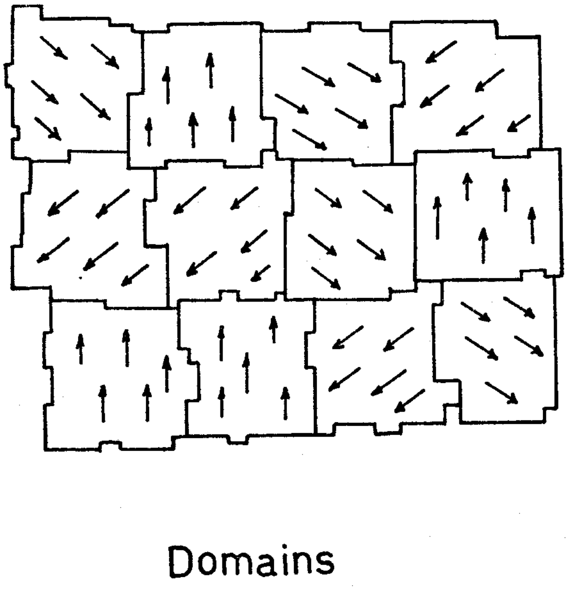

Fig. 10.3.2

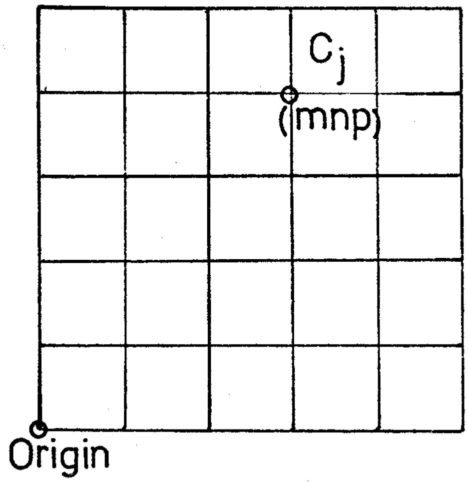

Fig. 10.3.3. Labelling of Domains.

The extent of each domain is the same. This seems reasonable because there is no a priori reason why one domain with a particular configuration should be favoured at the expense of the other. Every configuration should have the same probability of making a "mistake" and this, when strictly observed, should lead to equal extent for all domains.

Suppose now we could label the domains by (m,n,p). We may then ask the question: Given a domain with a certain configuration at the origin, what is the probability of finding the other configurations including itself at a location (m,n,p)? If we can answer this question, we can work out an estimate of the quantity Y(m,n,p) defined by Equation (10.2.2) which is required in estimating the intensity at a point (u,v,w) in reciprocal space, Equation (10.2.3).

The following Sections will be devoted to the calculation of Y(m,n,p).

10.4. Recurrence Relationships

Without loss of generality, suppose the configuration of the domain at the origin is A. Then,

Let $L_{m,n,p}(A)$ be the probability that the domain at (m,n,p) is A,

$L_{m,n,p}(B)$ be the probability that the domain at (m,n,p) is B, and

$L_{m,n,p}(C)$ be the probability that the domain at (m,n,p) is C.

We require

$$L_{m,n,p}(A) + L_{m,n,p}(B) + L_{m,n,p}(C) = 1. \tag{10.4.1}$$

Because of the layer structure of the system we shall divide the discussion into two parts: a first part dealing within each layer and a second part dealing between different layers.

Since we have only three configurations, it is simpler to describe the system with hexagonal indices. This we will do in the following. If, for p = 0, the layer has configuration A, B, or C, then for p = 1, the pyrophosphate groups will also have configurations A, B, or C, but in positions which are displaced $\underline{a}/3$ and $-\underline{b}/3$ relative to those for p = 0. We shall label the displaced configurations by A', B', and C'. For layers with p = odd, all domains will have primed configurations while for layers with p = even, they will have unprimed configurations. It is convenient to consider the layers with p = odd as one system intermingled with the layers with p = even as another system. We shall assume further that apart from the relative shifts of the pyrophosphate groups the two layer-systems are independent of each other, i.e. the "mistake" made in one system will not affect the other system.

Part I: Within the same layer

Let α be the probability that a mistake will occur which changes the configuration of a domain into one of the other two in the same layer. Then we have, for p = even

(i) $L_{m+1,n,p}(A) = L_{m,n,p}(A)(1-\alpha) + L_{m,n,p}(B)\alpha/2 + L_{m,n,p}(C)\alpha/2$

(ii) $L_{m+1,n,p}(B) = L_{m,n,p}(B)(1-\alpha) + L_{m,n,p}(C)\alpha/2 + L_{m,n,p}(A)\alpha/2$

(iii) $L_{m+1,n,p}(C) = L_{m,n,p}(C)(1-\alpha) + L_{m,n,p}(A)\alpha/2 + L_{m,n,p}(B)\alpha/2$

(10.4.2)

For p = odd, the above equations are still true if we replace the unprimed configurations with the primed configurations, i.e. A → A', B → B', and C → C'. It is readily verified that Equation (10.4.1) is true for the domain (m+1,n,p) as it should. Equations (10.4.2) are to be solved subject to the normalization condition (10.4.1) and the boundary conditions:

For p = even

$$(10.4.3)\qquad \begin{aligned} &\text{(i)} && L_{0,0,0}(A) = 1\\ &\text{(ii)} && L_{0,0,0}(B) = 0\\ &\text{(iii)} && L_{0,0,0}(C) = 0 \end{aligned}$$

For p = odd

$$(10.4.4)\qquad \begin{aligned} &\text{(i)} && L_{0,0,1}(A') = 1\\ &\text{(ii)} && L_{0,0,1}(B') = 0\\ &\text{(iii)} && L_{0,0,1}(C') = 0 \end{aligned}$$

We shall solve Equations (10.4.2) for p = even. We assume that the solution is in the following form:

$$(10.4.5)\qquad L_{m,n,p}(A) = R_A + S_A Q_A^{\,m+n} T_A^{\,p}$$

where R_A, S_A, Q_A and T_A are non-trivial constants independent of m,n, and p. The subscript A is used to designate configuration A. Expressions similar to (10.4.5) can be written for configurations B and C.

From Equation (10.4.1), we have

$$(10.4.6)\qquad \begin{aligned} L_{m+1,n,p}(A) &= L_{m,n,p}(A)(1-\alpha) + (1 - L_{m,n,p}(A))\alpha/2\\ &= \tfrac{1}{2}\alpha + L_{m,n,p}(A)(1 - 3\alpha/2) \end{aligned}$$

From (10.4.5), we have, on simplification

$$(10.4.7)\qquad \begin{aligned} R_A + S_A Q_A^{\,m+n+1} T_A^{\,p} &= \tfrac{1}{2}\alpha + R_A(1 - 3\alpha/2)\\ &\quad + S_A Q_A^{\,m+n} T_A^{\,p}(1 - 3\alpha/2) \end{aligned}$$

Equation (10.4.7) is true for all m, n, and p so that

(10.4.8)

$$\text{(i)} \quad R_A = \tfrac{1}{2}\alpha + R_A(1 - 3\alpha/2)$$

$$\text{(ii)} \quad S_A Q_A^{m+n+1} T_A^{\,p} = S_A Q_A^{m+n} T_A^{\,p}$$

(i) immediately gives $R_A = \frac{1}{3}$ while (ii) gives $Q_A = (1 - 3\alpha/2)$. To obtain S_A, we use the boundary condition (10.4.3(i)). Substituting it in 10.4.6), we have

$$L_{1,0,0}(A) = \tfrac{1}{2}\alpha + 1 \times (1 - 3\alpha/2)$$

But,

$$L_{1,0,0}(A) = R_A + S_A Q_A^{\,1} T_A^{\,0}$$

Therefore,

$$\tfrac{1}{3} + S_A(1 - 3\alpha/2) = \tfrac{1}{2}\alpha + 1 \times (1 - 3\alpha/2)$$

giving

(10.4.9) $$S_A = 2/3.$$

Hence, we obtain

(10.4.10) $$L_{m,n,p}(A) = \tfrac{1}{3} + \tfrac{2}{3}(1 - 3\alpha/2)^{m+n} T_A^{\,p}.$$

For $L_{m,n,p}(B)$ and $L_{m,n,p}(C)$ we can proceed in the same way to obtain

(10.4.11) $$L_{m,n,p}(B) = \tfrac{1}{3} - \tfrac{1}{3}(1 - 3\alpha/2)^{m+n} T_B^{\,p}$$

(10.4.12) $$L_{m,n,p}(C) = \tfrac{1}{3} - \tfrac{1}{3}(1 - 3\alpha/2)^{m+n} T_C^{\,p}$$

We still have to calculate $T_{A'}$, $T_{B'}$, and T_{C} which obviously can only be obtained by considering interactions between different layers.

If we proceed in a similar way for p = odd layers, making use of the boundary conditions (10.4.4), we have

(10.4.13) $L_{m,n,p}(A') = \frac{1}{3} + \frac{2}{3}(1 - 3\alpha/2)^{m+n} T_{A'}^{p-1}$

(10.4.14) $L_{m,n,p}(B') = \frac{1}{3} - \frac{1}{3}(1 - 3\alpha/2)^{m+n} T_{B'}^{p-1}$

(10.4.15) $L_{m,n,p}(C') = \frac{1}{3} - \frac{1}{3}(1 - 3\alpha/2)^{m+n} T_{C'}^{p-1}$

Part II: Between different layers

Let β be the probability that a mistake will occur which changes the configuration of a domain into one of the other two configurations in alternate layers up the c axis. Then we have, for p = even

(i) $L_{m,n,p+2}(A) = L_{m,n,p}(A)(1-\beta) + L_{m,n,p}(B)\beta/2 + L_{m,n,p}(C)\beta/2$

(ii) $L_{m,n,p+2}(B) = L_{m,n,p}(B)(1-\beta) + L_{m,n,p}(C)\beta/2 + L_{m,n,p}(A)\beta/2$

(iii) $L_{m,n,p+2}(C) = L_{m,n,p}(C)(1-\beta) + L_{m,n,p}(A)\beta/2 + L_{m,n,p}(B)\beta/2$

(10.4.16)

For p = odd, the above equations are still true when $A \rightarrow A'$, $B \rightarrow B'$ and $C \rightarrow C'$. Equations (10.4.16) can be solved in a way similar to (10.4.2) to give a solution to $T_{A'}$, $T_{B'}$, ...;

but a quicker way is to use Equations (10.4.10 - 10.4.12) in (10.4.16). Thus, we have, for example

$$1/3 + \frac{2}{3}(1 - 3\alpha/2)^{m+n}T_A{}^{p+2}$$

$$= \tfrac{1}{2}\beta + (1/3 + \frac{2}{3}(1 - 3\alpha/2)^{m+n}T_A{}^{p})(1 - 3\beta/2)$$

giving

$$T_A = (1 - 3\beta/2)$$

or

$$T_A = (1 - 3\beta/2)^{\frac{1}{2}}. \tag{10.4.17}$$

It can easily be verified that $T_B = T_C = T_{A'} = T_{B'} = T_{C'} = T_A$. Hence, we obtain the following complete solutions:

For p = even:

$$\begin{aligned} L_{m,n,p}(A) &= \frac{1}{3} + \frac{2}{3}(1 - 3\alpha/2)^{m+n}(1 - 3\beta/2)^{p/2} \\ L_{m,n,p}(B) &= \frac{1}{3} - \frac{1}{3}(1 - 3\alpha/2)^{m+n}(1 - 3\beta/2)^{p/2} \\ L_{m,n,p}(C) &= \frac{1}{3} - \frac{1}{3}(1 - 3\alpha/2)^{m+n}(1 - 3\beta/2)^{p/2} \\ L_{m,n,p}(A') &= L_{m,n,p}(B') = L_{m,n,p}(C') = 0 \end{aligned} \tag{10.4.18}$$

For p = odd:

$$\begin{aligned} L_{m,n,p}(A') &= \frac{1}{3} + \frac{2}{3}(1 - 3\alpha/2)^{m+n}(1 - 3\beta/2)^{\frac{1}{2}(p-1)} \\ L_{m,n,p}(B') &= \frac{1}{3} - \frac{1}{3}(1 - 3\alpha/2)^{m+n}(1 - 3\beta/2)^{\frac{1}{2}(p-1)} \\ &= L_{m,n,p}(C') \\ L_{m,n,p}(A) &= L_{m,n,p}(B) = L_{m,n,p}(C) = 0 \end{aligned} \tag{10.4.19}$$

10.5. Structure Factors of the Domains

Let $F(A)$, $F(B)$, and $F(C)$ be the structure factors of the domains A, B, and C respectively when they are in the even layers, and $F(A')$, $F(B')$, and $F(C')$ be the structure factors of the domains with the shifted configurations in the odd layers. Further, let

$$\text{(i)} \quad F(A) = Q;$$

then

$$
\begin{aligned}
&\text{(ii)} & F(B) &= Q \exp\,(i2\pi/3)\\
&\text{(iii)} & F(C) &= Q \exp\,(-i2\pi/3)\\
&\text{(iv)} & F(A') &= Q \exp\,(i2\pi(h-k)/3)\\
&\text{(v)} & F(B') &= Q \exp\,(i2\pi(h-k)/3) \exp\,(i2\pi/3)\\
&\text{(vi)} & F(C') &= Q \exp\,(i2\pi(h-k)/3) \exp\,(-i2\pi/3)
\end{aligned}
\tag{10.5.1}
$$

The factor $\exp\,(i2\pi/3)$ comes about because in a domain, configuration B can be obtained from configuration A by a rotation of $2\pi/3$ about an axis parallel to $\underline{c}$. Rotating $2\pi/3$ twice or $-2\pi/3$ gives configuration C. A further rotation of $2\pi/3$ gives back A. We conclude therefore that the phase difference between the configurations in the same layer must be $2\pi/3$. The factor $\exp\,(i2\pi(h-k)/3)$ comes about because the shifted positions are translated 1/3 along $\underline{a}$ and 2/3 along $\underline{b}$ (or, equivalently, -1/3 along $\underline{b}$) with respect to the normal unshifted layers.

It is convenient to display the real and imaginary parts of the structure factors explicitly. If we write f(A) and g(A) for the real and imaginary parts of F(A) respectively, we have

$$
(10.5.2)\qquad
\begin{aligned}
f(A) &= Q & g(A) &= 0\\
f(B) &= -\tfrac{1}{2}Q & g(B) &= \tfrac{1}{2}Q\sqrt{3}\\
f(C) &= -\tfrac{1}{2}Q & g(C) &= -\tfrac{1}{2}Q\sqrt{3}\\
f(A') &= QD & g(A') &= QE\\
f(B') &= -\tfrac{1}{2}QD - \tfrac{1}{2}QE\sqrt{3} & g(B') &= -\tfrac{1}{2}QE + \tfrac{1}{2}QD\sqrt{3}\\
f(C') &= -\tfrac{1}{2}QD + \tfrac{1}{2}QE\sqrt{3} & g(C') &= -\tfrac{1}{2}QE - \tfrac{1}{2}QD\sqrt{3}
\end{aligned}
$$

where we have written for short

$$D \equiv \cos 2\pi(h-k)/3$$

$$E \equiv \sin 2\pi(h-k)/3.$$

10.6. Evaluation of Y(m,n,p)

The quantity Y(m,n,p) as defined by Equation (10.2.2) can be expressed in terms of two other quantities J(m,n,p) and K(m,n,p) (Cf. Wilson [50]) as

$$(10.6.1)\qquad Y(m,n,p) = J(m,n,p) - i\,K(m,n,p)$$

where in the present case

$$(10.6.2)\qquad J(m,n,p) = \sum_{I} L_{m,n,p}(I)f(A)f(I)$$

and

$$(10.6.3)\qquad K(m,n,p) = \sum_{I} L_{m,n,p}(I)f(A)g(I)$$

where the summation on I is over all A, B, C, A', B', and C'. The quantities $L_{m,n,p}(I)$ are defined by (10.4.18 - 19).

Simplifying with Equations (10.5.2) we have

$$(10.6.4) \qquad J(m,n,p) = Q^2 L_{m,n,p}(A) - Q^2 L_{m,n,p}(B) + Q^2 D L_{m,n,p}(A') - Q^2 D L_{m,n,p}(B')$$

where we have used the equalities

$$L_{m,n,p}(B) = L_{m,n,p}(C) \quad \text{and} \quad L_{m,n,p}(B') = L_{m,n,p}(C').$$

We recall that the values of $L_{m,n,p}(I)$ depends on p being even or odd and it would be more convenient if we could get rid of the trouble of even or odd by building in some factors to take care of this. We know that for p = even, $L_{m,n,p}(I') = 0$; and for p = odd, $L_{m,n,p}(I) = 0$. Thus, we can prefix the factors $\frac{1}{2}(1 + (-1)^p)$ to $L_{m,n,p}(I)$ and $\frac{1}{2}(1 - (-1)^p)$ to $L_{m,n,p}(I')$ in Equation (10.6.4).

Simplifying further with Equations (10.4.18 - 19), we have,

$$(10.6.5) \qquad J(m,n,p) = \tfrac{1}{2}(1+(-1)^p)Q^2(1-3\alpha/2)^{m+n}(1-3\beta/2)^{\frac{1}{2}p} + \tfrac{1}{2}(1-(-1)^p)Q^2 D(1-3\alpha/2)^{m+n}(1-3\beta/2)^{\frac{1}{2}(p-1)}$$

Similar simplification on (10.6.3) for K(m,n,p) gives

$$(10.6.6) \qquad K(m,n,p) = \tfrac{1}{2}(1-(-1)^p)Q^2 E(1-3\alpha/2)^{m+n}(1-3\beta/2)^{\frac{1}{2}(p-1)}$$

Thus, we see that the quantity Y(m,n,p) as defined by (10.6.1) can be expressed in terms of the probabilities α and β.

10.7. Discussion

It has been shown that the intensity $I(u,v,w)$ at a point $\underline{s} = (u,v,w)$ in the vicinity of a reciprocal lattice point $\underline{h} = (h,k,l)$ is given by Equation (10.2.3), i.e.

$$I(u,v,w) = \sum_{mnp}\sum\sum W(m,n,p)Y(m,n,p)\exp\left[-2\pi i(mu+nv+pw)\right] \tag{10.7.1}$$

If s is small compared to the dimensions of the reciprocal lattice vectors, and $Y(m,n,p)$ is a smooth function, the summations can be replaced by integrals. If $\underline{a}'$, $\underline{b}'$ and $\underline{c}'$ are the dimensions of the domains, and if we write

$$x = ma'; \quad y = nb'; \quad z = pc'$$

the resulting integral can be expressed as

$$I(u,v,w) = \frac{1}{Ua'b'c'} \int dx \int dy \int dz\ W(x,y,z)\ Y(x,y,z)\ e^{-i\theta} \tag{10.7.2}$$

where U is the volume of each domain, and $W(x,y,z)$ and $Y(x,y,z)$ are the corresponding expressions with the substitutions and θ is given by

$$\theta = 2\pi\left\{\frac{ux}{a'} + \frac{vy}{b'} + \frac{wz}{c'}\right\} \tag{10.7.3}$$

In a crystal containing mistakes, $Y(x,y,z)$ may decrease so rapidly that the variations of $W(x,y,z)$ could be ignored. In that case, $W(x,y,z)$ can be taken out of the integration signs to give

$$(10.7.4) \qquad I(u,v,w) = \frac{W}{Ua'b'c'} \int dx \int dy \int dz\ Y(x,y,z)\ e^{-i\theta}\ .$$

With $Y(x,y,z)$ given by Equation (10.6.1) and $J(x,y,z)$ and $K(x,y,z)$ given by Equations (10.6.5 - 6) in terms of the disorder parameters α and β, we should be able, in principle at least, to solve for $I(u,v,w)$. If the model for the streaks is correct, the solution should contain the essential features of the streaks as described in Section(4.5), p. 50. However, simple as it may seem, Equation (10.7.4) cannot be evaluated readily and at the time of writing of this thesis, no solution has yet been obtained.

CHAPTER XI

SUMMARY AND DISCUSSION

IN this thesis it has been established that sodium pyrophosphate undergoes a series of first-order phase transformations between 405° and 550°C. and what probably corresponds to a transformation of the second kind near 600°C.

The first-order phase transformations are manifested primarily by changes in the periodicity along the $\underline{c}$ axis, the layer-stacking direction. The change at 405°C. is from a space group of $P2_12_12_1$ symmetry and $\underline{a}_o$, $\underline{b}_o$, $\underline{c}_o$ unit cell dimensions with adjacent rows within a layer along $\underline{a}_o$ related by a two-fold screw axis to space group C2/c with $\underline{a}_o$, $\underline{b}_o$, $2\underline{c}_o$ and these same rows related by the C-centering. This clearly indicates that changes also occur within the layers below the region where disorder is manifested by streaks in the diffraction patterns. The residual oxygen atom peaks in the difference electron density for phase II (p. 124) suggest that disorder has already occurred in the layer at this point. In region I above 520°C., after another first-order phase transformation, the structure is again monoclinic with the unit cell defined by $\underline{a} = b_o$, $\underline{b} = a_o$, $\underline{c} = 3c_o$ and probable symmetry C2/c. This latter symmetry preserves the two-fold axis and screw axis. In region II, above 540°C. the structure becomes orthorhombic with probable space group C2cm and unit cell dimensions $\underline{a}_o$, $\underline{b}_o$ and $\underline{c}_o$. The D.T.A. spectrum is suggestive of a series of first-order phase transformations in going from region I to region II. Further study will be required to ascertain whether the structure shows greater disorder within the layer in this region than at 405°C., as is anticipated.

Finally, the structure disorders with the pyrophosphate group adopting each of six possible configurations with equal frequency and increasingly less correlation between the pyrophosphate groups as the temperature is raised. At the same time, the diffuse diffraction streaks disappear into the background. Since the structure cannot proceed directly from $P2_12_12_1$ ($\underline{a}_o$, $\underline{b}_o$, $\underline{c}_o$) to $P6_3/mmc$ ($\underline{a}_o/\sqrt{3}$, $\underline{b}_o$, $\underline{c}_o$) by a transformation of the second-kind (Section 2.2, p. 8), it is not entirely surprising that it does so through a series of first-order transformations. However, the alternative path:

$$P2_12_12_1\ (\underline{a}_o,\underline{b}_o,\underline{c}_o) \rightarrow C222_1\ (\underline{a}_o,\underline{b}_o,\underline{c}_o) \rightarrow P6_322\ (\underline{a}_o/\sqrt{3},\underline{b}_o,\underline{c}_o)$$

is available by a series of second-order transformations leading to a hexagonal phase. As yet it has not been ascertained why this path is less favorable than the one actually found.

The sodium diarsenate system resembles sodium pyrophosphate in that it also exhibits a number of phase transformations above room temperature. The rich variety of phase transformations of the two compounds appears to be a feature common to alkaline pyro-compounds. Recently, similar results seemed to have been observed in sodium pyrovanadate [51]. It would be worthwhile, therefore, to study systematically the transformation properties of compounds of the general formula: $X_4Y_2O_7$ with X = Na, K, Li and Rb, and Y = P, As and V. As remarked previously (Chapter I), crystallographic data on these compounds are very scarce in the literature.

As a concluding remark, it might be said that pyrophosphates with organic derivatives play an important role in the metabolism of certain organic compounds, e.g. the adenosine-5'-diphosphate resulting from the hydrolysis of adenosine triphosphate is a source of immediate biological energy [52]. Sodium pyrophosphate, being readily soluble in water and other organic lipids, reacts with a number of biological materials. As pointed out in the beginning of the Introductory Chapter, it is important to know the structure of a compound in addition to its constituents if we were to study it properly. In this respect, understanding the structure of $Na_4P_2O_7$ as a "free" molecule might lead to some insight of the structure of those biological molecules containing a pyrophosphate ion, thereby to a better understanding of the functions of the biological materials themselves.

BIBLIOGRAPHY

1. Partridge, E.P., Hicks, V. and Smith, G.V. J. Am. Chem. Soc. 63, 454 (1941)

2. Kurian, E.M. and Tamhankar, R.V. Proc. Chem. Symp. Madras, 1, 143 (1971)

3. Landau, L.D. Phys. Zeitschr. Sowjet Union 11, 26 (1937)

4. Lyubarski, G. Ya. The Application of Group Theory in Physics. Chapter VIII. Pergamon Press, New York (1960)

5. Remy, F. Bull. Soc. Chim. de France 10, 3380 (1969)

6. Brown, I.D. and Calvo, C. J. Solid State Chem. 1, 173 (1970)

7. Wyckoff, R.W.G. Crystal Structures. Vol. 3. Wiley (Interscience), New York (1960)

8. Robertson, B.E. and Calvo, C. Acta Cryst. 22, 665 (1967)

9. Calvo, C. Private Communication

10. Baur, W.H. Trans. Am. Cryst. Assoc. 6, 129 (1970)

11. Brown, I.D. and Shannon, R.D. Acta Cryst. (to be published)

12. Landau, L.D. and Lifshitz, E.M. Statistical Physics. Chapter XIV. Addison-Wesley, Reading, Mass. (1969)

13. Seitz, F. Ann. Math. 37, 17 (1936)

14. Haas, C. J. Phys. Chem. Solids 26, 1225 (1965)

15. Lipson, H. and Cochran, W. The Determination of Crystal Structures. Cornell Univ. Press, Ithaca (1966)

16. Stout, G.H. and Jensen, L.H. X-ray Structure Determination. Macmillan, London (1968)

17. Waser, J. Rev. Sci. Instr. 22, 563 (1951)

18. International Tables for X-Ray Crystallography. Vol. II. p. 302ff and Vol. III. p.175ff. Kynoch Press, Birmingham (1967)

19. Cruickshank, D.W.J., Pilling, D.E., Bujosa, A., Lovell, F.M. and Truter, M.R. Computing Methods and the Phase Problem in X-ray Crystal Analysis. Pergamon Press, Oxford (1961)

20. Patterson, A.L. Z. Krist. A90, 517 (1935)

21, Woolfson, M.M. Direct Methods in Crystallography. Oxford University Press, New York (1961)

22. Hauptman, H. and Karle, J. Acta Cryst. 9, 45 (1956)

23. Karle, J. and Hauptman, H. Acta Cryst. 9, 635 (1956)

24. International Tables for X-Ray Crystallography. Vol. I. p. 374ff. Kynoch Press, Birmingham (1967)

25. Tien, T.Y. and Hummel, F.A. J. Am. Ceram. Soc. 44, 206 (1961)

26. von Sahnen, R. and Tammann, G. Ann. Phys. 10, 879 (1903)

27. DeLaMatter, D. M.Sc. Thesis. McMaster University (1972)

28. International Tables for X-Ray Crystallography. Vol. III. p. 202ff. Kynoch Press, Birmingham (1967)

29. McDonald, W.S. and Cruickshank, D.W.J. Acta Cryst. 22, 43 (1967)

30. Collin, R.L. and Willis, M. Acta Cryst. 27B, 291 (1971)

31. Gopal, R. Ph.D. Thesis. McMaster University (1972)

32. Sauerbrei, E. M.Sc. Thesis. McMaster University (1972)

33. Cruickshank, D.W.J., Lynton, H. and Barclay, G.A. Acta Cryst. 15, 491 (1962)

34. Ozog, J., Krishnamachari, N. and Calvo, C. Can. J. Chem. 48, 388 (1970)

35. Calvo, C. and Neelakantan, K. Can. J. Chem. 48, 890 (1970)

36. Pauling, L. The Nature of the Chemical Bond. Third Edition. Nornell University Press, Ithaca (1960)

37. Krishnamachari, N. Ph.D. Thesis. McMaster University (1971)

38. Ng, H.N. and Calvo, C. (to be published)

39. International Tables for X-Ray Crystallography. Vol. III. p.271. Kynoch Press, Birmingham (1967)

40. Finger, L.W. REFINE - A Computer Program for Structure Factor Calculation and Least-Squares Refinement of Crystal Structures. Carnegie Institution, Wash. (1969)

41. Cruickshank, D.W.J. Acta Cryst. 9, 747 (1956)

42. Busing, W.R. and Levy, H.A. Acta Cryst. 17, 142 (1964)

43. Schomaker, V. and Trueblood, K.N. Acta Cryst. B24, 63 (1968)

44. Pawley, G.S. and Willis, B.T.M. Acta Cryst. A26, 260 (1970)

45. Johnson, C.K. Crystallographic Computing. pp. 207-226. Munksgaard, Copenhagen (1970)

46. Scheringer, C. Acta Cryst. A28, 616 (1972)

47. Cruickshank, D.W.J. Acta Cryst. 9, 754 (1956)

48. Hamilton, W.C. Acta Cryst. 18, 502 (1965)

49. Okada, K. Phys. Rev. 164, 683 (1967)

50. Wilson, A.J.C. X-Ray Optics. Methuen, London (1949)

51. Calvo, C. Private Communication

52. van Wazer, J.R. Phosphorus and its Compounds. Chapter 10. Interscience, New York (1966)

53. Leung, K.Y. and Calvo, C. Can. J. Chem. 50, 2519 (1972)

54. Leung, K.Y. and Calvo, C. Can. J. Chem. (1973) (To be published)